Photochromism in Bile Salts

by

Cerize da Silva Santos
B.Sc, Universidade Estadual do Centro Oeste, Guarapuava, Brazil, 2004
M.Sc, Universidade de São Paulo, São Paulo, Brazil, 2008

A Thesis Submitted in Partial Fulfillment
of the Requirements for the Degree of

MASTER OF SCIENCE

in the Department of Chemistry

Supervisory Committee

Photochromism in Bile Salts

by

Cerize da Silva Santos
B.Sc, Universidade Estadual do Centro Oeste, Guarapuava, Brazil, 2004
M.Sc, Universidade de São Paulo, São Paulo, Brazil, 2008

Supervisory Committee

Dr. Cornelia Bohne (Department of Chemistry)
Supervisor

Dr. Irina Paci (Department of Chemistry)
Departmental Member

Dr. Geoff Steeves (Department of Physics and Astronomy)
Outside Member

Abstract

Supervisory Committee
Dr. Cornelia Bohne (Department of Chemistry)
Supervisor
Dr. Irina Paci (Department of Chemistry)
Departmental Member
Dr. Geoff Steeves (Department of Physics and Astronomy)
Outside Member

Photochromism is a phenomenon where two isomers with markedly different absorption spectra are interconverted by a reversible photochemical reaction. The photochromism of 1',3',3'-trimethyl-6-nitrospiro[2H-1]-benzopyran-2,2'-indoline (NSP) and 1,2-bis(2,4-dimethyl-5-phenyl-3-thienyl)-3,3,4,4,5,5-hexafluoro-1-cyclopentene) (DAE) was studied in aqueous solutions containing NaCl and the bile salts sodium cholate (NaC), sodium deoxycholate (NaDC) or sodium taurocholate (NaTC).

Bile salts are amphiphilic compounds that aggregate in water. These aggregates can solubilize hydrophobic organic compounds in water and affect the reactivity of the bound compounds. NSP and DAE are photochromic compounds that can be switched between a colored and a colorless isomer. The colored isomer of DAE can only be transformed into the colorless form by irradiation of light, while the colored isomer of NSP is also converted into the colorless form by a dark reaction.

The dark reaction rate constant of NSP increases at high concentrations of bile salt and NaCl. The bile salt structure also affects the dark reaction rate constant, which is smaller in NaTC and approximately the same in NaC and NaDC. The activation energy for the reaction in all conditions studied is similar to the value reported for polar organic solvents.

A method that employs HPLC was developed to determine the molar absorptivity coefficients of photochromic compounds. The values obtained were important to determine the quantum yields for photocoloration (Φ_{AB}) and photodecoloration (Φ_{BA}). Quantum yield values were determined by a photokinetic method that employs irradiation at a single wavelength and numerical analysis. The values of Φ_{AB} and Φ_{BA} for DAE in bile salts are the same as the values in cyclohexane. For NSP, Φ_{AB} is dependent on the structure of the bile salt and increases in the order NaTC < NaC < NaDC.

Table of Contents

List of Tables

List of Figures

List of Schemes

List of Abbreviations

A	colorless photochromic isomer
A	absorbance
a_i	pre-exponential factor for species i
B	colored photochromic isomer
CD	circular dichroism
cmc	critical micelle concentration
DAE	1,2-bis(2,4-dimethyl-5-phenyl-3-thienyl)-3,3,4,4,5,5-hexafluoro-1-cyclopentene
DAE_a	colorless isomer of DAE
DAE_b	colored isomer of DAE
DTAB	dodecyltrimethylammonium bromide
E_a	activation energy
ε	molar absorptivity coefficients
HPLC	high performance liquid chromatography
I_0	initial intensity
$I_{\mathbf{A}}^{\mathrm{Abs}}$	amount of light absorbed by **A**
K	Kelvin
K	equilibrium constant
k_2	decomposition rate constant
k_{obs1}	dark reaction rate constant
l	pathlength
M	molar
min	minute
mL	milliliter
mm	millimeter
NaC	sodium cholate
NaCl	sodium chloride
NaDC	sodium deoxycholate
NaTC	sodium taurocholate

nm	nanometer
NMR	nuclear magnetic resonance
NSP	1’,3’,3’-trimethyl-6-nitrospiro[2H-1]-benzopyran-2,2’-indoline
NSP_a	colorless isomer of NSP
NSP_b	colored isomer of NSP
^{o}C	degree Celsius
s	second
t	time
$\Delta H^{\ddagger}$	enthalpy of activation
$\Delta S^{\ddagger}$	entropy of activation
λ	wavelength
μM	micromolar
Φ_{AB}	quantum yield for the transformation of B into A
Φ_{AB}	quantum yield for the transformation of A into B

Acknowledgments

First of all, I would like to thank my supervisor Cornelia Bohne for the opportunity of being part of her research group and for being helpful in all the stages of the project;

I would like to thank Luis Netter for the assistance with equipments and for the help when I moved to Victoria;

I would like to thank Kentaro Morimitsu for the suggestions on the project;

I would like to thank Luise Wolf for reading the thesis and correcting the English;

I would like to thank Joanne Moszynski for the support and for the help with the HPLC;

I would like to thank Allyson Miller for the help with NSP experiments;

I would like to thank my supervisory committee for the suggestions on the project and on other aspects of grad school;

I would like to thank all my colleagues in the lab for their help and support, specially my friends: Allyson, Denis, Hao, Jason, Tamara, Yiyi and Xu;

I would like to thank my dear friend Michele from Brazil for being so patient and always helping me on my decisions;

I would like to thank my family for the unlimited support;

I would like to thank André, for his love, patience and for always encouraging me to pursue my dreams;

Finally, I would like to thank Xerox, NSERC and UVic for the financial support.

Dedication

To André

1 Introduction

1.1 Photochromism

Photochromism is the reversible photochemical transformation of a chemical species between its two isomers, A and B, which exhibit different absorption spectra.[1,2] The term "Photochromism" literally means "coloration by light", although it is known that this phenomenon may happen beyond the spectral range of visible light and applies to systems that absorb from the far UV to the IR.[1,3] In addition to the optical changes, other physicochemical properties undergo modification,[1,4] such as the refractive index, dielectric constant, oxidation/reduction potential, and geometrical structure.[4]

The first reports of photochromism date to the end of the 19th century and describe the change in color of some substances with daylight.[1,3] Nowadays, several families of compounds are known to exhibit photochromic properties, including spiropyrans, chromenes, fulgides and diarylethenes.[1]

In biological systems, photochromic proteins play a fundamental role in many processes, such as photosynthesis, photoperiodism and visual perception.[5,6] For instance, the initial process that later leads to the visual nervous impulse is the photochromic transformation of retinal from a 11-cis isomer to an all-trans configuration.[5]

1.2 Characteristics of Photochromic Systems

A photochromic reaction is reversible and light is required for one or both the forward and reverse reactions:

$$A \underset{h\upsilon_2 \text{ or } \Delta}{\overset{h\upsilon_1}{\rightleftharpoons}} B$$

The fundamental parameter that characterizes the photochemical path is the reaction's quantum yield. Consider isomer A in the ground state. After light is absorbed, an excited singlet or triplet state is formed. The excited molecule A* can either undergo a chemical transformation or be deactivated by internal conversion, intersystem crossing or fluorescence. The quantum yield is the fraction of absorbed photons that leads to a chemical transformation; a quantum yield close to 1 represents a highly effective system in which deactivation of the excited state is not significant.

Product B can be formed either in the ground or excited state. When there is a change between energy surfaces in the course of the reaction, B is formed in the ground state and the process is called diabatic. If the reaction happens on the same energy surface, B is formed in the excited state and the process is called adiabatic (Scheme 1.1).[7,8]

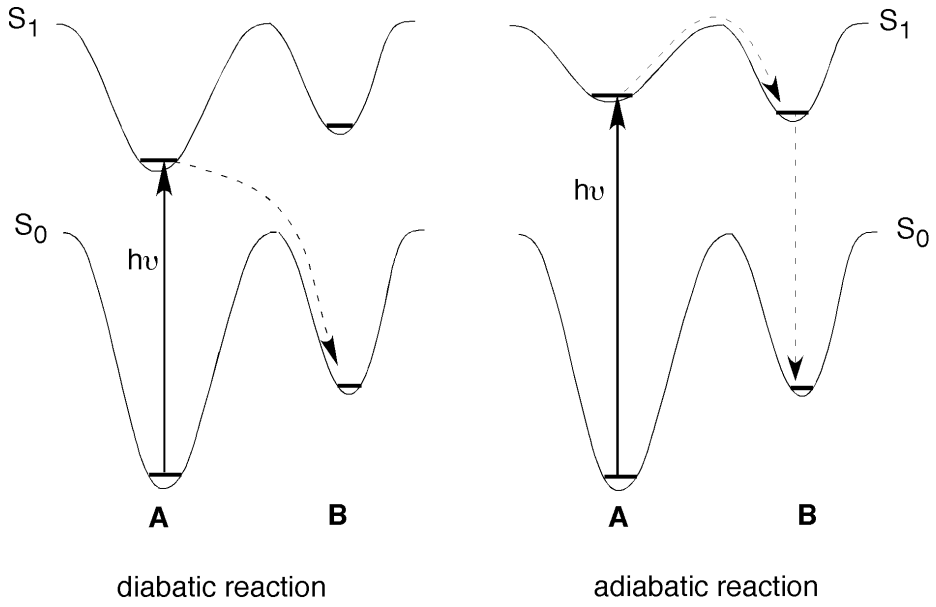

Scheme 1.1: Energy surface diagram for a diabatic and adiabatic photochemical transformation of A into B.

The quantum yield is related to the fate of the molecule after excitation, but gives no information about how efficiently the molecule absorbs the incident light. For this reason, another important parameter in the description of a photochromic system is the molar absorptivity of the species involved. The determination of both parameters is not trivial, since in many cases it is not possible to isolate the two isomers. Therefore, for the conversion of a colorless isomer into a colored one upon irradiation, a parameter called colorability ($A_0(\lambda)$) is commonly used. The colorability is the absorbance immediately after the reaction and is proportional to the quantum yield (Φ), the molar absorptivity coefficient of the colored isomer (ε_B) and the concentration of the colorless isomer (c_A). The light flux is included in the constant k.[1,9]

$$A_0(\lambda) = k\,\Phi\,\varepsilon_B\,c_A \qquad \mathbf{1}$$

The transformation of B into the thermodynamically stable isomer A can happen exclusively through a photochemical path or include a dark reaction. These two different types of reaction are called photochromism of type P and T, respectively. The majority of photochromic systems exhibit positive photochromism, which means the more stable isomer A is colorless or pale yellow and is transformed into the color isomer B upon irradiation. However, there are some systems that present negative photochromism described in the literature.[10-14] In these cases, the more stable isomer is colored and is formed spontaneously in the dark. The color is bleached by irradiation of UV or visible light. A few spiropyrans, especially those bearing free hydroxy, carboxy or amino groups, exhibit negative photochromism.[10] The phenomenon is related to the stabilization of the colored isomer, which is a zwitterionic merocyanine. This stabilization can also be achieved by using highly polar solvents, acidic medium[10,13] or by attaching the photochromic compound to nanoparticles.[12] In the case of negative photochromism induced by cadmium sulphide nanoparticles, the stabilization seems to be due the electrostatic interaction of the merocyanine ligand and the nanoparticle's defects.[12]

Decomposition reactions can happen concomitantly with the isomerization. This chemical degradation interferes with the photochromic activity and is called fatigue. The fatigue resistance of a photochromic compound is a measurement of how many isomerization cycles can be performed without significant decomposition. Side reactions can limit the use of a photochromic compound in many applications. The replacement of silver halides with organic photochromic molecules in the fabrication of photochromic ophthalmic lenses, for example, was possible after a indolinonaphthoxazine having a unique photostability was patented.[15]

Some photochromic compounds are also thermochromics. Thermochromism is a reversible change of color that is thermally induced. Spiropyrans and spirooxazines are examples of widely studied photochromic compounds that exhibit thermochromism.[1]

1.3 Photochromism of spiropyrans

The photochromic properties of spiropyrans were first reported by Fischer and Hirshberg in 1952.[16] They observed that the colored form of 1,3,3-trimethylindoline-2-spiro-6'-(2',3'-β-naphthopyran) could be obtained either through heating the solution or through irradiation at low temperature (Figure 1.1).

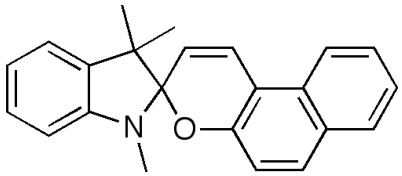

Figure 1.1: 1,3,3-trimethylindoline-2-spiro-6'-(2',3'-β-naphthopyran) whose photochromism was studied by Fischer and Hirshberg. [16]

Spiropyrans exhibit a photochromism of type T. When the closed-ring molecule is irradiated with UV light, a heterolytic cleavage of the bond between the oxygen and the spirocarbon occurs. The merocyanine formed has a series of conjugated double bonds, which shifts the absorption spectrum to the visible range. The reaction is reversible, and occurs either photochemically or in the dark. Many spiropyrans are also thermochromic, which means that a photobleached solution will become colored after ceasing the irradiation.[17-19] The compound studied and presented in this thesis, the 1',3',3'-trimethyl-6-nitrospiro[2H-1]-benzopyran-2,2'-indoline (NSP), has this characteristic (Scheme 1.2).

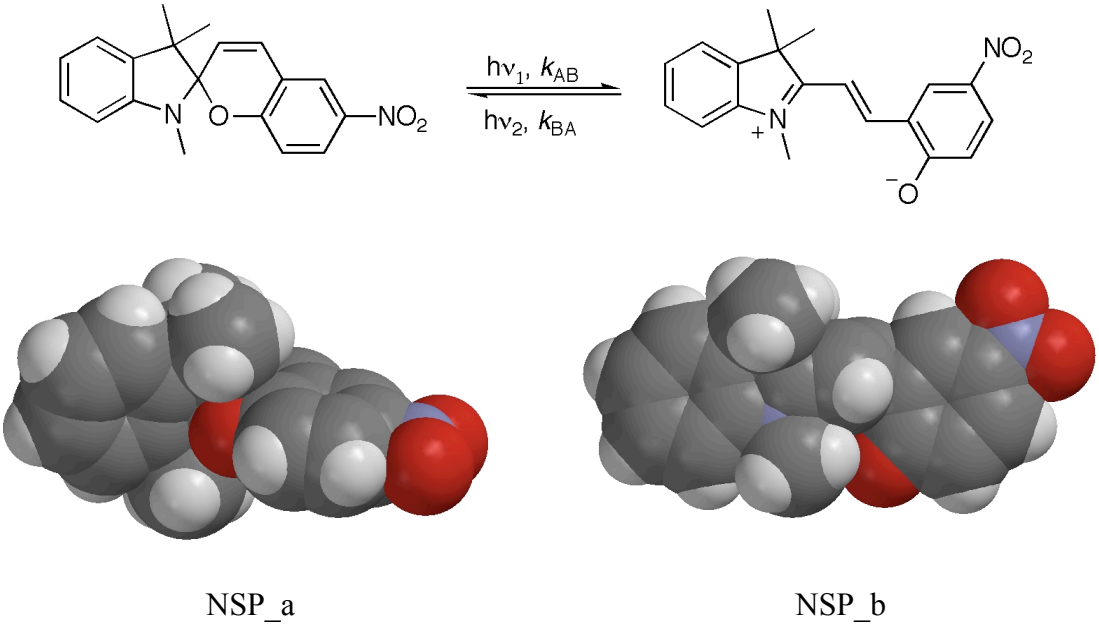

NSP_a NSP_b

Scheme 1.2: Photochromic and thermochromic reactions of NSP. Space-filling structures were created using SPARTAN'06 - Molecular mechanics, MMFF force field.

The thermal equilibrium between the colored and colorless isomers is largely affected by substituents on the pyran ring. The introduction of a nitro group in position 6 to give the compound shown in Scheme 1.2 causes an increase in the percentage of colored isomer at equilibrium from 3.0×10^{-5} % to 5.3×10^{-3} % in propanol at 0°C.[20] Also, the photocoloration quantum yield increases from 0.006 to 0.3 and the activation energy for the conversion of colored to colorless isomer increased from 17 kcal/mol to 22 kcal/mol.[20]

The spirocarbon in a spiropyran separates the molecule into two parts that are in an orthogonal position. When the C-O bond is broken the structure is rearranged in a planar geometry. The planarity is a requirement for conjugation. In fact, thermochromism is prevented in spiropyrans with hindered structure that precludes the formation of a

planar merocyanine. As an example, consider the two naphthospiropyrans **1a** and **2a** in Scheme 1.3. Thermochromism is only observed for **1a** because the formation of **2b** is inhibited due to steric requirements of the methyl group. [21]

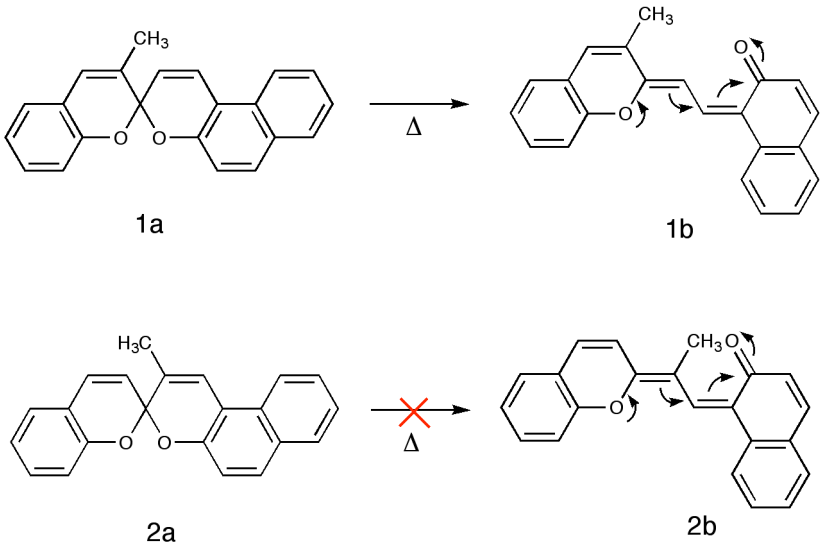

Scheme 1.3: Steric effects on the thermochromism of two naphthospiropyrans. Adapted from reference 21.

The colored product of spiropyrans can exist as an equilibrium of stereoisomers, as confirmed by several studies conducted at low temperature.[17,18,20,22] This equilibrium is reached in less than 10 ps after excitation for unsubstituted spiropyrans.[23] In principle, eight conformers having a quinoid or zwitterionic character are possible.[23] In polar solvent at ambient temperature the zwitterionic trans form of NSP_b (Scheme 1.2) is believed to be the most stable one.[24]

The UV irradiation of nitrosubstituted spiropyrans in nonpolar solvents can lead to the formation of aggregates containing the spiropyran A and the merocyanine B.[25] Krongauz et al.[26,27] reported the formation of AB dimers and A_nB (n = 2, 3) charge transfer complexes. The absorption spectra of the charge transfer complexes are red-

shifted 100 nm compared to the spectrum of the dimer. The relative amount of AB and A_nB species formed depends on the irradiation light intensity and temperature, since the formation of A_nB from AB and A has an activation energy of 5 kcal/mol. Larger aggregates containing more than 10^6 molecules are formed by the assembly of AB and A_nB. In their studies with polymers containing spiropyran units, Kalisky and Williams[28] observed that 100 μs after the laser pulse the transition absorption spectrum of the sample had bands from 500 nm to 700 nm. Absorption of B was assigned to the band at around 560 nm, AB around 600 nm and $(AB)_n$ or $(A_mB)_n$ at longer wavelengths.

The irradiation of NSP_a for long periods (>30 min) led to the precipitation of crystals with sizes ranging from 10 – 100 μm. [29,30] Raman spectroscopy suggested that the crystals formed are constituted by transoid merocyanine and the nitro group plays a fundamental role on the aggregation process. In contrast to merocyanine in solution, crystal-bound merocyanine is a long-lived species that remains unchanged in a dark environment for several days.

Interest in studying spiropyrans greatly increased after Hirshberg[31] described a system in which the color could be cyclically generated and erased by irradiation of monochromatic UV and visible light. He proposed that such a system could be used as a model to build a photochemical memory.

The photochromism of spiropyrans have been studied in supramolecular systems. In aqueous solutions of dodecyltrimethylammonium bromide (DTAB), NSP_a is solubilized when the concentration of surfactant is higher than the critical micelle concentration (cmc).[32] The presence of NaBr in solution causes a significant increase in the solubilization power of DTAB. This is attributed to the formation of rod-like

micelles, which are larger than the spherical micelles that are present in the absence of NaBr. NSP_a exhibits thermochromism in aqueous solution of DTAB, with an amount of colored isomer around 6% at equilibrium. Furthermore, a decrease in the cmc of DTAB was observed in the presence of NSP, possibly due to electrostatic interaction between the cationic DTAB micelles and the phenolate from NSP_b.

Cyclodextrins are supramolecular host systems constituted by glucose units linked to form a ring. Depending on the number of glucose units, the cyclodextrin is named as α (6 units), β (7 units) or γ (8 units). NSP_a forms inclusion complexes with γ-cyclodextrin that are insoluble in water.[33] In solid phase, the complex presents a high photochromic activity compared to NSP_a in the crystalline state. Given the same irradiation source, the coloration and decoloration that follow irradiation with UV and visible light are much faster for NSP_a bound to γ-cyclodextrin. For a water soluble derivative of NSP_a that has a sulfonate replacing the nitro group, the presence of β-cyclodextrin causes a shift in the equilibrium between colored and colorless isomer. After the addition of β-cyclodextrin, the absorbance at 510 nm decreases following first order kinetics, which indicates a decrease in the concentration of merocyanine in solution. The alcohol 1-adamantanol forms a very stable complex with β-cyclodextrin. The addition of 1-adamantanol to the solution increases the peak at 510 nm as the spiropyran is excluded from the cavity and the previous equilibrium is restored.

Zhou et al.[34] synthesized a derivative of NSP_a that contains a long alkyl chain. Although usually insoluble in water, the long hydrophobic chain can bind to β-cyclodextrin to form a soluble complex. Interestingly, when the sample is irradiated with UV light the produced merocyanine forms dimers with another merocyanine molecule

(Scheme 1.4). This behaviour contrasts with observations in homogeneous media, where the dimers are formed by a colored and a colorless isomer. The evidence for this mechanism is the thermal decoloration, which follows half-order kinetics.

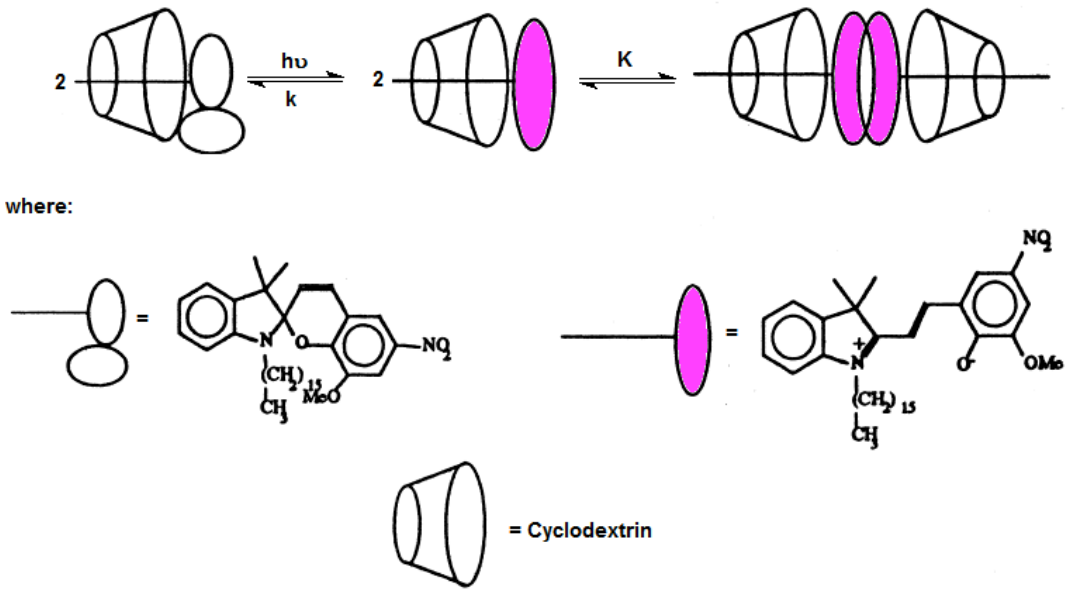

Scheme 1.4: Formation of dimer between complexes of nitrospiropyran and cyclodextrin. Adapted from reference 34.

1.4 Photochromism of diarylethenes

Diarylethene is the generic name of a molecule containing an aryl substituent on each carbon of an ethene unit. The photochemistry of the simplest diarylethene, stilbene, has been extensively studied and reviewed.[35-37] Upon irradiation, stilbene can undergo cis-trans isomerization or be transformed into phenanthrene by an oxidation process.[38-40] The cis isomer can also undergo a reversible cyclization; this reaction is the basis for the photochromic properties of diarylethenes (Scheme 1.5).

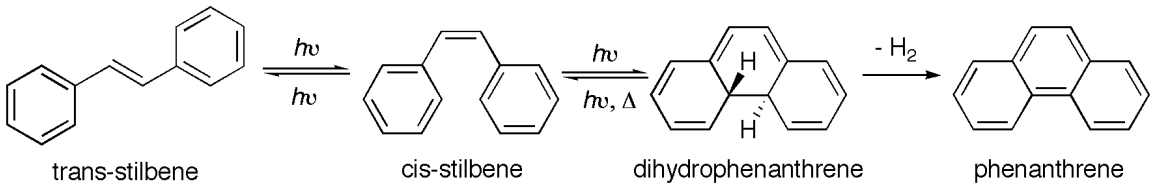

Scheme 1.5: Stilbene isomerization and oxidation reactions.

The thermal instability of the closed-ring isomer of most diarylethenes limits the use of these compounds in applications such as optical data storage media. In 1988, Irie and Mohri described the synthesis of a series of thermally stable and fatigue-resistant diarylethenes.[41] The structure of these compounds can be rationalized in three features (Figure 1.2, a): the presence of a heteroatom in the aryl group (X), the substituents in the ethene unit (R_1) and the substituents on the aryl group (R_2 and R_3).

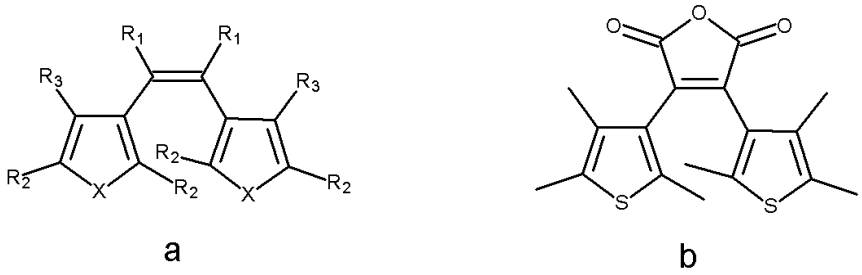

Figure 1.2: Thermally stable and fatigue resistant diarylethenes synthesized by Irie and Mohri.[41]

The inclusion of heterocyclic groups in the molecule was designed based on the reported thermal stability of 1,2-di(thienyl)ethenes.[42] Compared to a compound with X = S and R_1=R_2=R_3=H, the presence of CH_3 in R_2 leads to stabilization regarding the oxidation reaction. When R_3 is replaced by a cyano group, the absorption maximum of the closed-ring isomer is shifted to a longer wavelength. A further bathochromic shift in the absorption spectra and a better fatigue resistance was obtained for the acidic

anhydride derivative (Figure 1.2, b). As for the thermal stability towards the ring-opening reaction (cycloreversion reaction), all derivatives remained stable in the dark for more than 12 h at 80 ^{o}C. This increase in stability compared with phenyl derivatives is due to the difference in the ground state energy of these compounds. The heterocycles have smaller aromatic stabilization energy, which raises the activation energy for the cycloreversion according to calculations of state correlation diagrams.[43]

The introduction of electron-donating substituents in diarylperfluorocyclopentene derivatives provides compounds with higher molar absorptivity coefficients (ε) and lower ring-opening quantum yields. One of these derivatives, 1,2-bis(2,4-dimethyl-5-phenyl-3-thienyl)-3,3,4,4,5,5-hexafluoro-1-cyclopentene (DAE), was studied in the project presented in this thesis (Scheme 1.6). The absorption maximum for the closed-ring isomer in hexane is 562 nm with ε value of 1.1×10^4 cm^{-1} M^{-1}, and quantum yields of ring closing and opening equal to 0.46 and 0.015, respectively.[44]

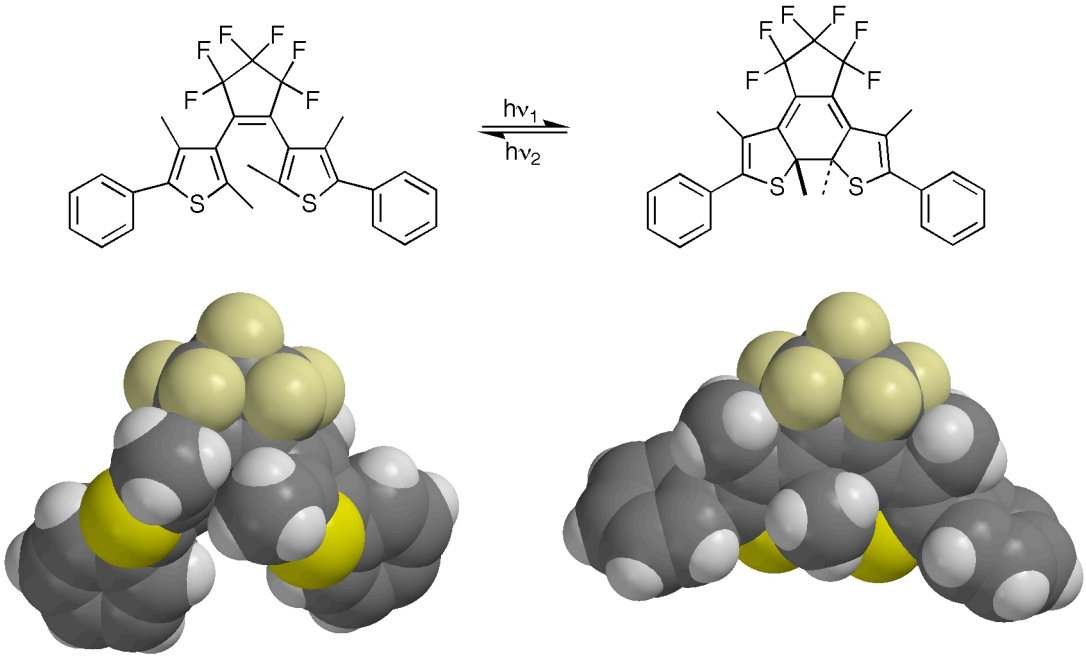

DAE_a DAE_b

Scheme 1.6: Photochromic reaction of 1,2-bis(2,4-dimethyl-5-phenyl-3-thienyl)-3,3,4,4,5,5-hexafluoro-1-cyclopentene. Space-filling structures were created using SPARTAN'06 Molecular mechanics, MMFF force field.

The quantum yield obtained for the formation of the colored isomer, 0.46, is close to the maximum expected for diarylperfluorocyclopentenes, which is 0.50. A maximum quantum yield smaller than 1 is expected because two conformers are in equilibrium in solution. The photochemical reaction is allowed for the conformer in the conrotatory mode, with the two aryl rings in a C_2 symmetry.[43,44] The ratio between the two conformers in hexane is 1:1 as estimated by NMR measurements.[44]

An interesting gated photochromic system involving a diarylethene was proposed by Irie et al. in 1992.[45] The photochromic activity of the molecule can be switched on and off in the presence of ethanol but is completely extinguished in cyclohexane. The formation of intramolecular hydrogen bonds in cyclohexane keeps the molecule in a

parallel configuration and does not allow a conrotatory cyclization, which explains this phenomenon (Scheme 1.7).

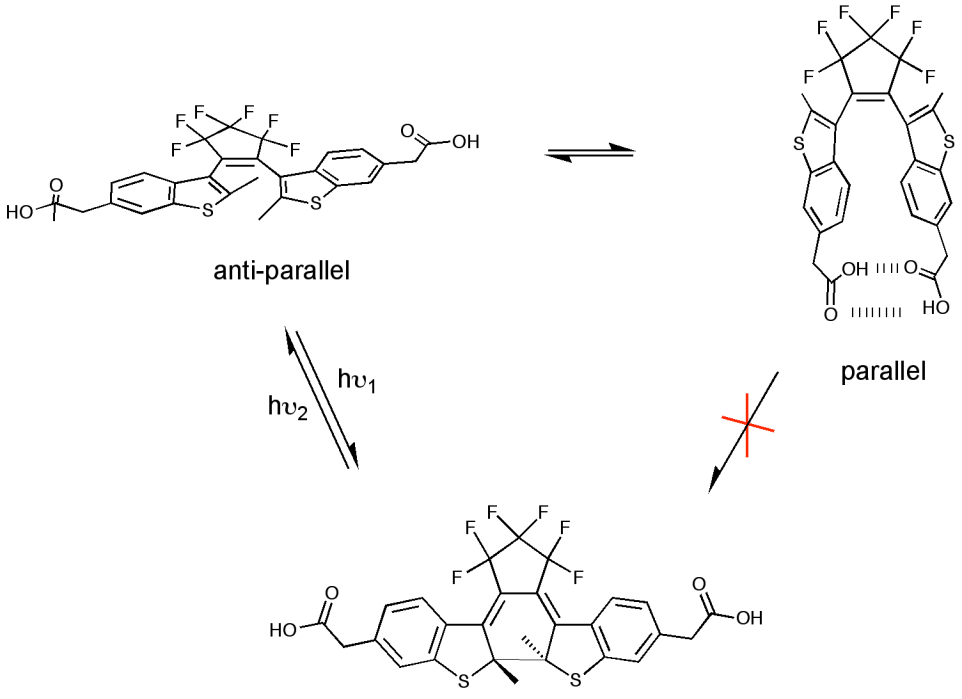

Scheme 1.7: Example of a gated photochromic system. Adapted from reference 45.

The photocoloration of some diarylethenes was studied in aqueous solutions containing β-cyclodextrin (Figure 1.3).[46,47,48] The ^{1}H-NMR spectra of these solutions shows that the presence of β-cyclodextrin increases the anti-parallel configuration. Consequently, the photocoloration quantum yield increased by a factor of 1.5. The complexation with β-cyclodextrin also induces circular dichroism (CD).[47] The signal of the CD spectrum changes from negative to positive when the samples are irradiated at 313 nm. The reason for this change is that when the compound isomerizes there is a change in the transition moment of the chromophore inside the β-cyclodextrin cavity. Calculations of transition moment confirmed this interpretation.

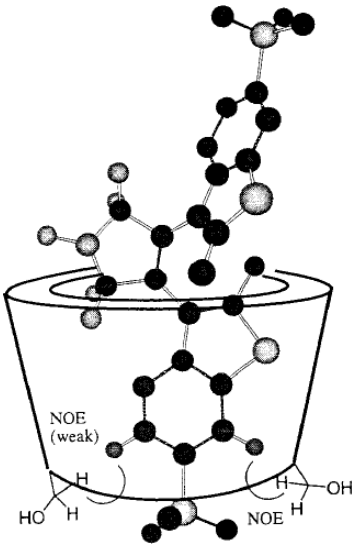

Figure 1.3: Proposed structure of a complex of Sodium 2,2'-Dimethyl-3,3'-(perfluorocyclopentene-1,2-diyl)bis(benzo[*b*]thiophene-6-sulfonate) and β-cyclodextrin. Reprinted with permission from reference 47. Copyright 1998, American Chemical Society.

1.5 Bile Salt Aggregates

Bile salts are amphiphilic compounds present in vertebrates.[49] They are formed in the metabolism of cholesterol[49] and act as surfactants that allow the absorption of dietary lipids. Other biological functions include protection against bacteria[50,51] and solubilization of cholesterol in bile.[52] In humans, bile salts are stored in the gallbladder, where their concentration can be as high as 300 mM.[49]

The structure of bile salt molecules contains a saturated steroid nucleus attached to a polar head group. There are three six-membered rings (A, B and C) and one five-membered ring. One of the differences between the structure of bile salts and cholesterol is the double bond present in the steroid skeleton in the cholesterol molecule (Figure 1.4). This double bond makes the molecule flat. Bile salt molecules can also be flat or bent if

the rings A/B have a trans or cis configuration, respectively. It is interesting that flat bile salts are found in most primitive vertebrates but not in mammals.[49,53] The cis configuration provides much more efficient detergent properties, and for this reason was preferred in the evolutionary process.[53]

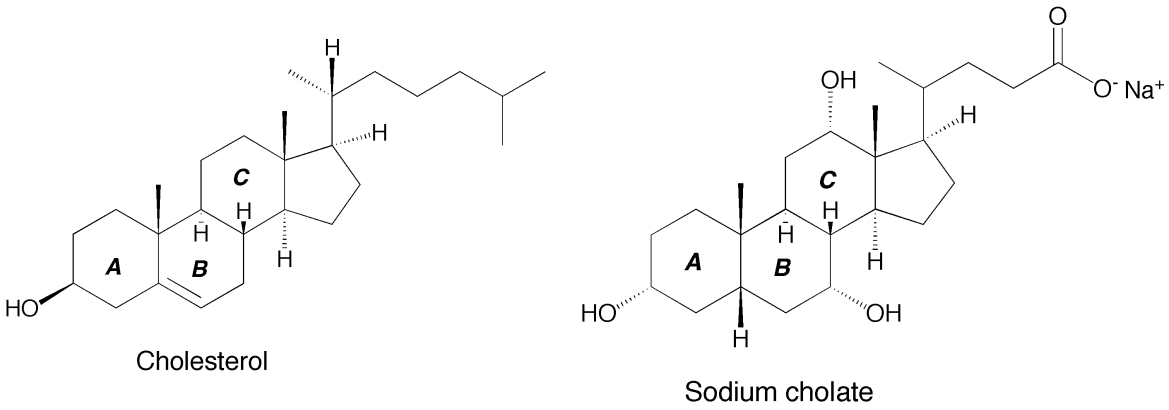

Figure 1.4: Structure of cholesterol and sodium cholate, one of the most common bile salts.

The bile salts studied in this project were sodium cholate (NaC), sodium deoxycholate (NaDC) and sodium taurocholate (NaTC) (Figure 1.5). The difference between these bile salts is the number of hydroxyl groups in the steroid nucleus and the head group.

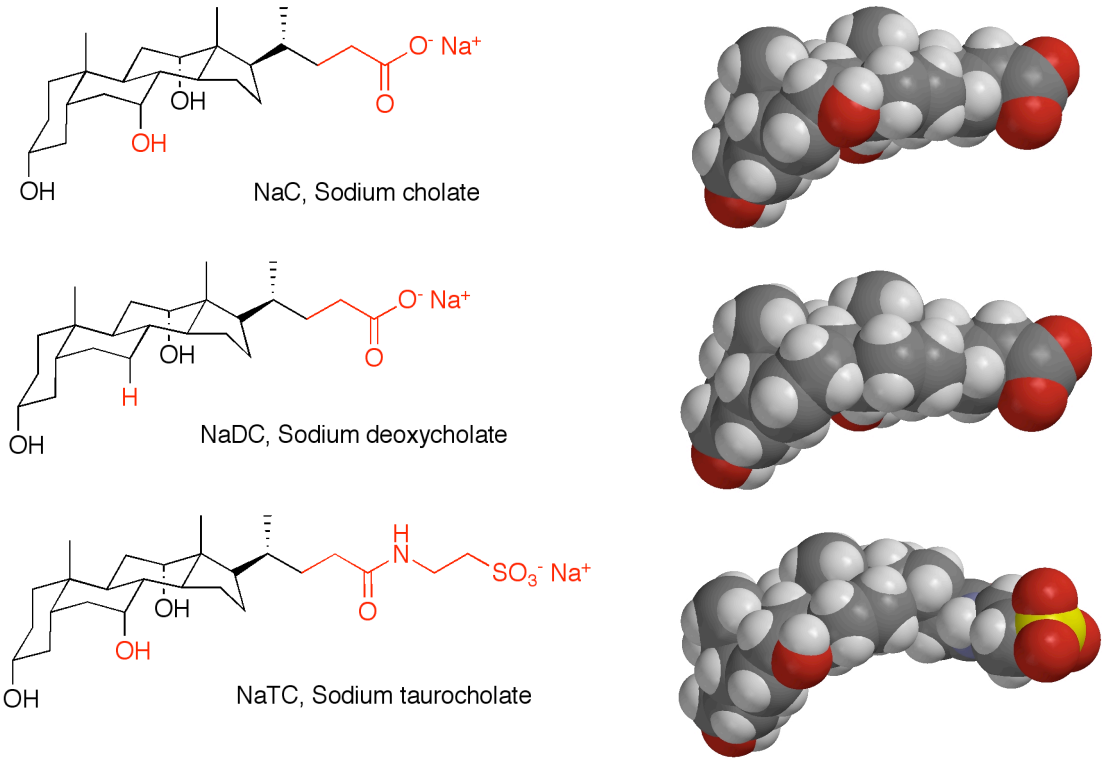

Figure 1.5: Structure of the bile salts employed in this project. Space-filling structures were created using SPARTAN'06 Molecular mechanics, MMFF force field.

The solubilizing properties of bile salts are due to the formation of aggregates in aqueous solutions. The formation of these aggregates is driven by the amphiphilic nature of bile salt molecules. The structure has a hydrophobic convex face, a polar head group and a concave face which is hydrophilic due to hydroxyl groups.[54]

Different models were proposed to explain the aggregation mechanism. Kawamura et al.[55] investigated a series of dihydroxy and trihydroxy bile salts with spin-label techniques, and suggested that only disk-like micelles are present in solution. Another strategy employed[56,57] was to explain the results obtained in solution based on the crystalline structure, which is helical. The hydrophobic faces are positioned at the outside of the helix and the stabilization of the aggregates in this case would be mainly by

polar interactions. This model, therefore, assumes that these polar interactions are strong enough to compensate the unfavorable interaction between the hydrophobic faces and water.[58]

The majority of the studies reveal that, unlike conventional micelles, the aggregation of bile salts does not happen at a specific concentration. Instead, the aggregation is a gradual process. O'Connor et al.[59] observed that the surface tension plots of bile salt solutions - sodium cholate, deoxycholate, chenodeoxycholate, dehydrocholate and lithocholate – exhibit discontinuities. This behavior was explained by a stepwise aggregation model. A similar model was also used to explain the conductance curves of aqueous solutions of bile salts and bile acids.[60]

The most accepted model is the primary/secondary aggregate model. This model, which is also confirmed by studies performed in Bohne's research group,[61-64] was first proposed by Small et al.[54] In the first step, at moderate monomer concentrations (10^{-4} – 10^{-3} mol/L),[59] small aggregates containing up to 10 monomers are formed through hydrophobic interactions of the convex faces. When the concentration of bile salt is increased, these primary aggregates self associate by hydrogen bonds to form bigger structures called secondary aggregates. The size of the aggregates continuously increases with the concentration of monomer and are polydisperse. [65]

Supramolecular systems, such as those composed by cyclodextrin and a guest molecule, commonly have their structure and the interactions of the host-guest system very well characterized. [66-68] For bile salts, this information has not been reported for any system yet. Therefore, the description of the environment inside bile salt aggregates is usually made based on more general terms, such as the polarity of the environment

instead of being based on specific host-guest interactions.[64] Bile salts aggregates are adaptable to the structure of the probe. The location of a molecule in an aqueous bile salt solution will depend on the polarity of this molecule. The primary aggregates have a hydrophobic environment and therefore bind to more hydrophobic molecules. More polar molecules, like the ones containing hydroxyl groups, bind to secondary aggregates.[62,63] Compared with guest molecules located in secondary aggregates, compounds bound to primary aggregates have a longer residence time and are more protected against quenching.[62] The shape of the guest molecule influences the efficiency of this protection, which is larger for smaller and more symmetrical molecules.[61] All these studies suggest that investigations using only one fluorescent probe give limited information about the characteristics of bile salt aggregates, and that all measurements refer to a specific guest-aggregate complex, not to the aggregates themselves.[64] In Figure 1.6, the concave face of the bile salt molecules are shown in blue and the negatively charged head groups in red.

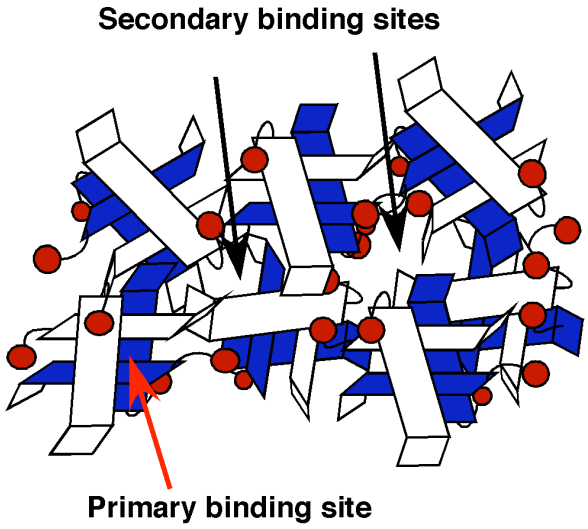

Figure 1.6: Cartoon representation of bile salt aggregates in aqueous solution. Reprinted with permission from reference [69]. Copyright 2006, American Chemical Society.

The structure of the bile salt monomer, like the number and position of hydroxyl groups, affects the properties of the aggregates. Aggregation happens at a lower concentration if the molecule has less -OH groups, as concluded in earlier studies with solubilization of fluorescence probes[70] and surface tension measurements.[71] The aggregates are less affected by the nature of the head group, as can be inferred by quenching experiments.[64] The presence of salts in solution decreases the concentration in which the primary aggregates are formed, but does not affect the formation of secondary aggregates.[62]

The term "critical micellar concentration", although extensively used in the literature, should be avoided since the aggregation process is gradual over a broad range of concentrations. Roda et al.[71] suggest that the term "noncritical multimer concentration" would be more appropriate.

1.6 Thesis objectives

Bile salt aggregates are interesting supramolecular systems with a structure that is adaptable to the guest molecule.[61,64] This feature provides the solubilization of hydrophobic organic compounds in aqueous solution. Such compounds can then be used in different media without synthesizing water-soluble derivatives. Unlike conventional micelles, bile salts do not have a critical micelle concentration. Instead, the aggregates are continuously modified with the increase in monomer concentration. At high concentrations two binding sites are found. The result is a more sophisticated host system that can be optimized for each application.

Photochromic systems have been employed in several applications such as ophtalmological lenses,[15,72] data storage[73,74] and photoswitchable biomaterials.[75] The objective of this thesis is to study photochromic compounds in aqueous solutions containing bile salts. This investigation can impact technological applications that require aqueous media, since the two photochromic compounds studied – NSP and DAE – are commercially available but insoluble in water. This study also aims to explore bile salt aggregates as nanoreactors, a feature that has not been largely investigated in the supramolecular field.

The main parameter of a photochromic system is the quantum yield. Given that methods to determine this parameter in photochromic reactions are still a matter of investigation, the first specific objective of this thesis is to develop a methodology to determine the quantum yield. The second specific objective is to use this method to investigate the effect of different bile salts and different NaCl concentrations on the quantum yields of forward and backward reactions of DAE and NSP.

The isomerization of NSP also happens through a dark reaction. The third specific objective of this thesis is to verify the effect of bile salt concentration and structure, NaCl concentration and temperature on the dark reaction of NSP.

2 Experimental Section

2.1 Materials

Sodium chloride, (NaCl, ACP, ≥ 99.0%), sodium cholate hydrate, (NaC, Aldrich, 98%), sodium deoxycholate (NaDC, Fluka, ≥ 98.0%), sodium taurocholate hydrate, (NaTC, Sigma, ≥ 97.0%), 1',3',3'-trimethyl-6-nitrospiro[2H-1]-benzopyran-2,2'-indoline, (NSP, TCI), 1,2-bis(2,4-dimethyl-5-phenyl-3-thienyl)-3,3,4,4,5,5-hexafluoro-1-cyclopentene), (DAE, TCI), potassium oxalate monohydrate, (Sigma, ≥ 99%), ferric chloride, (Fisher Scientific), 1,10-phenanthroline monohydrate, (Aldrich, 99%), sulphuric acid (Caledon, ≥ 95.0%), sodium acetate, (NaAc, BDH, ≥ 98%), anhydrous ethyl alcohol, (Commercial Alcohols), hexane, (Caledon, spectro grade, ≥ 98.5%) methanol, (EMD, HPLC grade, ≥ 99.8%) and acetonitrile (EMD, HPLC grade, ≥ 99.8%) were used as received. Deionized water (≥ 17.8 MΩ cm^{-1}, Sybron Barnstead system) was employed for sample preparation.

2.2 Solutions of photochromic compounds

All aqueous solutions of photochromic compounds contained bile salt (NaC, NaDC or NaTC, 40 – 100 mM) and NaCl (0.030 M - 1.0 M) and were prepared the day prior to

the experiment to shake overnight. The photochromic compound was incorporated in the bile salt solution by injecting a stock solution made in acetonitrile (maximum final volume of acetonitrile was equal to 1 % of the final solution). On the day of the experiment, these solutions were heated at 50 ^{o}C for 30 min and left to cool before carrying out any measurements. This procedure was applied to dissolve any gel that could have formed after the long period of time that the bile salt solution was left stirring.[76]

Solutions in other solvents were prepared on the day they were used by either the dilution of the stock solution with the solvent or, in the cases when the solvent is immiscible with acetonitrile (e.g. hexane and cyclohexane), by evaporation of acetonitrile followed by addition of the required solvent.

2.3 Equipment

Absorption spectra were taken at room temperature using either a Varian Cary 100 or a Varian Cary 1 spectrophotometer. NSP dark reaction kinetics were followed using either a Varian Cary 100 or a Varian Cary 5 spectrophotometer containing a 6 × 6 cell holder attached to a water bath. A PTI Xe-arc lamp model A-1010B operating at 74 W was employed for irradiation and the excitation wavelength was selected with a monochromator. Different slit bandwidths were used. The temperature during irradiation was kept constant using a water bath attached to the cell holder. For the molar absorptivity experiments, a Hewlett Packard 1100 Series HPLC was employed with an Agilent Zorbax SB-C18 column (5 μm, 4.6×250 mm) and a photodiode array detector. The kinetics of photocoloration were followed using an Ocean Optics spectrophotometer (see section 5.1 for details).

2.4 NSP dark reaction

An aqueous solution of 50 μM NSP in the presence of bile salt (volume of 2.5 mL) was placed in a quartz 10 × 10 mm cell and irradiated at 338 nm for 10 min (slit bandwidths = 10 nm). The temperature during irradiation was kept the same as the temperature at which the kinetics were followed. Immediately following irradiation, absorbance of the sample was measured at 517 nm with 1 min intervals until the absorbance did not decrease significantly. Due to experimental limitation, no kinetics were followed for more than 30 h. In the same measurement, the absorbance of the blank (bile salt solution with no NSP) was registered to take into account small fluctuations in the spectrophotometer lamp. The data for the blank was subtracted from the data for the NSP solution and the kinetic curve obtained was initially fit to a sum of two exponentials (equation 2). In some cases k_2 was found to have a negative value. Since it is physically meaningless to have a negative rate constant, the curve was fit as one exponential function (equation 3, see chapter 4 for details).

$$A = a_1 e^{k_{obs1} t} + a_2 e^{k_2 t} \qquad 2$$

$$A = a_0 + a_1 e^{k_{obs1} t} \qquad 3$$

where:

A: absorbance;

a_1, a_2: pre-exponential factors;

a_0: absorbance when $t \rightarrow \infty$;

t: time;

k_{obs1}, k_2: reaction rate constants.

Another detail for the absorbance measurement is the position where the sample is placed in the cell holder. Cell holders with multiple sample positions are set to irradiate sample position 1 in downtime between measurements. This intermittent radiation can cause artifacts for determining the dark reaction rate constant; therefore the NSP sample was never placed in position 1. A possible artifact includes the photoreaction of NSP_b producing NSP_a, which would lead to higher dark reaction rate constants.

2.5 Determination of molar absorptivity coefficients

Described in details in section 3.1.

2.6 Photokinetic method

This method consists of following the formation of NSP_b or DAE_b while the sample is continuously irradiated with monochromatic light at the isosbestic point. During irradiation, the temperature of the sample was kept constant at 15 ^{o}C. The curves obtained were numerically fit using the software Scientist 3.0 from Micromath. Details about the procedure are given in section 5.1.

2.7 Actinometry with potassium ferrioxalate

2.7.1 Synthesis of potassium ferrioxalate

$K_3Fe(C_2O_4)_3.3H_2O$ was synthesized according to a procedure reported in the literature:[77] 100 mL of potassium oxalate 1.5 M was mixed with 33.3 mL of ferric chloride 1.5 M and the resulting solution vigorously stirred for 30 min. The resulting dark

green crystals were vacuum filtrated, recrystallized three times from hot water and dried on filter paper by aspiration for 10 min. The procedure was performed while protecting the solutions and crystals from ambient light.

2.7.2 General procedure

The procedure followed is reported in the literature:[77] the work solution of $K_3Fe(C_2O_4)_3.3H_2O$ 0.006 M was prepared by diluting the salt in $H_2SO_{4(aq)}$ 0.05 M. The ferrioxalate solution (2.5 mL) was placed in a 10 × 10 mm absorbance cell and irradiated for 3 minutes. This irradiation time was enough to reduce an amount of Fe^{3+} to Fe^{2+} suitable to be determined by absorption spectrophotometry after complexation with 1,10-phenanthroline. The irradiation wavelength and the monochromator slit bandwidth were the same as those set up to irradiate the photochromic compound in the photokinetic method. After the irradiation, 0.5 mL of a solution containing 0.1% w/v 1,10-phenanthroline in NaAc 1.8 M / H_2SO_4 0.54 M was added to the cell. The blank was prepared by repeating the procedure without irradiation. After 30 min, the absorption spectrum was registered and the absorbance at 510 nm (after subtraction of the absorbance of the blank) was used to determine the light flux of the lamp, I_0:

$$I_0 = \frac{A_{510}\mathrm{V}}{\varepsilon_{510}\, l \Phi \mathrm{t}} \qquad 4$$

where:

A_{510} : Absorbance at 510 nm;

V=3.0 10^{-3} L, final volume of the solution;

$\varepsilon_{510} = 1.11 \times 10^4$ L mol^{-1} cm^{-1};[78]

l = 1 cm, path length;

Φ: quantum yield at the irradiation wavelength, given in the literature [78];

t= irradiation time.

For all photocoloration experiments, the light flux was measured before and after collecting the kinetic trace and the average value was used for the fit of the kinetic traces. Solutions of potassium ferrioxalate were protected from ambient light during the procedure.

In order to verify if the irradiation lamp was stable during a whole photocoloration experiment, the intensity of the light was determined along 8 hours. The absorbance at 510 nm was plotted as a function of the irradiation time and, as expected for a stable lamp, a linear relationship was observed (Figure 2.1).

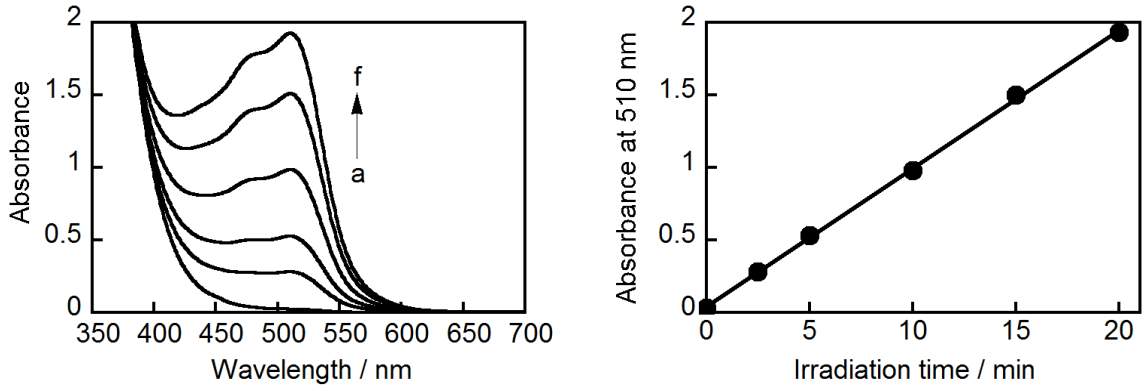

Figure 2.1: Actinometry with potassium ferrioxalate. **Left**: Absorption spectra of aqueous solutions of potassium ferrioxalate irradiated at 340 nm (slits bandwidth of 3 nm) followed by addition of 1,10- phenanthroline. Irradiation time: a) 0 min; b) 2.5 min; c) 5 min; d) 10 min; e) 15 min; f) 20 min. **Right**: Absorbance at 510 nm as a function of the irradiation time.

3 Molar Absorptivity Coefficients of DAE and NSP

Part of the material presented in this chapter has been published. Reproduced in part with permission from *Langmuir* (2014) **30**, 11319-11328. Copyright 2014 American Chemical Society.

3.1 Method development

The molar absorptivity coefficients (ε) of any compound in a given solvent can be determined if the absorption spectrum and the concentration of this compound in the solution is known. The isomers DAE_b and NSP_b can be obtained by irradiating the solution of DAE and NSP with UV light. However, a photostationary state is achieved and the final concentrations of DAE_b and NSP_b are unknown.

The methods to determine the values of ε for stable compounds like DAE_b usually involves the isolation of the colored isomer after chromatographic separation.[44,79 80]. The solution collected is then concentrated and the absorption spectra measured. This method cannot be used to determine the values of ε for unstable compounds like NSP_b because after isolation the dark reaction will lead to formation of NSP_a. Although possible, the values of ε for DAE_b in aqueous solutions containing bile salts are very difficult to be determined by isolating DAE_b. After separation in the HPLC column, the organic solvent from the mobile phase would have to be evaporated and the crystals redissolved in the bile salt solution. This step is problematic and the complete dissolution would probably only occur using a large volume of bile salt solution, which would result in a

solution of DAE_b too diluted to obtain precise values of absorbance. Another difficulty is that, after isolation, all the manipulation of the solutions has to be done in the dark. Therefore, a new method to determine the values of ε for DAE_b and NSP_b was developed during the presented project.

If the concentration of the colorless isomer NSP_a/DAE_a can be quantified in a sample, then the concentration of the colored isomer can also be determined since the total concentration of NSP or DAE in the sample is known. The concentration of NSP_a/DAE_a in a solution that also contains the colored isomer cannot be assessed by the absorption spectrum because it overlaps with the spectrum of NSP_b/DAE_b. Therefore, HPLC (high performance chromatography) was employed to separate and determine the concentration of NSP_a/DAE_b in a solution that had been irradiated with UV light and contains a mixture of isomers. HPLC is a technique used to separate compounds based on their interactions with a liquid mobile phase and a solid stationary phase. The HPLC column contains the stationary phase. The mobile phase is a solvent or mixture of solvents that is pumped through the column. The mixture of compounds is injected in the column and the individual compounds elute with different rates, which leads to separation. The detector is located after the column and can measure, for example, the absorbance of the sample. A chromatogram is a graph of the measured property as a function of time. As the compounds exit the column they can be isolated when a preparative HPLC method is used. [81]

The steps followed in the development of this method were: a) find the HPLC conditions that allow the separation of NSP_a from NSP_b and DAE_a from DAE_b; b) based on the area under the peak assigned as NSP_a and DAE_a, build a response curve

using solutions of known concentration of these isomers, **c**) evaluate any shortcoming in the procedure that could affect the accuracy of the molar absorptivity coefficients obtained, especially for the case of NSP which undergoes a dark reaction.

3.2 Molar absorptivity coefficients of DAE

In order to find the HPLC conditions to separate the isomers DAE_a and DAE_b, two samples (samples 1 and 2) of 2.5 mL of DAE 50 μM in hexane were irradiated at 285 nm (slit bandwidth = 3 nm) at 15 ^{o}C. The absorbance at 563 nm was recorded over time. Irradiation was interrupted after reaching the photostationary state (Figure 3.1, left). Hexane was chosen as the solvent in order to compare the values of ε obtained with the ones reported in the literature by Irie *et al.*[44] The irradiation conditions chosen were the same as a typical photokinetic experiment. The absorption spectra were registered before and after the irradiation (Figure 3.1, right).

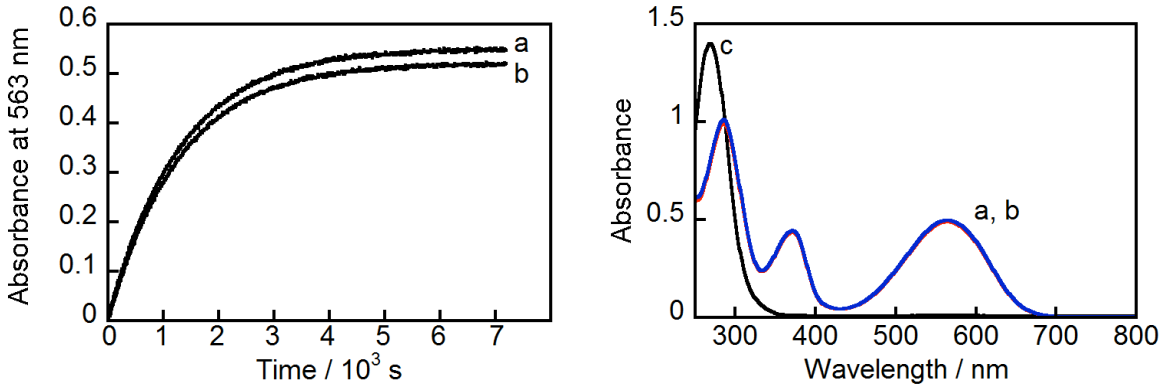

Figure 3.1: **Left**: Absorbance at 563 nm of sample 1 (a) and sample 2 (b) of DAE 50 μM in hexane during irradiation at 285 nm. **Right**: Absorption spectra of these samples before (c) and after irradiation (a – red and b - blue).

After collecting the absorption spectra, the samples were kept in the dark and put in HPLC vials covered with aluminum foil. The HPLC chromatogram was registered by injecting 8 µL of the sample and using detection wavelengths of 269 and 562 nm, the maximum in the absorption spectra of DAE_a and DAE_b respectively. The mobile phase with optimal peak separation for DAE_a and DAE_b was 30% acetonitrile/70% MeOH with a flow rate of 1.5 mL/min (Figure 3.2).

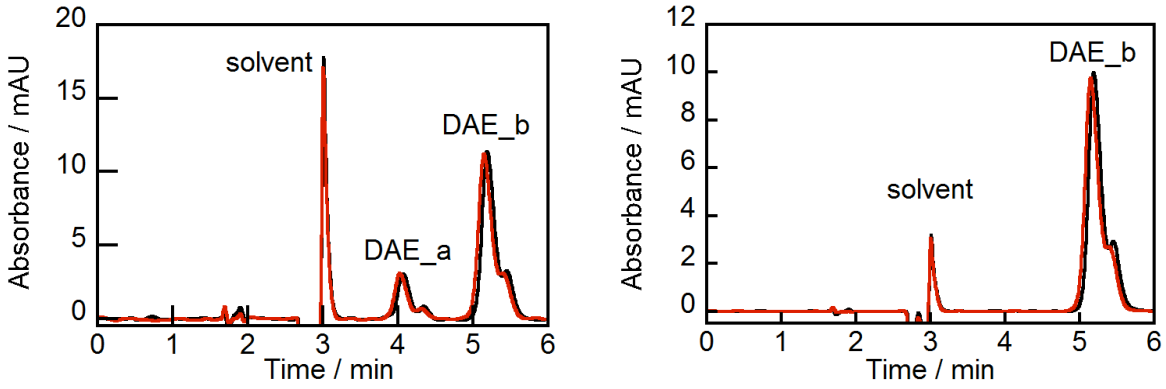

Figure 3.2: HPLC chromatogram of sample 1 (black) and sample 2 (red) of DAE 50 µM in hexane irradiated at 285 nm. Detection wavelength: 269 nm (right) and 562 nm (left); mobile phase: 30% acetonitrile/70% MeOH, flow = 1.5 mL/min, Agilent Zorbax SB-C18 column (5 µm, 4.6×250 mm).

Peaks in the chromatogram were assigned based on the absorption spectra registered during the chromatogram. For the detection wavelength of 269 nm, the absorption spectrum of the peak at 4.1 min (Figure 3.3, curve "a") is similar to the spectra of DAE_a (Figure 3.1, right, curve "c"). The spectrum of the peak at 5.2 min has an absorption maximum at 562 nm, which suggests it is due to the isomer DAE_b. For the chromatogram collected at 562 nm, only the peak at 5.2 min is observed, since only DAE_b absorbs at this wavelength (Figure 3.3, curve "b"). The peak assigned as "solvent" also appears in the chromatogram of the blank (hexane).

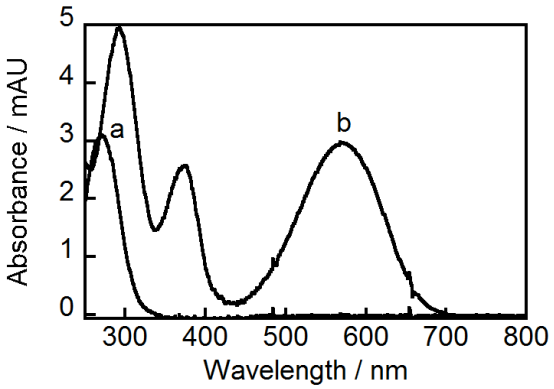

Figure 3.3: Absorption spectra for the peaks at 4.1 min (a) and 5.2 min (b) registered during the HPLC chromatogram presented in Figure 3.2.

Both the peaks of DAE_a and DAE_b in the chromatogram exhibit a shoulder or small second peak at longer time. This second peak was also detected when the solution of DAE was prepared in cyclohexane, but not when an aqueous solution of DAE containing bile salt was injected. The relative areas of the peak and the shoulder change in different mobile phases. These facts suggest that the presence of a shoulder is due to poor miscibility of hexane and cyclohexane in the mobile phase. The absorption spectra collected during the HPLC chromatogram shows that both the main peak and the shoulder belong to the same compound (Figure 3.4). For this reason, the area of the shoulder was taken into account in the calculations.

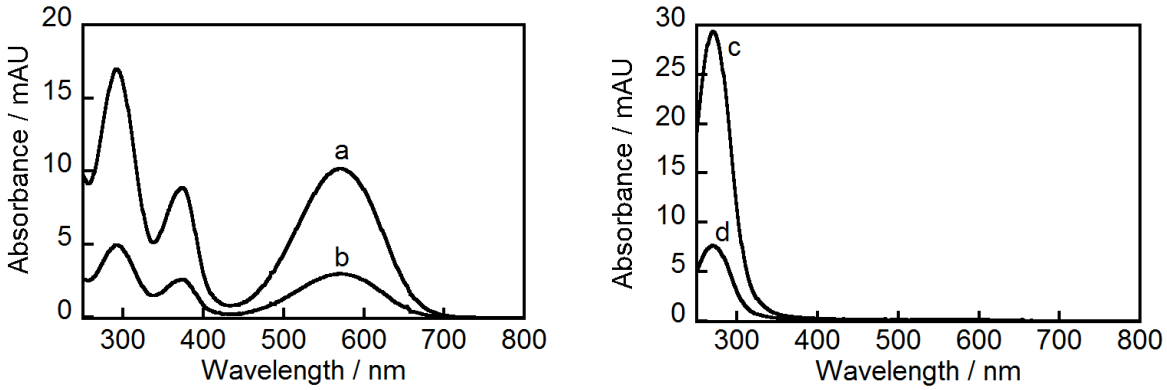

Figure 3.4: Absorption spectra registered during the HPLC chromatogram of DAE 50 μM in hexane irradiated at 285 nm. **Left**: peak at 5.2 min (a) and the shoulder at 5.4 min (b). **Right**: peak at 4.1 min (c) and the shoulder at 4.3 min (d).

In order to investigate possible decomposition of DAE when irradiated at 285 nm, sample 1 was exposed to ambient light after collecting the HPLC chromatogram shown in Figure 3.2 to convert all DAE_b into DAE_a. Subsequently, a new chromatogram was obtained for this colorless solution. This chromatogram was compared with the chromatogram of a sample of DAE 50 μM in hexane (sample 3) that was not irradiated with UV light (Figure 3.5). The area under the peak at 4.1 min is equal to 404 mAU*s for sample 1 and 405 mAU*s for sample 3. There is no other peak in the chromatogram that could be due to a decomposition product, which suggests that DAE does not undergo any other reaction other than the isomerization during the irradiation at 285 nm.

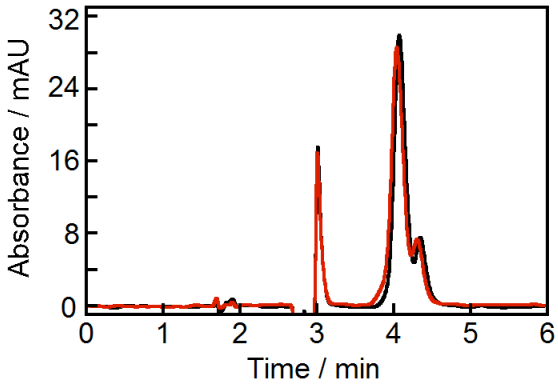

Figure 3.5: HPLC chromatogram of DAE 50 µM in hexane exposed to visible light, sample 3 (black) and sample 1 after irradiation at 285 nm followed by exposition to visible light (red). Detection wavelength: 269 nm; mobile phase: 30% acetonitrile/70% MeOH, flow = 1.5 mL/min, Agilent Zorbax SB-C18 column (5 µm, 4.6×250 mm).

Once ideal HPLC conditions to separate DAE_a and DAE_b were found, the area under the peak at 4.1 min was plotted as a function of the concentration of DAE_a to obtain an HPLC response curve. A solution of DAE 50 µM in hexane was prepared and exposed to ambient light to convert DAE to the colorless isomer DAE_a. The complete conversion was ensured by checking the absorbance of this sample at 562 nm, which was equal to zero. Since this absorption spectrum belongs to a solution of pure DAE_a that has a known concentration, the ε values for DAE_a were directly determined by dividing the spectrum by the concentration (Figure 3.6, left).

HPLC chromatograms were collected for solutions of DAE_a 25 µM and 5 µM in hexane. The sum of the area under the peak at 4.1 min and the shoulder centered at 4.3 min was plotted against the concentration of DAE_a in each sample, resulting in a linear relationship (Figure 3.6, right).

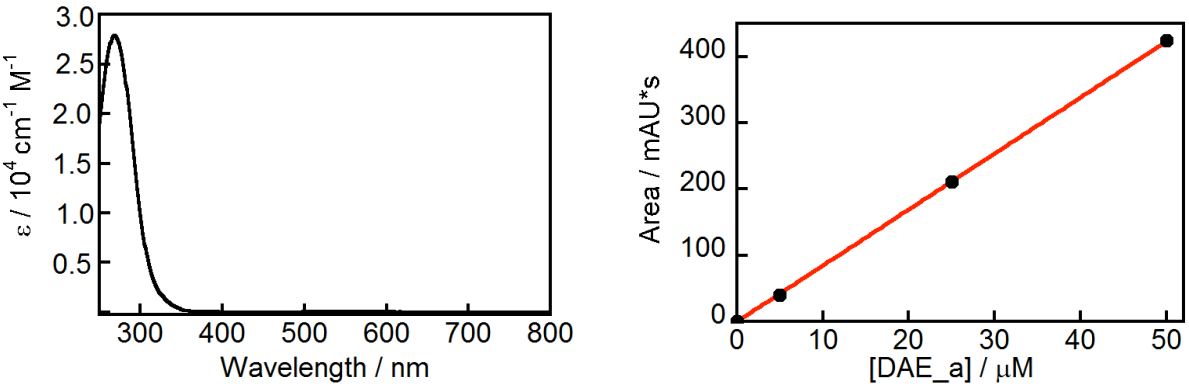

Figure 3.6: Left: Absorption spectra of DAE_a in hexane. Right: HPLC response curve of DAE_a in hexane; the linear fit was set to pass through zero and has a slope of 8.463; the correlation coefficient is 0.99996.

Although the experiments previously shown were performed with solutions in the photostationary state, this condition is not required for the method to work. The irradiated solution, though, must have an amount of DAE_b high enough to be detected by absorption and an amount of DAE_a high enough to be detected by HPLC, best achieved if the conversion is kept between 20% and 80%. In order to shorten the irradiation process, the slit bandwidth for the entrance of the monochromator was opened to 16 nm and kept equal to 3 nm at the exit. Using this set up, a suitable amount of DAE_b was formed in 2 min. After the irradiation, the absorption spectrum of the sample containing DAE 50 μM in hexane was collected (Figure 3.7, left). The sample was placed in a HPLC vial covered with aluminum foil to protect from ambient light and the chromatogram was registered (Figure 3.7, right).

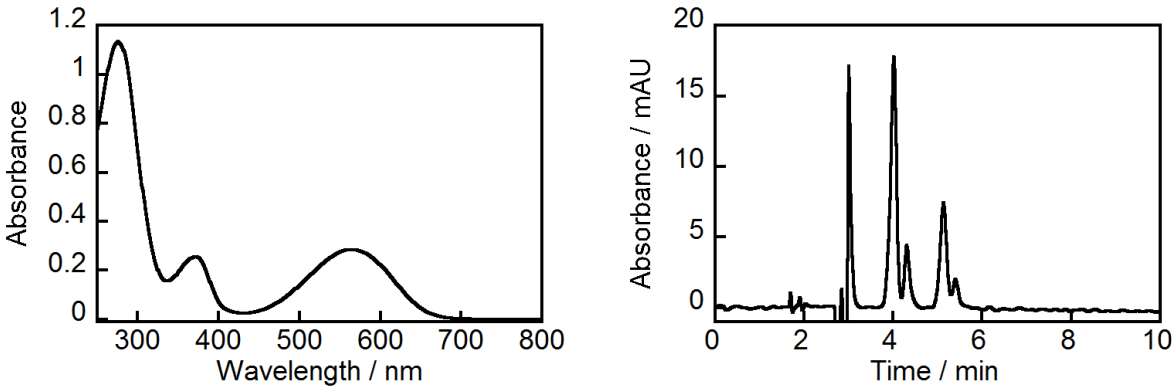

Figure 3.7: Absorption spectrum of DAE 50 μM in hexane irradiated at 287 nm (left) and its HPLC chromatogram (right).

The sum of the areas under the peak at 4.1 min and the peak at 4.3 min was 212.18 mAU×s. Based on the response curve in Figure 3.6, this area represents a concentration of DAE_a equal to 25.1 μM. Since the total concentration of DAE in the irradiated solution was 50.0 μM, the concentration of DAE_b must be equal to 24.9 μM. The absorption spectrum of the irradiated sample shown in Figure 3.7 is the sum of the spectra of DAE_a and DAE_b. The molar absorptivity coefficients of DAE_a in hexane have been previously determined (Figure 3.6), so the spectrum of a solution of DAE_a 25.1 μM can be calculated by multiplying ε by this concentration (Figure 3.8, left). If the calculated spectrum is subtracted from the spectrum of the irradiated sample, the result is the absorption spectrum of DAE_b 24.9 μM in hexane (Figure 3.8, right).

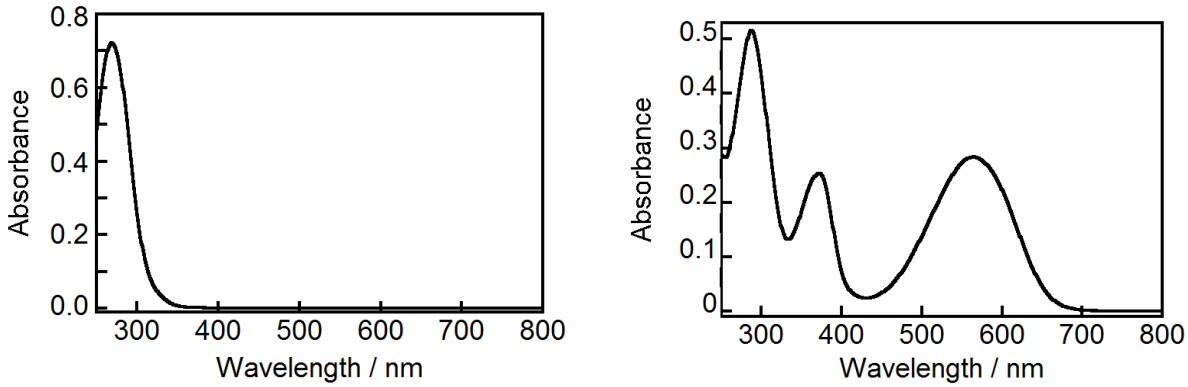

Figure 3.8: Calculated absorption spectra of DAE_a 25.1 µM (left) and DAE_b 24.9 µM (right) in hexane.

The ε values of DAE_b can be obtained by dividing the absorption spectrum in Figure 3.8, right, by 24.9 µM. At 562 nm, the ε value was found to be equal to (1.11 ± 0.03) × 10^4 cm^{-1} M^{-1} (Figure 3.9). The value reported in the literature is 1.1 × 10^4 cm^{-1} M^{-1}.[44]

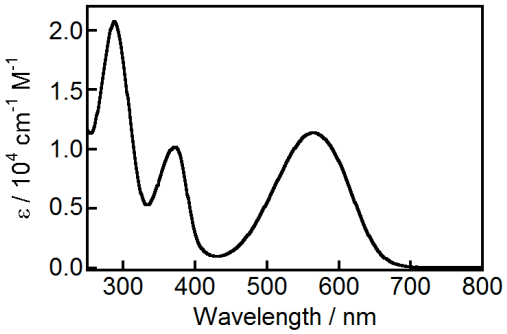

Figure 3.9: Absorption spectrum of DAE_b in hexane.

The experiment was repeated for solutions of DAE in NaC 80 mM/NaCl 0.2 M. The main concern about using this solution was that the salts could precipitate and clog the HPLC column. The damage was minimized by washing the column with methanol for at least 40 min after each experiment. The pressure in the column did not increase while

the experiments were performed, which indicates that the precipitation of salts was not significant.

With the detection wavelength at 269 nm, the HPLC chromatogram of an aqueous solution of DAE containing bile salt irradiated at 287 nm exhibits a sharp single peak at 5.4 min for the isomer DAE_b and another at 4.3 min for the isomer DAE_a. In all experiments the identity of the peaks were confirmed by the absorption spectrum registered during the chromatogram.

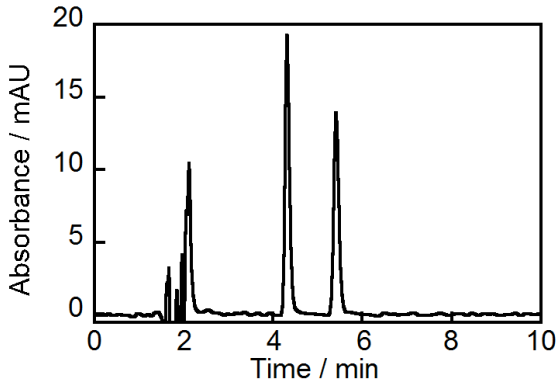

Figure 3.10: HPLC chromatogram of an aqueous solution of DAE 50 μM in NaC 80 mM/NaCl 0.2 M irradiated at 287 nm.

3.3 Molar absorptivity coefficients of NSP

The same strategy employed to develop a method to assess the ε values of DAE_b was applied in the case of NSP_b. The main challenge for experiments with NSP is the possibility of conversion of NSP_b into NSP_a inside the column, which would make isomer separation difficult.

An aqueous solution of NSP 50 μM in the presence of NaTC 80 mM/NaCl 0.2 M was exposed to ambient light. The absorption spectrum was collected and, since only

NSP_a was present, the ε values for this isomer were determined by dividing the absorbance by the total NSP concentration, 50.0 μM (Figure 3.11). An aliquot of this solution was irradiated at 338 nm and used to determine the best mobile phase to be employed in the HPLC.

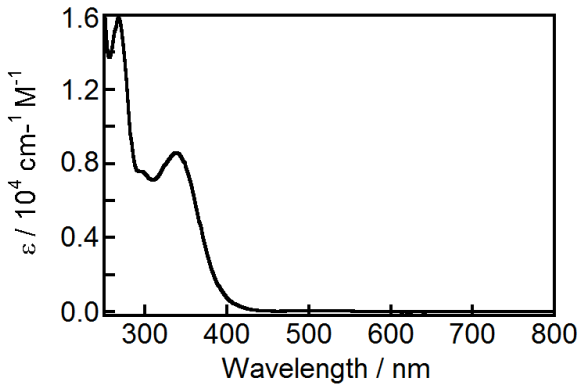

Figure 3.11: Absorption spectrum of NSP_a 50 μM in the presence of NaTC 80 mM/NaCl 0.2 M.

The best peak separation was observed for 20% water/80% MeOH with a flow rate of 1.2 mL/min. The wavelengths followed during the chromatogram were 338 nm and 517 nm, corresponding to the maximum absorption of NSP_a and NSP_b, respectively. For the signal at 338 nm, the HPLC chromatogram exhibits a broad peak at 3.1 min and a sharp peak at 12.8 min. For the signal at 517 nm there is a broad peak at 3.1 min (Figure 3.12).

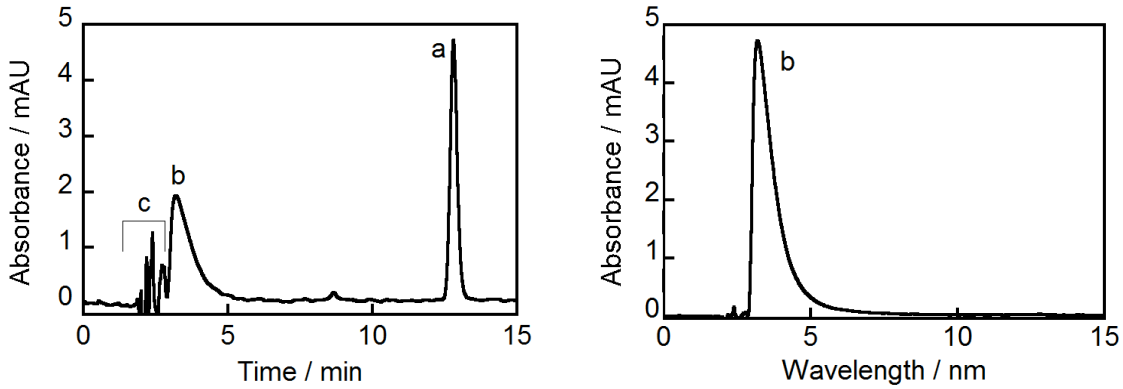

Figure 3.12: HPLC chromatogram of an aqueous solution of NSP 50 μM in the presence of NaTC 80 mM/NaCl 0.2 M irradiated with UV light. Signal at 338 nm (left) and 517 nm (right). a) peak assigned as NSP_a; b) peak assigned as NSP_b; c) peaks assigned as impurities in the bile salt.

The absorption spectra suggest that the peak at 3.1 min corresponds to NSP_b and the peak at 12.8 min corresponds to NSP_a (Figure 3.13, left). Other peaks are due to impurities in the bile salt and also appear in the chromatogram of the blank (Figure 3.13, right). Some of these impurities is fluorescent and have already been observed in previous studies.[82]

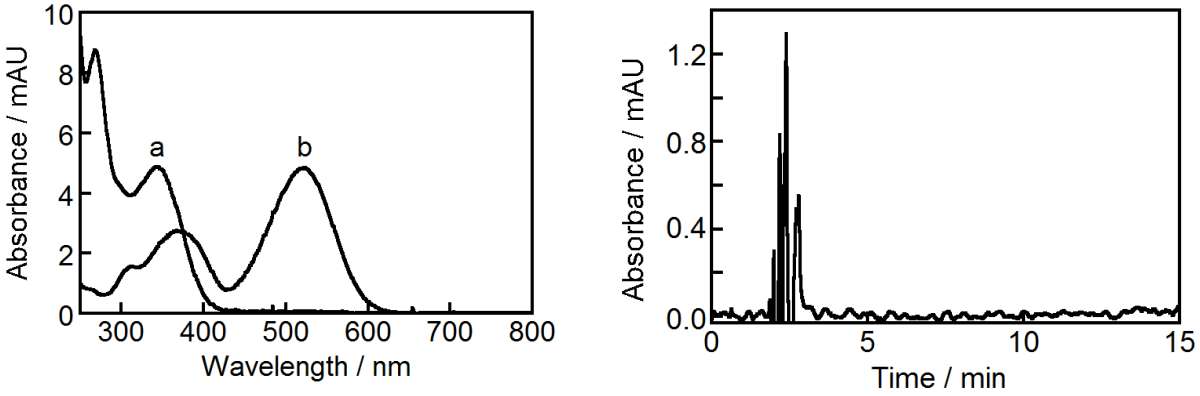

Figure 3.13: Left: Absorption spectra of the peaks at 12.8 min (a) and 3.1 min (b). Right: HPLC chromatogram of an aqueous solution of NaTC 80 mM/NaCl 0.2 M.

Once the conditions to perform the experiment were defined, another experiment was done to obtain a response curve. The chromatogram of four solutions of NSP containing only the isomer NSP_a (blank, 5.0 µM, 25 µM and 50 µM) was registered. The areas under the peak at 12.8 min and detection at 338 nm were used to plot a response curve (Figure 3.14).

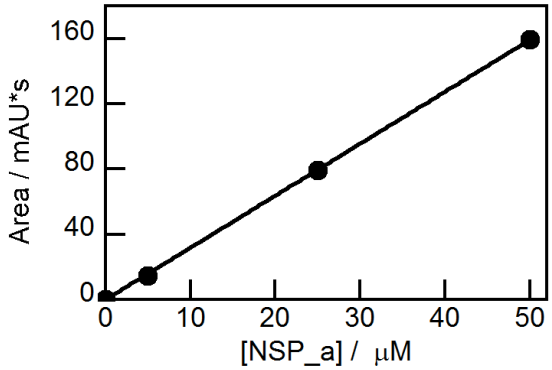

Figure 3.14: HPLC response curve of NSP_a in the presence of NaTC 80 mM/NaCl 0.2 M, signal at 338nm; the linear fit was set to pass through zero and has a slope of 3.19 with a correlation coefficient of 0.99995.

Immediately before collecting the chromatogram shown in Figure 3.12, the absorption spectrum of the solution of NSP irradiated at 338 nm was registered (Figure 3.15). For the signal at 338 nm, the peak at 12.8 min has an area equal to 80.60 mAU*s. Based on the response curve above, this area correspond to a concentration of NSP_a equal to 25.3 µM. The total concentration of NSP in the sample was 50.0 µM, thus the concentration of NSP_b was equal to 24.7 µM.

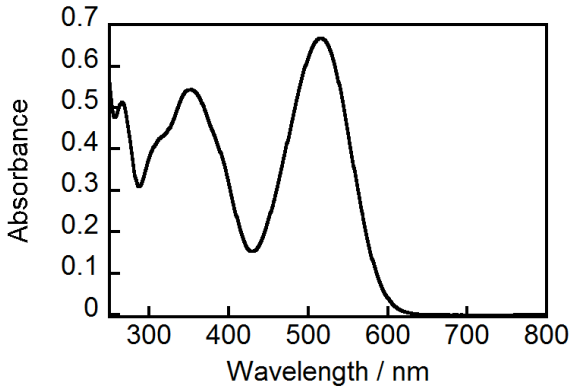

Figure 3.15: Absorption spectrum of NSP 50 µM in NaTC 80 mM/NaCl 0.2 M irradiated at 338 nm. The concentration of NSP_a was 25.3 µM and the concentration of NSP_b was is 24.7 µM.

The ε values of NSP_a are known (Figure 3.11), thus the absorption spectrum of NSP_a was obtained multiplying the ε values by 25.3 µM (Figure 3.16, a). The absorption spectrum of NSP_b at 24.7 µM was calculated by subtracting the spectrum of NSP_a at 25.3 µM from the spectrum of the irradiated sample (Figure 3.16, b).

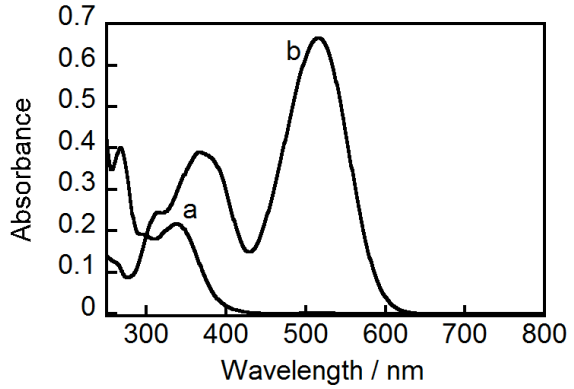

Figure 3.16: Calculated absorption spectra of NSP_a 25.30 µM (a) and NSP_b 24.70 µM (b) in NaTC 80 mM/NaCl 0.2 M.

The ε values of NSP_b were obtained dividing the spectrum b shown in Figure 3.16 by 24.7 µM (Figure 3.17).

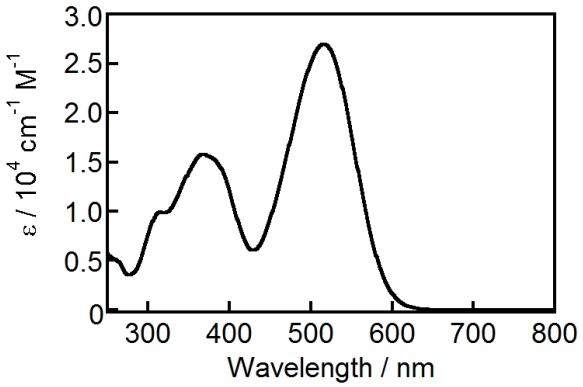

Figure 3.17: Absorption spectrum of NSP_b in NaTC 80 mM/NaCl 0.2 M.

The extension of the dark reaction of NSP during the experiment was investigated by performing control experiments. An aqueous solution of NSP 50 μM containing NaC 80 mM/NaCl 0.2 M at 10 ^{o}C was irradiated at 338 nm for 2 minutes. The absorption spectrum was collected and an aliquot of the solution was transferred to a covered HPLC vial. The remaining solution and the HPLC vial were kept in an ice bath. The HPLC chromatogram was registered 6 min after the spectrum was collected. During this run, the HPLC vial was kept in the ice bath and another chromatogram was registered after the first one, 22 min after the spectrum was taken. While the first chromatogram was running, a second absorption spectrum of the NSP solution remaining in the cell was collected (13 min after the first spectrum). This second spectrum was very similar to the first one (Figure 3.18, left) and for the two chromatograms collected the areas under the peak at 12.7 min are almost the same - 114.87 mAU*s for the first and 114.97 mAU*s for the second chromatogram (Figure 3.18, right). Based on these results, it is assumed that the dark reaction does not occur to a large extent during the time of the experiment if the solutions are maintained at low temperature.

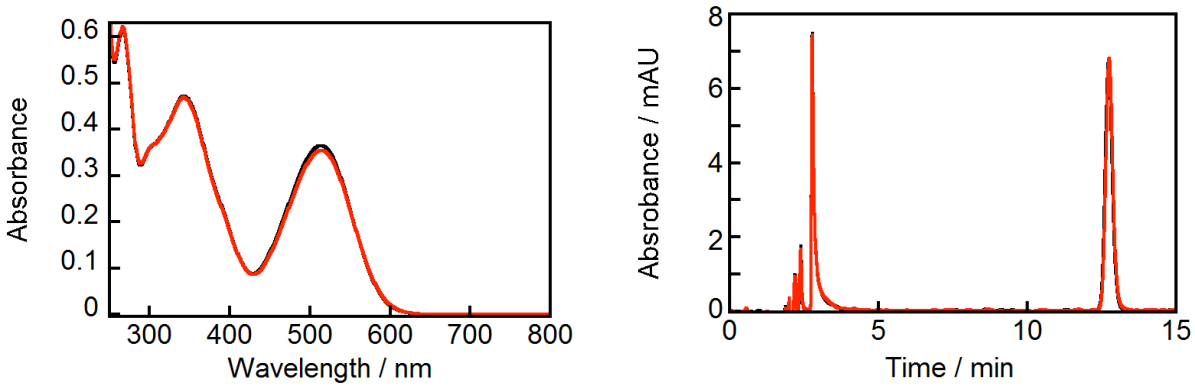

Figure 3.18: NSP 50 µM in NaC 80 mM/NaCl kept at low temperature: **Left**: Absorption spectra collected at time 0 min (black) and time 13 min (red) after the first spectrum; **Right**: HPLC chromatogram registered at time 6 min (black) and time 22 min (red) after the first spectrum.

For other experiments the solutions were kept in an ice bath for at least 15 min before the irradiation, irradiated at 338 nm for 2 min, the absorption spectrum was register, the solutions transferred to a covered HPLC vial and the chromatogram was collected as soon as was possible. For the irradiation, the slit bandwidth at the entrance of the monochromator was 16 nm and the slit bandwidth at the exit of the light was 3 nm.

The peaks for NSP_b have different positions (2.8 – 3.2 min) and shapes in different chromatograms (Figure 3.19). However, these peaks have the same absorption spectrum (Figure 3.20). It is possible that a partial conversion of NSP_b into NSP_a inside the column leads to broad peaks. However, this does not affect the determination of the ε values; the quantitative information is obtained from the peak for NSP_a, which is kinetically stable and has always the same shape and position (12.7 – 12.8 min). Furthermore, the peak of NSP_b did not overlap with the peak of NSP_a in any chromatogram.

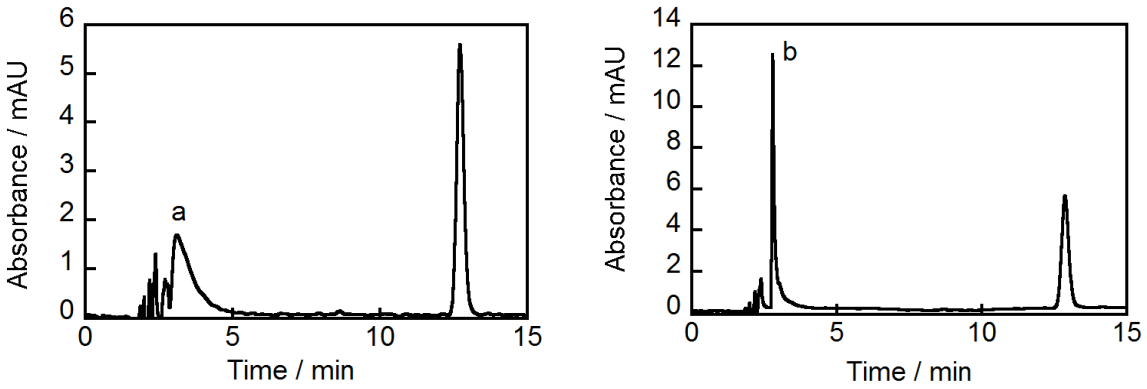

Figure 3.19: HPLC chromatogram of NSP 50 µM irradiated with UV light in NaTC 80 mM/NaCl 0.2 M (left) and NaC 80 mM/NaCl 0.2 M (right). The peaks identified as "a" at 3.1 min and "b" at 2.8 min are due to NSP_b. Signal at 338 nm.

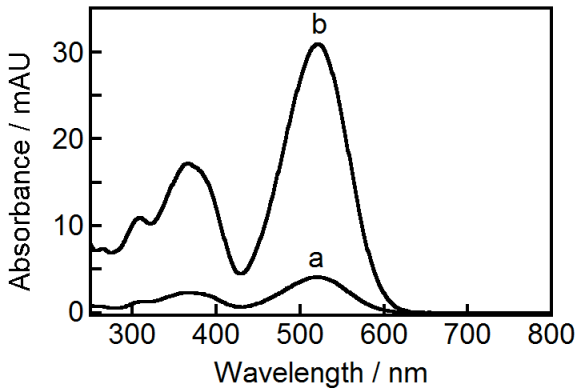

Figure 3.20: Absorption spectra of the peaks at a) 3.1 min, Figure 3.19, left and b) 2.8 min, Figure 3.19, right.

The method was validated by repeating the procedure using a solution of NSP in ethanol. The value found for ε value at 537 nm was (3.68 ± 0.03) × 10^4 cm^{-1} M^{-1}. A literature value of 3.5 × 10^4 cm^{-1} M^{-1} was reported by Flannery. [83]

In summary, the HPLC conditions to determine the molar absorptivity coefficients of DAE and NSP were as follows (Table 3.1):

Table 3.1: HPLC settings for the detection of DAE and NSP

	DAE	NSP
Mobile phase	30% acetonitrile 70% MeOH	20% H_2O 80% MeOH
Flow rate	1.5 mL/min	1.2 mL/min
Detection wavelengths	269 nm and 562 nm	338 nm and 517 nm
Temperature	25 ^oC	25 ^oC

3.4 Results

Using the procedure described above, the ε values for the colorless and colored isomers of DAE and NSP were determined. For DAE (Figure 3.21), the absorption spectra of both DAE_a and DAE_b are very similar in different media. A small bathochromic shift is observed for DAE_b when the compound is taken from a non-polar to a polar environment. The experiment was not performed in NaTC 80 mM/NaCl 0.2 M due to solubility limitations. Even when using a high concentration of this bile salt - 80 mM - the solution of DAE 50 μM was turbid. The average values obtained for ε of DAE_b at the wavelength of maximum absorbance are summarized in Table 3.2.

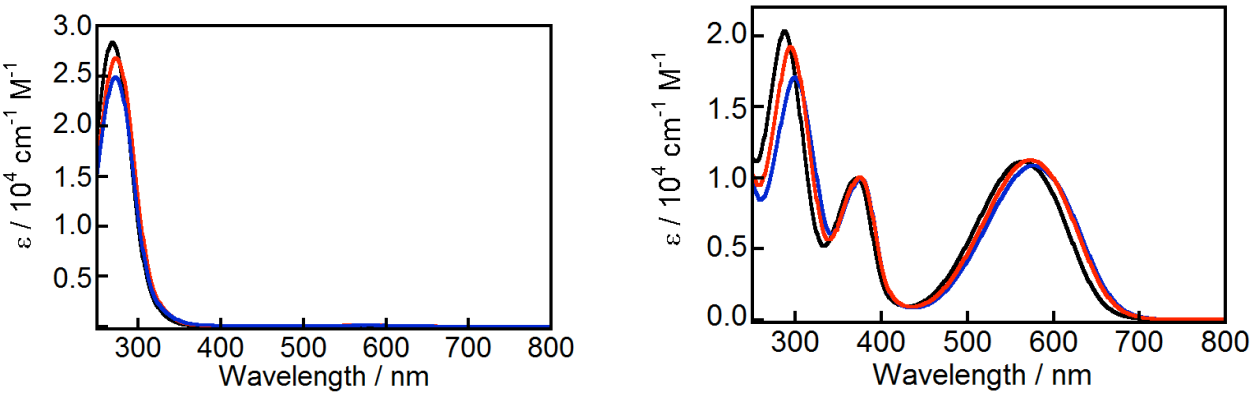

Figure 3.21: Absorption spectra of DAE_a (left) and DAE_b (right) in: hexane (black); NaC 80 mM/NaCl 0.2 M (blue) and NaDC 80 mM/NaCl 0.2 M (red).

Table 3.2: ε values of DAE_b at the wavelength of maximum absorption in the visible region:[a]

Solvent	**ε / 10^4 cm^{-1} M^{-1}**
Hexane / 562 nm (2)	1.11 ± 0.03
NaC 80 mM/NaCl 0.2 M / 577 nm (2)	1.09 ± 0.04
NaDC 80 mM/NaCl 0.2 M / 577 nm (2)	1.1 ± 0.1
NaTC 80 mM/NaCl 0.2 M / 577 nm	Solubility limitation

[a]The numbers in parenthesis correspond to independent experiments. The errors are average deviations.

For NSP (Figure 3.22), the ε values were determined in ethanol and three aqueous solutions containing NaCl 0.2 M and different bile salts. The absorption spectrum of NSP_a and NSP_b are very similar in aqueous solutions, but exhibit a large bathochromic shift in ethanol. The average values of ε obtained for NSP_b in different media are given in Table 3.3.

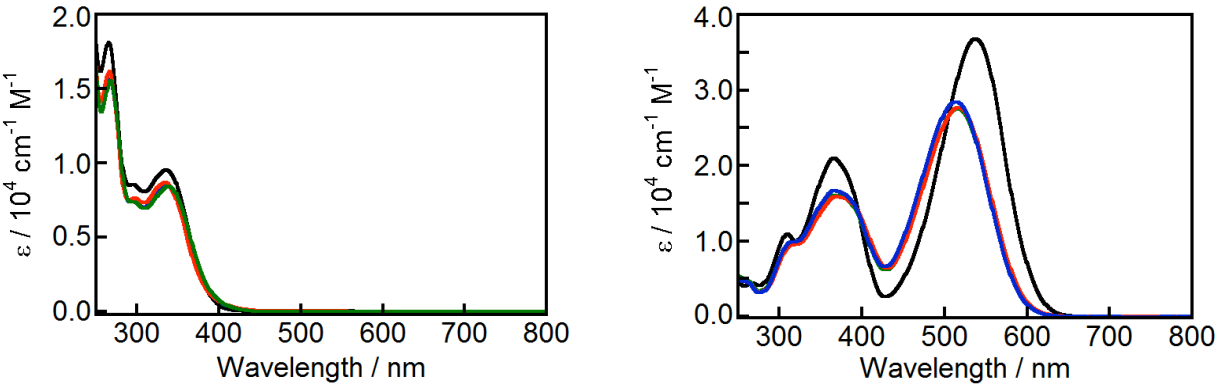

Figure 3.22: Absorption spectra of NSP_a (left) and NSP_b (right) in: ethanol (---, black); NaC 80 mM/NaCl 0.2 M (blue, overlapped with green trace on the left); NaDC 80 mM/NaCl 0.2 M (red); NaTC 80 mM/NaCl 0.2 M (green, overlapped with red trace on the right).

Table 3.3: ε values of NSP_b at the wavelength of maximum absorption in the visible region:[a]

Solvent	**ε / 10^4 cm^{-1} M^{-1}**
Ethanol / 537 nm (2)	3.68 ± 0.03
NaC 80 mM/NaCl 0.2 M / 517 nm (2)	2.84 ± 0.06
NaDC 80 mM/NaCl 0.2 M / 517 nm (2)	2.77 ± 0.05
NaTC 80 mM/NaCl 0.2 M / 517 nm (2)	2.76 ± 0.06

[a]The numbers in parenthesis correspond to independent experiments. The errors are average deviations.

Values of ε were not determined for DAE_b or NSP_b in the presence NaC 80 mM/NaCl 1 M. This concentration of NaCl is very high and could damage the HPLC column. The bands at 577 nm for DAE_b and at 517 nm for NSP_b are broad and no shift is observed when the concentration of NaCl increases from 0.2 M to 1 M. For the calculation showed in chapters 4 and 5, the values of ε in the presence of NaC 80

mM/NaCl 1 M were assumed to be equal to the values in the presence of NaC 80 mM/NaCl 0.2 M.

3.5 Discussion

The determination of ε values for the colored isomers of photochromic compounds has intrinsic difficulties. Because the absorption spectra of both colored and colorless compounds overlap in the UV region, irradiation of the sample with UV light leads to a photostationary state, and the spectrum of the irradiated sample corresponds to the sum of the spectra of the colored and colorless isomers. Also, since the colorless isomer absorbs only in this overlapping region, it is not possible to determine its concentration by analysing the absorption spectrum of the irradiated solution.

For DAE and other compounds that do not undergo a dark reaction, methods to determine ε values generally involve isolation of the colored isomer from the mixture. Separation is usually achieved by HPLC,[44,79] although the use of silica TLC plates has also been reported[80]. A drawback of these methods is that the sample is manipulated in different steps of the procedure and has to be protected from ambient light all the time.

For thermally unstable compounds like NSP_b, the isolation of this isomer cannot be done easily because the dark reaction represents a major source of error. These limitations are probably the reason why it is difficult to find methods to determine ε values in the literature. Most of the papers[24,84,85] use the values cited by Flannery[83] in 1968. Flannery assumed that the value of ε for NSP_b in polar solvents was the same as the value of ε in ethanol, 3.5×10^4 cm^{-1} M^{-1}. This was determined by Heller[86] et al. under

the assumption that a solution of NSP contained between 51% and 100% of NSP_b in the photostationary state. This gives an ε between 4.68×10^4 and 2.40×10^4 cm^{-1} M^{-1}, with a mean value of 3.54×10^4 cm^{-1} M^{-1}. This thesis presents a value of ε for NSP_b equal to $(3.68 \pm 0.03) \times 10^4$, which is very similar to the average value estimated by Heller. Another approach to determine ε values of spiropyrans is the photokinetic method,[87-89] which involves setting ε as an unknown in the fit of kinetic curves; the difficulties on applying this method are discussed in chapter 5.

The wavelength of maximum absorption for NSP_b increases in less polar solvents.[90] In ethanol, the maximum occurs at 537 nm and in aqueous solutions containing bile salts the maximum occurs around 517 nm. Therefore, NSP_b is located in a very polar environment in the interior of the bile salt aggregates. In aqueous solutions containing bile salts, the molar absorptivity coefficient of NSP_b was found to be 2.8×10^4 cm^{-1} M^{-1} at 517 nm, which is considerably different from the value in ethanol. Thus the assumption commonly made in the literature that the molar absorptivity coefficients for NSP_b are the same for all polar solvents may need revision.

The method described in this work is very useful for analysing photochromic compounds because the quantification is made without isolation of the isomers, which is an advantage compared to other methods described in the literature. [44,79] [80]After irradiation, the only step that needs to be conduct in the dark is to transfer the solution to a covered HPLC vial, which is convenient from the experimental point of view. The procedure is fast enough that the dark reaction of NSP does not interfere with the results and has also shown good reproducibility.

4 NSP Dark Reaction

Part of the material presented in this chapter has been published:

Li, R.; Santos, C. S.; Norsten, T. B.; Morimitsu, K.; Bohne, C. *Chem. Commun*. **2010**, *46*, 1941. DOI: 10.1039/B926351A – Reproduced by permission of The Royal Society of Chemistry

Part of the material presented in this chapter has been published. Reproduced in part with permission from *Langmuir* (2014) **30**, 11319-11328. Copyright 2014 American Chemical Society.

The switch between closed and open-ring isomers of NSP can be induced photochemically in both directions. Another path for the isomerization occurs by a dark reaction, *i.e.*, by a process that does not require the absorption of light (Scheme 1.2).[1] In this chapter the effect of bile salt aggregates on the kinetics of the NSP dark reaction will be presented and discussed.

4.1 Results

When an aqueous solution of NSP containing bile salt was irradiated with UV light a reddish solution was obtained. The absorption spectrum of this irradiated solution exhibit a broad band with a maximum around 515 nm (Figure 4.1). The maximum shows a small shift depending on the concentration[91] and structure of the bile salt, as shown on Chapter 3.

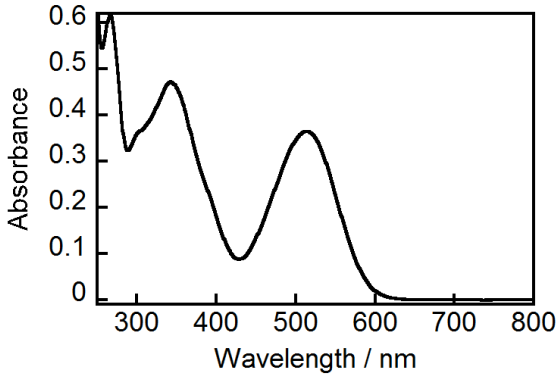

Figure 4.1: Aqueous solution of NSP 50 µM containing NaC 80mM/NaCl 0.20 M irradiated at 338 nm.

In order to monitor the kinetics of the dark reaction, the solutions containing NSP were placed in the spectrophotometer after irradiation at 338 nm. This wavelength was chosen for being an absorption maximum for the isomer NSP_a. The absorbance of the solutions were then registered each 1 min at 517 nm. As a result of the dark reaction, the absorbance decreased until equilibrium was reached. A solution containing only NSP_a was obtained by exposing the solution of NSP to ambient light. The absorbance of this colorless solution was monitored at 517 nm and, as a result of the dark reaction, the absorbance increased until reaching equilibrium. The equilibrium position obtained for the coloration and for the fading of the color in the dark were the same, which shows the process monitored is the relaxation kinetics. For aqueous solutions of NSP containing NaC and NaCl, the amount of NSP at equilibrium showed to be affected by the concentration of NaCl (Figure 4.2).

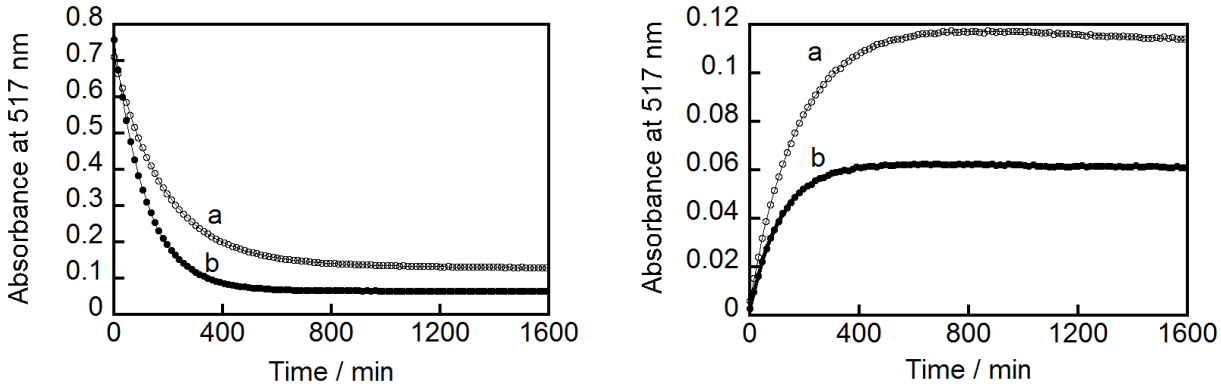

Figure 4.2: Kinetics for the relaxation of NSP 50 µM in aqueous solution of NaC 80 mM and NaCl 0.20 M (a) or NaCl 1.0 M (b). **Left**: after irradiation at 338 nm; **Right**: after exposure to ambient light.

The curves shown in Figure 4.2 are better fit as the sum of 2 exponentials (Equation 5). If the curves are fit as a one exponential function the residuals from the fit are considerably larger and systematic deviations are observed. The first term of equation 5 is related to the dark reaction, and the second was assumed to be the decomposition by hydrolysis. The absorption spectra of an aqueous solution of NSP_a containing NaC exhibited an increase in absorbance at 405 nm over time[91] (Figure 4.3). The same changes were observed[92] in aqueous solutions containing water soluble derivatives of NSP and were attributed to the formation of hydrolysis products. Another indication of decomposition is that a fit with smaller least squares deviation was obtained when the value of absorbance at $t \rightarrow \infty$ was set to zero, which is expected since the decomposition is an irreversible process (Equation 5).

$$A = a_1 \, e^{-k_{obs1} t} + a_2 \, e^{-k_2 t} + 0 \qquad \textbf{5}$$

where:

- A = Absorbance at 517 nm;

- a_1, a_2 = pre-exponential factors;
- k_{obs1} = dark reaction rate constant;
- k_2 = decomposition rate constant;
- t = time.

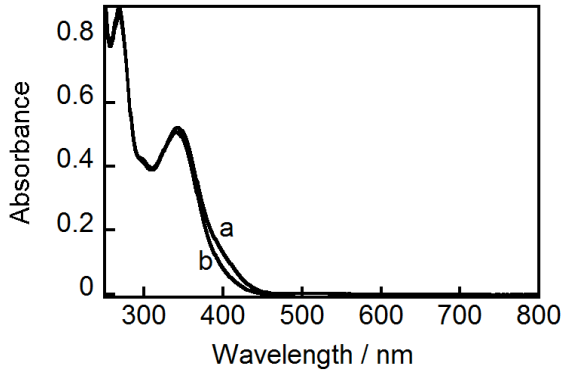

Figure 4.3: Absorption spectra of an aqueous solution of NSP_a 50 µM containing NaC 80 mM/NaCl 0.20 M after sample preparation (a) and after 29 h (b).

The same values of k_{obs1} and k_2 determined by the fit of the decoloration curve on the left of Figure 4.2 were found from the fit of the coloration curve (Figure 4.2, right), as expected for relaxation kinetics (Table 4.1).

Table 4.1: Rate constants for the relaxation of NSP_b to NSP_a (k_{obs1}, k_2) and for the relaxation of NSP_a to NSP_b (k'_{obs1}, k'_2) measured for aqueous solutions of NSP 50 µM at 25 °C.[a]

[NaCl] / M	k_{obs1} / 10^{-3} min^{-1}	k_2 / 10^{-5} min^{-1}	k'_{obs1} / 10^{-3} min^{-1}	k'_2 / 10^{-5} min^{-1}
0.20	5.6 ± 0.1 (3)	5.4 ± 0.8 (3)	5.4 ± 0.2 (4)	5.1 ± 0.8 (4)
1.0	8.74 ± 0.06 (3)	3 ± 1 (3)	8.4 ± 0.3 (4)	2.6 ± 0.7 (4)

[a]The numbers in parenthesis correspond to independent experiments. The errors are standard deviations.

A comprehensive study was performed to evaluate the effect of bile salt concentration, NaCl concentration, bile salt structure and temperature on the dark reaction of NSP. Since k_{obs1} and k_2 can be evaluated by either the relaxation of NSP_b to NSP_a or the relaxation of NSP_a to NSP_b, only the decoloration process was studied in these experiments. When indicated accordantly, the experiments were performed by Allyson Miller, a co-op student who was supervised by me in the period of January to April 2010.

4.2 Effect of NaC concentration on the dark reaction of NSP

Full solubilization of NSP 50 μM in water was achieved using NaC 40 mM. Therefore, the dark reaction was investigated in solutions containing from 40 mM to 100 mM of NaC (Figure 4.4). The values obtained for the dark reaction and decomposition rate constants are given in Table 4.2. The increase in the concentration of NaC from 40 mM to 50 mM led to an increase in k_{obs1}, but the further increase of NaC concentration until 80 mM resulted, within error, in the same values of k_{obs1}. When the concentration of NaC was increase from 80 mM to 100 mM the value of k_{obs1} increased from $(5.6 \pm 0.2) \times 10^{-3}$ min^{-1} to $(6.5 \pm 0.2) \times 10^{-3}$ min^{-1}. The values obtained for k_2 in different independent experiments were not reproducible. The decomposition rate constant was found to be around 100 times smaller than the rate constant for the dark reaction, and for this reason the time the kinetics were followed was too short to determine a precise value of k_2. Consider for example a k_2 value of 5×10^{-5} min^{-1}. The lifetime considering only this decay is 20000 min, which is 10 times longer than the period of time for which each

kinetic curve was collected. The data collected, therefore, were not sufficient to determine precise values of k_2. As a consequence, no trend was observed on the value of k_2 with the increase of NaC concentration or with the change of any other parameter. The individuals values of k_2 obtained on each experiment were presented instead of calculating standard or average deviations.

The concentration of NaC also seems to affect the amount of NSP_b at equilibrium, as verified by the final absorbance in the kinetic curves (Figure 4.4). Except for the concentration equal to 50 mM, the increase in NaC concentration led to a decrease in the absorbance at 517 nm for the system at equilibrium.

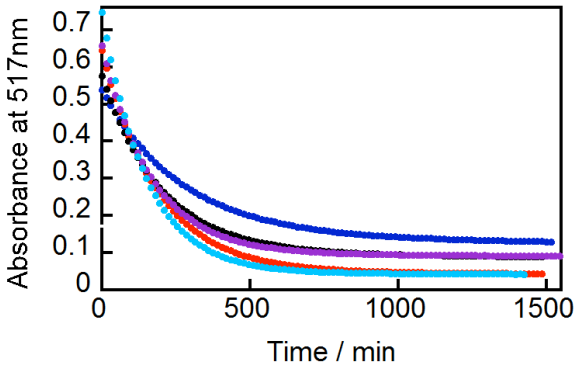

Figure 4.4: Kinetics for the decay of NSP_b to NSP_a at 25 °C measured at 517 nm. Aqueous solutions of NSP 50 µM in NaCl 0.2 M and NaC 40 mM (blue), 50 mM (red), 60 mM (black), 80 mM (purple) and 100 mM (cyan). Experiments performed by Allyson Miller.

Table 4.2: Rate constants for the dark reaction, k_{obs1}, and decomposition, k_2, of NSP in aqueous solutions of NaC/NaCl 0.2 M at 25 ^{o}C.[a]

NaC / mM	k_{obs1} / 10^{-3} min^{-1}	k_2 / 10^{-5} min^{-1}
40 (3)	4.0 ± 0.5	6, 7, 8
50 (2)	5.4 ± 0.1	4, 5
60 (3)	5.4 ± 0.5	6, 7, 8
80 (3)	5.6 ± 0.1	5, 5, 6
100 (2)	6.5 ± 0.2	2, 4

[a]Experiments performed by Allyson Miller. The numbers in parenthesis correspond to independent experiments. The errors are standard deviations where the number of independent experiments are equal or larger than 3 or average deviations where only 2 independent experiments were performed. For k_2 the values obtained for each trial are reported.

4.3 Effect of NaCl concentration on the dark reaction of NSP

The relaxation of NSP was evaluated in aqueous solutions containing NaC 80 mM and different concentrations of NaCl (Figure 4.5). The fit of the kinetic curves showed that the value of k_{obs1} increased as the concentration of NaCl was increased. The values of k_2 could not be determined precisely, and the wide range of values obtained for this parameter overlaped for all the concentrations of NaCl evaluated.

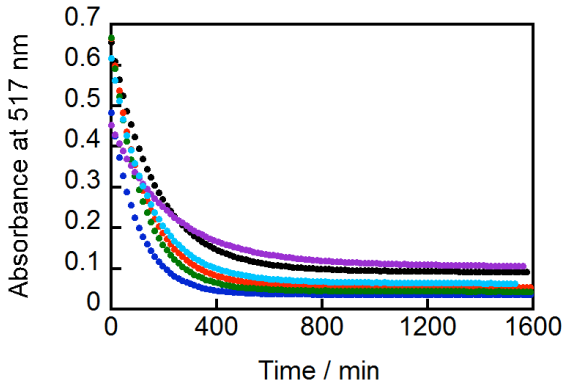

Figure 4.5: Kinetics for the decay of NSP_b to NSP_a at 25 °C measured at 517 nm. Aqueous solutions of NSP 50 µM in NaC 80 mM and NaCl 1.0 M (blue), 0.8 M (green), 0.6 M (red), 0.4 M (cyan), 0.2 M (---, black) and 0.03 M (purple). Experiments performed by Allyson Miller.

Table 4.3: Rate constants for the dark reaction, k_{obs1}, and decomposition, k_2, of NSP in aqueous solutions of NaC 80 mM/NaCl at 25 °C.[a]

NaCl / M	k_{obs1} / 10^{-3} min^{-1}	k_2 / 10^{-5} min^{-1}
0.03 (2)	4.63 ± 0.06	6, 9
0.2 (3)	5.6 ± 0.1	5, 5, 6
0.4 (2)	7.17 ± 0.08	6, 6
0.6 (3)	7.93 ± 0.01	5, 5, 6
0.8 (3)	8.71 ± 0.04	4, 5, 7
1.0 (3)	9.5 ± 0.1	1, 2, 8

[a]Experiments performed by Allyson Miller. The numbers in parenthesis correspond to independent experiments. The errors are standard deviations where the number of independent experiments are equal or larger than 3 or average deviations where only 2 independent experiments were performed. For k_2 the values obtained for each trial are reported.

4.4 Effect of bile salt structure on the dark reaction of NSP

The experiments presented so far were performed in solutions containing NaC. This bile salt contains a carboxyl head group and 3 hydroxyl groups on the concave face. In order to compare the effect of bile salt structure on the relaxation kinetics of NSP, the reaction was carried out in aqueous solutions containing NaDC and NaTC. The difference between these bile salts and NaC is that NaDC has only 2 hydroxyl groups on the concave face and NaTC has a different head group (Figure 1.5).

The amount of NSP_b at equilibrium was found to depend on the bile salt structure. The absorbance at 517 nm for the system at equilibrium has the largest value in the presence of NaTC and the smallest one in the presence of NaDC (Figure 4.6). The dark reaction of NSP in solutions containing NaDC and NaC exhibited a similar rate constant, while in the presence of NaTC the relaxation process is slower (Table 4.4). In organic solvents the dark reaction rate constant changes with the polarity of the medium, as will be discussed later. Different bile salt structures lead to different aggregates, which can have different polarities.

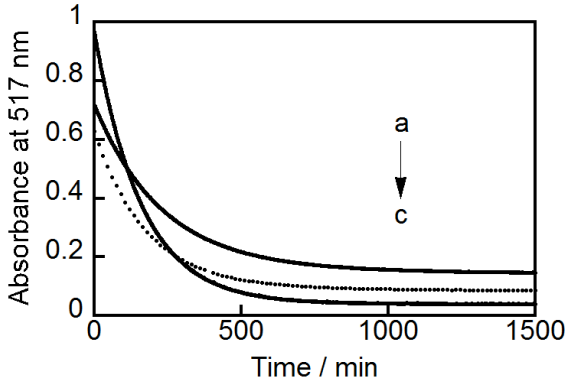

Figure 4.6: Kinetics for the decay of NSP_b to NSP_a at 25 °C measured at 517 nm. Aqueous solutions of NSP 50 μM in NaCl 0.20 M and NaTC 80 mM (a), NaC 80 mM (b) and NaDC 80 mM (c).

Table 4.4: Rate constants for the dark reaction, k_{obs1}, and decomposition, k_2, of NSP in aqueous solutions containing NaCl 0.20 M and different bile salts at 25 ^{o}C.[a]

Bile salt	k_{obs1} / 10^{-3} min^{-1}	k_2 / 10^{-5} min^{-1}
NaC (3)	5.6 ± 0.1	5, 5, 6
NaDC (2)	6.26 ± 0.06	0, 1
NaTC (2)	4.336 ± 0.008	5, 5

[a]The numbers in parenthesis correspond to independent experiments. The errors are standard deviations where the number of independent experiments are equal or larger than 3 or average deviations where only 2 independent experiments were performed. For k_2 the values obtained for each trial are reported.

In one of the experiments in the presence of NaDC presented on Table 4.4 the fit of the kinetic curve using equation 5 led to a negative value for k_2. Since the existence of a negative rate constant is physically meaningless, the curve was fit as a one exponential decay and k_2 was indicated as being equal to zero (equation 6). Under some other conditions studied, especially at higher temperatures, the decomposition rate constant was also found to be negative in one or more independent experiments. In all these cases the curve could be fit using equation 6 with a small least squares deviation, and the value of k_2 was indicated as being zero.

$$A = a_0 + a_1 e^{k_{obs1} t} \qquad \textbf{6}$$

4.5 Temperature studies

In order to evaluate the effect of bile salt structure and NaCl concentration on the activation energy, the dark reaction rate constant was determined at different temperatures for the following conditions:

- NaC 80 mM/NaCl 0.20 M
- NaC 80 mM/NaCl 1.0 M
- NaDC 80 mM/NaCl 0.20 M
- NaTC 80 mM/NaCl 0.20 M

In the absence of light, a solution containing NSP will reach the equilibrium between the colored and colorless isomers via opposing first-order reactions.[83] The reaction rate constant experimentally determined, k_{obs1}, is equal to the sum of the rate constant for the conversion of NSP_b into NSP_a, k_{BA}, and the rate constant for the conversion of NSP_a into NSP_b, k_{AB} (Equation 7). The determination of k_{BA} and k_{AB} is necessary to assess the activation energy of both the forward and backward reactions.

$$k_{obs1} = k_{AB} + k_{BA} \qquad 7$$

The equilibrium constant for the reaction in Scheme 1.2 is:

$$K = \frac{[\text{NSP\_b}]}{[\text{NSP\_a}]} \qquad 8$$

The concentration of NSP_b at equilibrium was determined considering the parameters obtained from the fit with Equation 5. The absorbance for the system at

equilibrium in the absence of decomposition is equal to the absorbance at the beginning of the kinetics (when t = 0) minus the pre-exponential factor a_1. The concentration of NSP_a was determined by subtracting the concentration of NSP_b from the total concentration of NSP (50 μM). At 25 ^{o}C the equilibrium constant was smaller in the presence of NaC 80 mM/NaCl 1.0 M than in the presence of NaC 80 mM/NaCl 0.2 M. For the reaction in the presence of NaCl 0.2 M and different bile salts, *K* increased in the order NaDC < NaC < NaTC (Table 4.5). The polarity inside the aggregates is probably the reason for this trend, as will be discussed later.

Table 4.5: Equilibrium constant for the dark reaction of NSP_a to NSP_b at 25 ^{o}C.[a]

Medium	K / 10^{-2}
NaC 80 mM/NaCl 0.20 M (3)	10 ± 1
NaC 80 mM/NaCl 1.0 M (2)	2.2 ± 0.4
NaDC 80 mM/NaCl 0.20 M (2)	2.9 ± 0.1
NaTC 80 mM/NaCl 0.20 M (2)	12.5 ± 0.2

[a]The numbers in parenthesis correspond to independent experiments. The errors are standard deviations where the number of independent experiments are equal to 3 or average deviations where only 2 independent experiments were performed.

The equilibrium constant is related to the rate constant as follows:

$$K = \frac{k_{AB}}{k_{BA}} \qquad \textbf{9}$$

After the determination of *K* with equation 8, equation 7 and 9 were rearranged to allow the determination of k_{BA} (Equation 10). Values of k_{AB} were determined with equation 7.

$$k_{BA} = \frac{k_{obs1}}{1 + K} \qquad \textbf{10}$$

The reaction in the presence of NaC 80 mM/NaCl 0.20 M was performed with the temperature ranging from 15 ^{o}C to 45 ^{o}C (Figure 4.7). As expected, the values determined for k_{obs1}, k_{AB} and k_{BA} increased with temperature (Table 4.6). The values found for k_2 were not very reproducible and did not follow any trend with temperature.

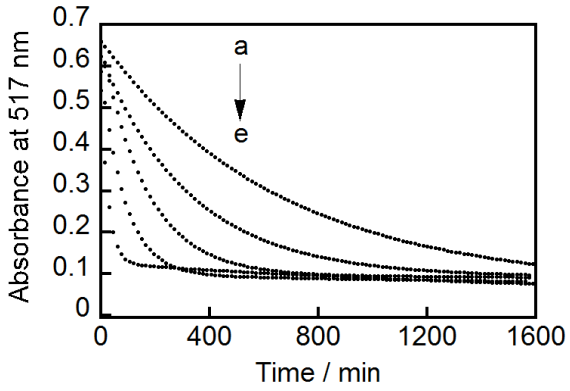

Figure 4.7: Kinetics for the decay of NSP_b to NSP_a measured at 517 nm. Aqueous solutions of NSP 50 μM in NaC 80 mM/NaCl 0.2 M at 15 ^{o}C (a), 20 ^{o}C (b), 25 ^{o}C (c), 30 ^{o}C (d) and 40 ^{o}C (e). Experiments performed by Allyson Miller

Table 4.6: Rate constants for the dark reaction - k_{obs1}, k_{AB}, k_{BA} - and decomposition - k_2, - of NSP in aqueous solutions of NaC 80 mM/NaCl 0.2 M at different temperatures.[a]

T / °C	k_{obs1} / 10^{-3} min^{-1}	k_2 / 10^{-5} min^{-1}	k_{BA} / 10^{-3} min^{-1}	k_{AB}/ 10^{-3} min^{-1}
15 (3)	1.75 ± 0.03	38, 39, 39	1.54 ± 0.03	0.207 ± 0.004
20 (2)	3.3 ± 0.3	4, 52	3.1 ± 0.3	0.28 ± 0.07
25 (3)	5.6 ± 0.1	5, 5, 6	5.1 ± 0.2	0.51 ± 0.06
30 (2)	11.3 ± 0.1	11, 12	10.6 ± 0.1	0.72 ± 0.04
35 (4)	21 ± 1	18, 18, 18, 20	19 ± 1	1.74 ± 0.04
40 (2)	37 ± 3	30, 36	33 ± 4	3.3 ± 0.1
45 (2)	78 ± 1	6, 32	73 ± 1	5.5 ± 0.2

[a]Experiments performed by Allyson Miller. The numbers in parenthesis correspond to independent experiments. The errors are standard deviations where the number of independent experiments are equal or larger than 3 or average deviations where only 2 independent experiments were performed. For k_2 the values obtained for each trial are reported.

The activation energy was determined using an Arrhenius plot (equation 11), while the enthalpy and entropy of activation were determined by an Eyring plot (equation 12). The plot of these equations resulted in a line for both k_{BA} (Figure 4.8) and k_{AB} (Figure 4.9).

$$\ln(k) = \ln(A) - \frac{E_a}{R}\left(\frac{1}{T}\right) \qquad \textbf{11}$$

$$\ln\left(\frac{k}{T}\right) = \ln\left(\frac{k_b}{h}\right) + \frac{\Delta S^{\neq}}{R} - \frac{\Delta H^{\neq}}{R}\left(\frac{1}{T}\right) \qquad \textbf{12}$$

where:

- k = reaction rate constant
- T = absolute temperature
- R = gas constant
- k_b = Boltzmann constant
- h = Planck's constant
- E_a = activation energy
- $\Delta H^{\ddagger}$ = enthalpy of activation
- $\Delta S^{\ddagger}$ = entropy of activation

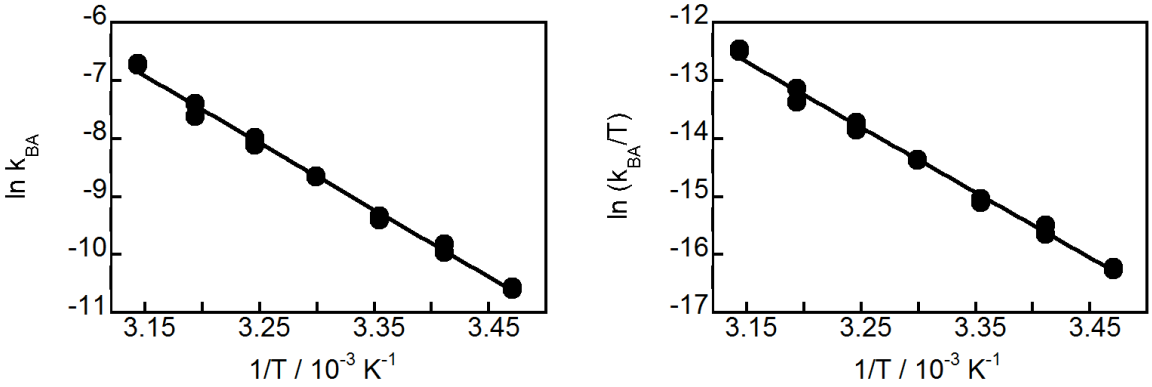

Figure 4.8: Temperature studies for the decoloration of NSP in NaC 80 mM/NaCl 0.2 M. Left: Arrhenius plot for k_{BA}. Right: Eyring plot k_{BA}.

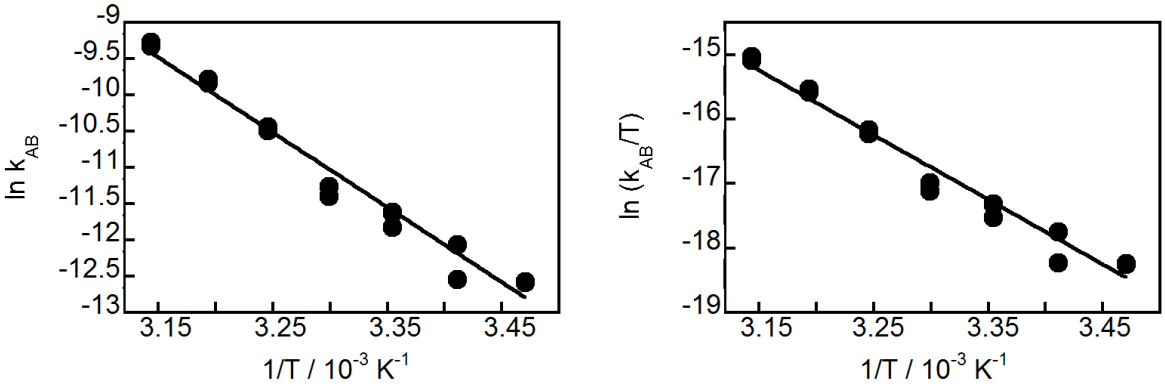

Figure 4.9: Temperature studies for the coloration of NSP in NaC 80 mM/NaCl 0.2 M. Left: Arrhenius plot for k_{AB}. Right: Eyring plot k_{AB}.

The same analysis presented before for NaC 80 mM/NaCl 0.2 M was performed for the other conditions. For NaDC 80 mM/NaCl 0.2 M (Figure 4.11, Table 4.8, Figure B.3, Figure B.4) the experiment could not be performed at 15 ^{o}C and 20 ^{o}C because a gel formed at that temperature. For NaTC 80 mM/NaCl 0.2 M (Figure 4.12, Table 4.9, Figure B.5, Figure B.6) the experiment was not done at 15 ^{o}C because the reaction was very slow at that temperature; it would take more than 30 hours to collect each kinetic curve.

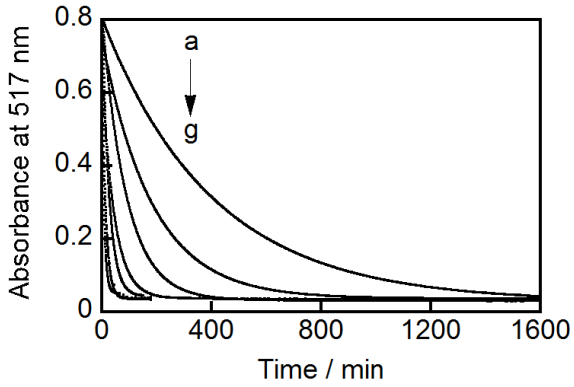

Figure 4.10: Kinetics for the decay of NSP_b to NSP_a measured at 517 nm. Aqueous solutions of NSP 50 µM in NaC 80 mM/NaCl 1.0 M at 15 ^{o}C (a), 20 ^{o}C (b), 25 ^{o}C (c), 30 ^{o}C (d), 35 ^{o}C (e), 40 ^{o}C (f) and 45 ^{o}C (g).

Table 4.7: Rate constants for the dark reaction - k_{obs1}, k_{AB}, k_{BA} - and decomposition - k_2, - of NSP in aqueous solutions of NaC 80 mM/NaCl 1.0 M at different temperatures.[a]

T / °C	k_{obs1} / 10^{-3} min^{-1}	k_2 / 10^{-5} min^{-1}	k_{BA} / 10^{-3} min^{-1}	k_{AB} / 10^{-3} min^{-1}
15 (2)	2.746 ±0.002	55, 85	2.54 ± 0.06	0.20 ± 0.06
20 (2)	5.508 ± 0.007	1, 3	5.37 ± 0.01	0.13 ± 0.02
25 (2)	11.15 ± 0.05	3, 6	10.9 ± 0.1	0.24 ± 0.04
30 (2)	22.15 ± 0.06	6, 8	21.6 ± 0.1	0.57 ± 0.03
35 (4)	40 ± 4	0, 13, 9, 426	39 ± 4	1.1 ± 0.5
40 (4)	66 ± 7	0, 13, 17, 19	64 ± 7	1.9 ± 0.5
45 (2)	127.19 ± 0.04	0, 0	124.0 ± 0.2	3.2 ± 0.2

[a]The numbers in parenthesis correspond to independent experiments. The errors are standard deviations where the number of independent experiments are equal or larger than 3 or average deviations where only 2 independent experiments were performed. For k_2 the values obtained on each trial are reported.

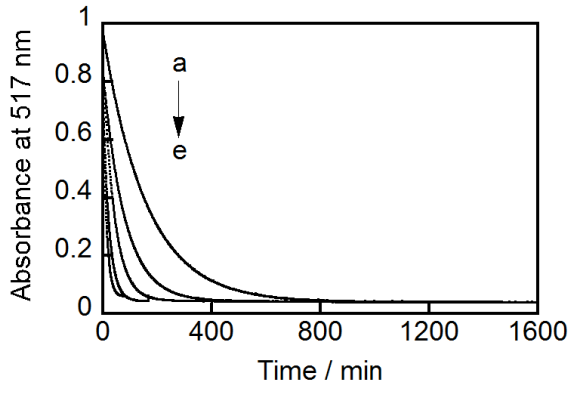

Figure 4.11: Kinetics for the decay of NSP_b to NSP_a measured at 517 nm. Aqueous solutions of NSP 50 µM in NaDC 80 mM/NaCl 0.20 M at 25 °C (a), 30 °C (b), 35 °C (c), 40 °C (d) and 45 °C (e).

Table 4.8: Rate constants for the dark reaction - k_{obs1}, k_{AB}, k_{BA} - and decomposition - k_2, - of NSP in aqueous solutions of NaDC 80 mM/NaCl 0.2 M at different temperatures.[a]

T / °C	k_{obs1} / 10^{-3} min^{-1}	k_2 / 10^{-5} min^{-1}	k_{BA} / 10^{-3} min^{-1}	k_{AB} / 10^{-3} min^{-1}
25 (2)	6.26 ± 0.06	0, 1	6.08 ± 0.06	0.177 ± 0.005
30 (2)	12.55 ± 0.03	5, 7	12.15 ± 0.05	0.375 ± 0.008
35 (3)	23 ± 1	6, 6, 12	23 ± 2	0.9 ± 0.2
40 (2)	43 ± 1	0, 24	42 ± 1	1.3 ± 0.2
45 (2)	80.2 ± 0.2	0, 0	77.6 ± 0.4	2.7 ± 0.1

[a]The numbers in parenthesis correspond to independent experiments. The errors are standard deviations where the number of independent experiments are equal or larger than 3 or average deviations where only 2 independent experiments were performed. For k_2 the values obtained for each trial are reported.

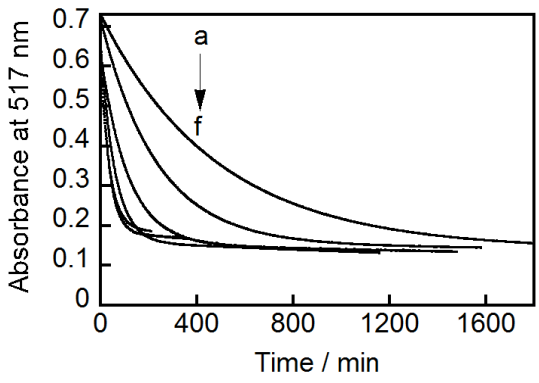

Figure 4.12: Kinetics for the decay of NSP_b to NSP_a measured at 517 nm. Aqueous solutions of NSP 50 μM in NaTC 80 mM/NaCl 0.20 M at 20 °C (a), 25 °C (b), 30 °C (c), 35 °C (d), 40 °C (e) and 45 °C (f).

Table 4.9: Rate constants for the dark reaction - k_{obs1}, k_{AB}, k_{BA} - and decomposition - k_2, - of NSP in aqueous solutions of NaTC 80 mM/NaCl 0.2 M at different temperatures.

T / ^{o}C	k_{obs1} / 10^{-3} min^{-1}	k_2 / 10^{-5} min^{-1}	k_{BA} / 10^{-3} min^{-1}	k_{AB} / 10^{-3} min^{-1}
20 (2)	2.093 ± 0.007	3, 4	1.86 ± 0.01	0.231 ± 0.009
25 (2)	4.336 ± 0.008	5, 5	3.85 ± 0.01	0.48 ± 0.02
30 (2)	8.88 ± 0.01	8, 9	7.87 ± 0.03	1.01 ± 0.03
35 (3)	16.9 ± 0.5	16, 16, 21	15.0 ± 0.7	1.9 ± 0.2
40 (2)	30.5 ± 0.5	0, 25	27 ± 1	3.3 ± 0.6
45 (2)	55 ± 1	29, 47	48 ± 1	7.4 ± 0.2

[a]The numbers in parenthesis correspond to independent experiments. The errors are standard deviations where the number of independent experiments are equal to 3 or average deviations where only 2 independent experiments were performed. For k_2 the values obtained for each trial are reported.

The parameters found for the analysis in all conditions are given on Table 4.10. The values of $\Delta S^{\ddagger}$ are in all cases close to zero. The values of E_a and $\Delta H^{\ddagger}$ are larger for k_{AB} than for k_{BA} in all conditions except in NaC 80 mM/NaCl 0.20 M. For k_{BA}, the enthalpy of activation was found to be the same in solutions containing NaC and different concentrations of NaCl, and a larger value was found for solutions containing NaDC and NaTC compared to NaC.

Table 4.10: Kinetic parameters for the dark reaction of NSP in bile salts.

Medium		E_a / kJ mol^{-1}	$\Delta S^{\ddagger}$ / kJ mol^{-1}	$\Delta H^{\ddagger}$ / J mol^{-1} K^{-1}
NaC 80 mM/NaCl 0.20 M	k_{BA}	96 ± 2	93 ± 1	-9 ± 6
	k_{AB}	86 ± 4	83 ± 3	-62 ± 12
NaC 80 mM/NaCl 1.0 M	k_{BA}	97 ± 2	94 ± 2	0 ± 6
	k_{AB}	82 ± 7	80 ± 7	-77 ± 23
NaDC 80 mM/NaCl 0.20 M	k_{BA}	100 ± 1	97 ± 3	5 ± 4
	k_{AB}	105 ± 5	102 ± 6	7 ± 18
NaTC 80 mM/NaCl 0.20 M	k_{BA}	101 ± 1	98 ± 1	4 ± 4
	k_{AB}	105 ± 3	102 ± 3	1 ± 9

4.6 Discussion

The capacity of bile salts to affect reactivity has been explored for the abstraction of hydrogens by excited ketones[84] and for the cleavage of C-C and C-O bond in a series of photoreactions.[93,94] In the later case, selectivity of photoproducts was achieved because bile salt aggregates control the rotational and translational motion of reaction intermediates. In the present project, the relaxation kinetics of NSP was studied at different temperatures, bile salts and concentrations of NaC and NaCl. In all those conditions the dark reaction was found to be much faster than the decomposition process. In the presence of NaC 80 mM/NaCl 0.2 M at 25 ^{o}C the decomposition rate constant was in the range of (3-8) $\times 10^{-5}$ min^{-1}. For a water soluble derivative of NSP the value for the decomposition rate constant was reported[92] as being equal to 3.6×10^{-3} min^{-1} at pH 8.0 (10 mM phosphate buffer) and 25 ^{o}C. According to this study, the decomposition occurs by hydrolysis of the isomer NSP_b. Therefore, the presence of bile salt reduced the decomposition by a factor of 45-120 times.

The dark reaction of NSP has been studied in different solvents.[24,83,90] In organic solvents the observed rate constant k_{obs1} decreases by increasing the solvent polarity, and has a value of 3.76×10^{-4} s^{-1} in ethanol and 1.120×10^{-1} s^{-1} in benzene.[83] Keum et al.[90] observed that k_{obs1} has a linear relationship with the solvent parameter E_T, which is a measure of the ionizing power of a solvent. For a series of nine solvents, the value of k_{obs1} decreased with the increase of E_T. In a series of imidazolium-based ionic liquids the value of k_{obs1} also shows a dependence on the polarity of the medium.[85] For the reaction carried out in different aqueous solutions containing bile salts, the value of k_{obs1} was

affected by the concentration of NaC, the concentration of NaCl and the structure of the bile salt monomer. The differences can be related to the polarity inside the bile salt aggregates.

The presence of NaCl influences the formation of bile salt aggregates. When the concentration of NaCl is increased the aggregates start to form at lower concentrations of bile salt,[95,96] are bigger,[65,97,98] more compact[82] and, as suggested by studies with pyrene I/III ratio, more hydrophobic.[82] The values of k_{obs1} increased when the concentration of NaCl was increased from 0.03 to 1.0 M. This result corroborates the evidence that NaCl causes a decrease in the polarity inside the aggregates. The increase in NaCl concentration also led to a decrease of NSP_b concentration at equilibrium. For the reaction in organic solvents, the amount of NSP_b at equilibrium decreases when the polarity of the solvent is decreased.[83]

The concentration of NaC was varied from 40 to 100 mM. Under these conditions the solution contains both primary and secondary bile salt aggregates. Although it is not possible to assign the location of NSP_a, NSP_b is problably located in secondary aggregates due to its zwitterionic structure. The value of k_{obs1} in the presence of 40 mM NaC is $(4.0 \pm 0.5) \times 10^{-3}$ min^{-1} and in the presence of 100 mM NaC is $(6.5 \pm 0.2) \times 10^{-3}$ min^{-1}, which represents an overall small increase of k_{obs1} with the NaC concentration. However, for concentrations of NaC from 50 to 80 mM the value of k_{obs1} was constant. These results can indicate that the polarity in the environment where NSP_b is located does not seem to change a lot with increasing the concentration of NaC. In fact, for probes in secondary aggregates, the protection efficiency towards quenching does not

change significantly from 20 to 40 mM NaC.[62] The amount of NSP_b at equilibrium presents an overall decrease with increasing the concentration of NaC.

NaDC, a dihydroxyl bile salt, can form larger aggregates than NaC, a trihydroxyl bile salt.[64,65,99] The structure of the bile salts also influences the binding efficiency and protection efficiency towards quenching, which are higher for NaDC than for NaC.[64] Nevertheless, the number of hydroxyl group in the concave face seems to have only a small effect on k_{obs1}. In organic solvents, the value of equilibrium constant (K) increases by increasing the polarity of the medium. The value of K is higher in the presence of NaC, which can indicate that NSP is located in a more polar environment in the presence of NaC. In order to evaluate the bile salt head group in the dark reaction of NSP, this reaction was also performed in the presence of NaTC. The value of k_{obs1} is smaller and the value of K is higher in the presence of NaTC, which indicates a higher polarity in the aggregates compared to NaC. Probably the fact that there is a larger amount of NSP_b at equilibrium in more polar environment is because this ionic isomer is more stable in such media.

The activation energy for the conversion of NSP_b to NSP_a in all bile salts is similar to other polar solvents like ethanol (103 kJ/mol) and chloroform (98 kJ/mol).[83] The values for both the energy and enthalpy of activation are expected to be higher for the conversion of NSP_a to NSP_b. However, for the reaction performed in NaC 80 mM/NaCl 1.0 M and NaC 80 mM/NaCl 0.20 M, E_a and $\Delta H^{\ddagger}$ calculated from k_{AB} are smaller than the ones calculated from k_{BA}. These results may have occurred because the Arrhenius and Eyring plots for those conditions did not exhibit a good linear fit. Because

for all the conditions the values of E_a, $\Delta H^{\ddagger}$ and $\Delta S^{\ddagger}$ are very close, no mechanistic information could be obtained from these numbers.

5 Photocoloration of NSP and DAE in Bile Salts

Part of the material presented in this chapter has been published. Reproduced in part with permission from *Langmuir* (2014) **30**, 11319-11328. Copyright 2014 American Chemical Society.

The quantum yield is a fundamental parameter in the description of a photochemical reaction. In a photochromic system, obtaining quantum yields is not trivial. Absorption spectra for the two isomers overlap in the UV range, and UV radiation can lead to both forward and backward reactions (Scheme 5.1, Scheme 5.2). Other processes such as dark reactions and decomposition can occur, which further complicates data analysis.[89]

The photocoloration of DAE and NSP was investigated in aqueous solutions of bile salts. The method developed to conduct this study and the effect of the medium on the reaction quantum yields will be presented in this chapter.

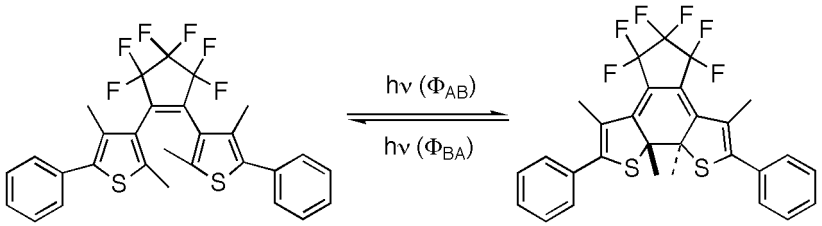

Scheme 5.1: Isomerisation of DAE during irradiation with UV light.

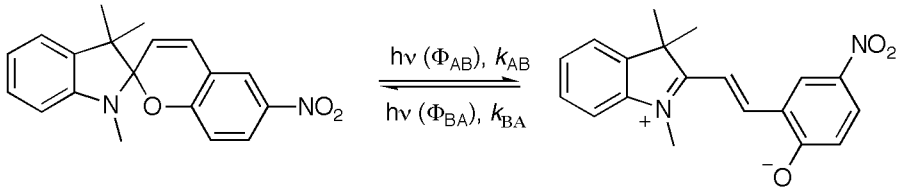

Scheme 5.2: Isomerisation of NSP during irradiation with UV light.

5.1 Method development

The photokinetic method for the determination of quantum yields involves following the kinetics of the photochemical reaction under continuous irradiation. [89,100,101] In order to apply this method, experimental and mathematical problems must be overcome.[101]

In a photochromic system the two isomers have very different absorption spectra, therefore the reaction can be monitored measuring the absorbance of the solution at a suitable wavelength. The first idea to perform the experiments was to irradiate the sample with monochromatic light and record the absorption spectrum at specific time intervals. With this approach, however, the dark reaction of NSP cannot be properly accounted for as the absorption spectra are being collected. A set-up was designed by Luis Netter and Tamara Pace to measure absorption of a sample undergoing irradiation. A PTI irradiation lamp and monochromator were connected to a cell compartment from a fluorimeter attached to a water bath. The absorbance of the sample was monitored using an Ocean Optics detector and a PTI lamp, both connected to the cell holder by fiber optics. Because the Ocean Optics detector is not as stable as a conventional spectrophotometer, the absorbance of a reference was measured alternately with the absorbance of the sample and the fluctuations corrected by the software. A FOS-2x2-TTL Inline Fiber Optic Shutter controlled the measurements of reference and sample, and the sample cell holder had a magnetic stirrer (Figure 5.1).

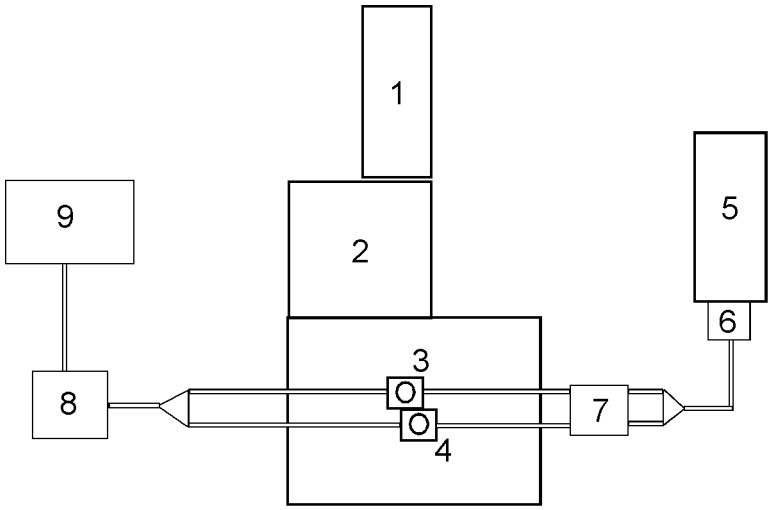

Figure 5.1: Equipment used in the photocoloration experiments: 1) irradiation lamp; 2) monochromator; 3) sample cell holder with magnetic stirrer; 4) reference cell holder; 5) monitoring lamp; 6) shutter; 7) FOS-2x2-TTL Inline Fiber Optic Shutter; 8) Ocean Optics detector; 9) computer.

The analysis of kinetic traces is another challenge in the study of a photochromic system. Usually it is necessary to make approximations to obtain analytical expressions[101] and, depending on the complexity of the system, no analytical method can be employed.[102] Therefore, the strategy employed in this investigation was to analyze the kinetic equations numerically by using the software Scientist 3.0 from Micromath.

Consider the simplest photochemical process in which **A** is irreversibly transformed into **B**:

$$A \xrightarrow{h\upsilon\ (\Phi_{AB})} B$$

If Φ_{AB} is the quantum yield of the conversion and $I_{\mathbf{A}}^{\mathrm{Abs}}$ is the amount of light absorbed by **A**, the rate equation for this process is:

$$\frac{d[\mathbf{A}]}{dt} = -\Phi_{AB}\, I_{\mathbf{A}}^{Abs} \qquad \mathbf{13}$$

Equation 13 can be written in terms of the light flux incident in the sample, I_0, and the absorbance of **A**, $Abs_{\mathbf{A}}$:

$$\frac{d[\mathbf{A}]}{dt} = -\Phi_{AB} I_0\, (1-10^{-Abs_{\mathbf{A}}}) \qquad \mathbf{14}$$

For an optical path length of 1 cm, the absorbance can be replaced by the product of the concentration of **A** and its molar absorptivity coefficient at the irradiation wavelength, $\varepsilon_{\mathbf{A}}$:

$$\frac{d[\mathbf{A}]}{dt} = -\Phi_{AB} I_0\, (1-10^{-\varepsilon_{\mathbf{A}}[\mathbf{A}]}) \qquad \mathbf{15}$$

For the photochromic reaction of DAE, irradiation with UV light leads to both forward and backward reactions; another term needs to be included in equation 15 regarding the conversion of **B** into **A:**

$$\frac{d[\mathbf{A}]}{dt} = -\Phi_{AB} I_0\, (1-10^{-\varepsilon_{\mathbf{A}}[\mathbf{A}]}) + \Phi_{BA} I_0\, (1-10^{-\varepsilon_{\mathbf{B}}[\mathbf{B}]}) \qquad \mathbf{16}$$

The isomerization of NSP also occurs via a dark reaction. Consequently, four processes have to be included in the kinetic model for this compound (Scheme 5.3):

$$A \underset{h\upsilon\ (\Phi_{BA}),\ k_{BA}}{\overset{h\upsilon\ (\Phi_{AB}),\ k_{AB}}{\rightleftharpoons}} B$$

$$A \xrightarrow{h\nu} B \qquad v_1 = I_0\,(1\text{-}10^{-\varepsilon_A[A]})\,\Phi_{AB}$$

$$A \xrightarrow{k_{AB}} B \qquad v_2 = k_{AB}\,[A]$$

$$B \xrightarrow{h\nu} A \qquad v_3 = I_0\,(1\text{-}10^{-\varepsilon_B[B]})\,\Phi_{BA}$$

$$B \xrightarrow{k_{BA}} A \qquad v_4 = k_{BA}\,[B]$$

Scheme 5.3: Processes involved in the photochromism of NSP and their respective rate equations.

The sum of the rate equations for the individual processes gives the differential equation that describes the change in the concentration of **A** when the system is continuously irradiated:

$$\frac{d[\mathbf{A}]}{dt} = -I_0\left(1-10^{-\varepsilon_A[\mathbf{A}]}\right)\Phi_{AB} - k_{AB}[\mathbf{A}] + I_0\left(1-10^{-\varepsilon_B[\mathbf{B}]}\right)\Phi_{BA} + k_{BA}[\mathbf{B}] \qquad \textbf{17}$$

At longer wavelengths in the visible range of the absorption spectrum, only **B** absorbs, therefore the reaction can be monitored for the formation of **B**:

$$Abs_{\mathbf{B}}^{vis} = \varepsilon_{\mathbf{B}}^{vis}\,[\mathbf{B}] \qquad \textbf{18}$$

where $Abs_{\mathbf{B}}^{vis}$ and $\varepsilon_{\mathbf{B}}^{vis}$ are the absorbance and the molar absorptivity coefficient of **B** at the monitoring wavelength, respectively. The concentrations of **B** and **A** are correlated and the concentration of **B** can be expressed as the difference between the total concentration of photochromic compound, $\mathbf{A}_0$, and the concentration of **A**:

$$[\mathbf{B}] = [\mathbf{A}_0] - [\mathbf{A}] \qquad \textbf{19}$$

5.2 The photokinetic factor and the absorbance at the irradiation wavelength

The rate equations for the photochemical reactions considered above were written as a function of the light absorbed by the individual components **A** and **B**. However, it is not possible to directly measure the light absorbed by each one of these compounds since their absorption spectra overlap. On the other hand, the light absorbed by the whole system, I_S^{Abs}, can be directly measured by the absorbance of the solution at the irradiation wavelength. Equation 13 can be written considering I_S^{Abs} if multiplied by a factor that represents the portion of light absorbed by **A:**

$$\frac{d[\mathbf{A}]}{dt} = -\Phi_{AB}\, I_S^{Abs}\left(\frac{I_{\mathbf{A}}^{Abs}}{I_S^{Abs}}\right) \qquad \textbf{20}$$

For absorbance values smaller than 0.1, the factor $I_{\mathbf{A}}^{Abs} / I_S^{Abs}$ is approximately equal to the ratio between the absorbance of **A** and the absorbance of the solution:

$$\frac{d[\mathbf{A}]}{dt} = -\Phi_{AB}\, I_S^{Abs}\left(\frac{Abs_{\mathbf{A}}}{Abs_S}\right) \qquad \textbf{21}$$

If I_0 is the light flux incident in the sample, one can substitute as follows:

$$\frac{d[\mathbf{A}]}{dt} = -\Phi_{AB}\, I_0\left(1-10^{-Abs_S}\right)\left(\frac{Abs_{\mathbf{A}}}{Abs_S}\right) \qquad \textbf{22}$$

The photokinetic factor F is defined as

$$F = \frac{\left(1-10^{-Abs_S}\right)}{Abs_S} \qquad \textbf{23}$$

Replacing F in Equation 22 and considering a light path of 1 cm, the result is

$$\frac{d[\mathbf{A}]}{dt} = -\Phi_{\mathrm{AB}}\, I_0 F\, Abs_{\mathbf{A}} \qquad \textbf{24}$$

$$\frac{d[\mathbf{A}]}{dt} = -\Phi_{\mathrm{AB}} I_0 F \varepsilon_{\mathbf{A}}[\mathbf{A}] \qquad \textbf{25}$$

Equation 25 is the main equation used in the photokinetic model. This equation assumes that the ratio between the light absorbed by **A** and the light absorbed by the solution is equal to the ratio between the absorbance of **A** and the absorbance of the solution. As already discussed, this assumption is only valid for absorbance smaller than 0.1. The absorbance at the irradiation wavelength should not be higher than this value. Nevertheless, this equation is often used without respecting this absorbance limit or discussing the intrinsic error associated with it.[89,101,103,104] Simulations performed with typical conditions for the photocoloration of DAE revealed that when the absorbance at the irradiation wavelength is 0.2 the error introduced on the quantum yields is around 10 %.

The use of Equation 25 rather than Equation 15 is probably due to the difficulty of integrating the latter. Since numerical analysis was the method chosen to fit the kinetic traces, Equation 15 can be applied. In principle, the solutions employed could have any absorbance at the irradiation wavelength. However, if the absorbance at the irradiation wavelength is too high, the entire incident light is absorbed by a thin layer of solution at the side of the cell facing the irradiation lamp. The accumulation of products in this layer can cause unwanted degradation reactions[8] and stirring may not be sufficient to ensure a homogeneous distribution of product. This, in turn, will affect the absorbance readout.

Therefore, the absorbance of the solutions employed in all the experiments was kept smaller than 0.30 at the irradiation wavelength.

5.3 Φ_{AB} and Φ_{BA} for DAE isomerization

The isomerization of DAE occurs exclusively through a photochemical reaction, which makes the study of this system easier from a mathematical point of view. A solution of DAE in cyclohexane was irradiated at the isosbestic point, 287 nm, and the absorbance at several wavelengths was monitored during the irradiation (Figure 5.2). The temperature was kept at 15 ^{o}C and the slit of the monochromator was set to achieve a bandwidth of 3 nm for both the entrance and exit of light. Although ideally monochromatic light should be employed, small slit bandwidths results in lower light flux and longer collection times for the kinetics. The absorbance measured had a periodic oscillation. This point will be addressed below.

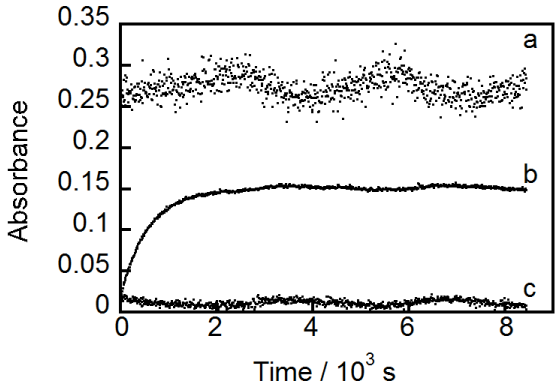

Figure 5.2: Absorbance at a) 287 nm, b) 562 nm and c) 800 nm during irradiation of DAE at 287 nm in cyclohexane. T = 15 ^{o}C.

The absorbance at 562 nm, $Abs_{\mathbf{B}}^{\text{vis}}$, corresponds to the maximum of absorption for the colored isomer of DAE. The kinetic trace at this wavelength was fit using the following model (Scheme 5.4):

Dependent variable: [**A**], [**B**], $Abs_{\mathbf{B}}^{\text{vis}}$

Independent variable: t

Parameters: I_0, $\varepsilon_{\mathbf{A}}$, $\varepsilon_{\mathbf{B}}$, $\varepsilon_{\mathbf{B}}^{\text{vis}}$, Φ_{AB}, Φ_{BA}

//**Equations**:

$$\frac{d[\mathbf{A}]}{dt} = -\Phi_{AB} I_0 \left(1 - 10^{-\varepsilon_{\mathbf{A}}[\mathbf{A}]}\right) + \Phi_{BA} I_0 \left(1 - 10^{-\varepsilon_{\mathbf{B}}([\mathbf{A}_0]-[\mathbf{A}])}\right)$$

$$[\mathbf{B}] = [\mathbf{A}_0] - [\mathbf{A}]$$

$$Abs_{\mathbf{B}}^{\text{vis}} = \varepsilon_{\mathbf{B}}^{\text{vis}} [\mathbf{B}]$$

//**Initial condition**:

t = 0

[**A**] = [$\mathbf{A}_0$]

Scheme 5.4: Model in Scientist 3.0 to fit the kinetics of DAE photocoloration.

The initial condition is an important information in the model, and for the experiments performed it indicates that in the beginning of the kinetics the concentration of **A** is equal to the total concentration of photochromic compound. Experimentally this condition was obtained by exposing the sample with ambient light until a complete conversion to isomer **A** was achieved.

The parameters in a model are quantities that have either their values fixed or allowed to change in order to obtain the best fit for the kinetics. In the above model, there

are six parameters; three of them - I_0, $\varepsilon_{\mathbf{A}}$ and $\varepsilon_{\mathbf{B}}$ - are determined in independent experiments and therefore can have their values fixed.

The light flux I_0 was determined using potassium ferrioxalate as an actinometer.[77] The molar absorptivity coefficient of **A** at the irradiation wavelength, $\varepsilon_{\mathbf{A}}$, was determined based on the absorption spectra of a solution of DAE containing only the isomer **A**. Since the irradiation was performed at the isosbestic point, the value of $\varepsilon_{\mathbf{B}}$ is equal to the value of $\varepsilon_{\mathbf{A}}$. As described in chapter 3, the molar absorptivity coefficients of **B** at other wavelengths are not readily available since it is not possible to obtain a solution containing only **B** unless some isolation method is employed. Initially, the curves were first fit without fixing $\varepsilon_{\mathbf{B}}^{\text{vis}}$. The values of $\varepsilon_{\mathbf{B}}^{\text{vis}}$, Φ_{AB} and Φ_{BA} obtained by this method were random, changing each time new guess values were input into the model. These initial guess values are numbers close to what is believed to be the real values, and are used by the software in the beginning of the calculations. The statistics of the fit revealed a large standard deviation for the parameters calculated. Constraining the possible values for the quantum yields between the theoretical values of 0 and 1, the parameters obtained in one of the attempts to fit curve b on Figure 5.2 were:

$\Phi_{AB} = 0.14 \pm 1.01$

$\Phi_{BA} = 0.31 \pm 0.49$

$\varepsilon_{\mathbf{B}}^{\text{vis}} = 3.5 \times 10^4 \pm 2.5 \times 10^5$

The large standard deviations and the dependence on initial guess values indicate that the parameters are underdetermined, *i.e.* there are several combinations of values that provide equally good fits to the data. The same underdetermination resulted when the reaction was monitored at several wavelengths and the curves were fit together.

These results suggest that the value of $\varepsilon_{\mathbf{B}}^{vis}$ has to be fixed in order to determine precise values for Φ_{AB} and Φ_{BA}. This requirement was the main motivation to develop an HPLC method to obtain the molar absorptivity coefficients of **B** (Chapter 3). If the value of $\varepsilon_{\mathbf{B}}^{vis}$ is fixed, the quantum yields are determined with a small standard deviation and the same values are found independently of the initial guess values. For curve b in Figure 5.2 the values of Φ_{AB} and Φ_{BA} were determined to be equal to 0.397 ± 0.002 and 0.0775 ± 0.0005, respectively (Figure 5.3).

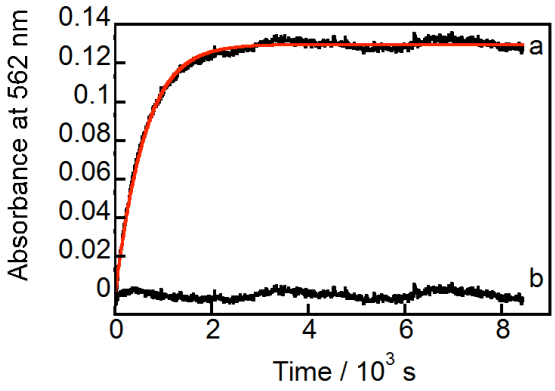

Figure 5.3: Absorbance at 562 nm during irradiation of DAE at 287 nm in cyclohexane. a) Experimental data (black) and numerical fit (red); b) Residuals between the experimental data and the fit. T = 15 °C.

A noise with a sinusoidal shape was observed for the detection at all wavelengths. This noise is more noticeable when the measurement is done with no sample in the cell holder or for wavelengths that should not change over time, like the curves at 287 nm and 800 nm (Figure 5.2, a and c). The data at 562 nm has the same type of noise, and for this reason the residuals of the fit also have a sinusoidal shape instead of being random around zero. In order to ensure that the noise would be taken into account in the fit, the

kinetics were followed for at least one cycle of oscillation after reaching the photostationary state.

5.4 Φ_{AB} and Φ_{BA} for NSP isomerization

The same method developed to analyze the photocoloration of DAE was applied to NSP, with extra consideration for the dark reaction (Scheme 5.5). The dark reaction rate constants k_{AB} and k_{BA} are known parameters (Chapter 4); therefore, their values were fixed when fitting the kinetic curve.

Dependent variable: [**A**], [**B**], $Abs_{\mathbf{B}}^{vis}$

Independent variable: t

Parameters: I_0, $\varepsilon_{\mathbf{A}}$, $\varepsilon_{\mathbf{B}}$, $\varepsilon_{\mathbf{B}}^{vis}$, k_{AB}, k_{BA}, Φ_{AB}, Φ_{BA}

//**Equations**:

$$\frac{d[\mathbf{A}]}{dt} = -I_0 \left(1-10^{-\varepsilon_{\mathbf{A}}[\mathbf{A}]}\right) \Phi_{AB} - k_{AB}[\mathbf{A}] + I_0 \left(1-10^{-\varepsilon_{\mathbf{B}}([\mathbf{A}_0]-[\mathbf{A}])}\right) \Phi_{BA} + k_{BA}([\mathbf{A}_0]-[\mathbf{A}])$$

$$[\mathbf{B}] = [\mathbf{A}_0]-[\mathbf{A}]$$

$$Abs_{\mathbf{B}}^{vis} = \varepsilon_{\mathbf{B}}^{vis}[\mathbf{B}]$$

//**Initial condition**:

t = 0

[**A**] = [$\mathbf{A}_0$]

Scheme 5.5: Model in Scientist 3.0 to fit the kinetics of NSP photocoloration.

Most of the photocoloration experiments with DAE and NSP were performed at 15 ^{o}C. This temperature was chosen for two reasons: as it minimizes evaporation of the organic solvents during irradiation and disfavours the dark reaction of NSP. For aqueous solutions containing NaDC, however, the experiments were performed at 25 ^{o}C to avoid the formation of a gel.

5.5 Results

The photocoloration of DAE was performed in cyclohexane (Figure 5.4) and in aqueous solutions containing NaC 80 mM/NaCl 0.2 M (Figure 5.5), NaC 80 mM/NaCl 1M (Figure 5.6) and NaDC 80 mM/NaCl 0.2 M (Figure 5.7). Two independent experiments were carried out for each of these conditions. Due to solubility limitations, the experiment was not performed in the presence of NaTC.

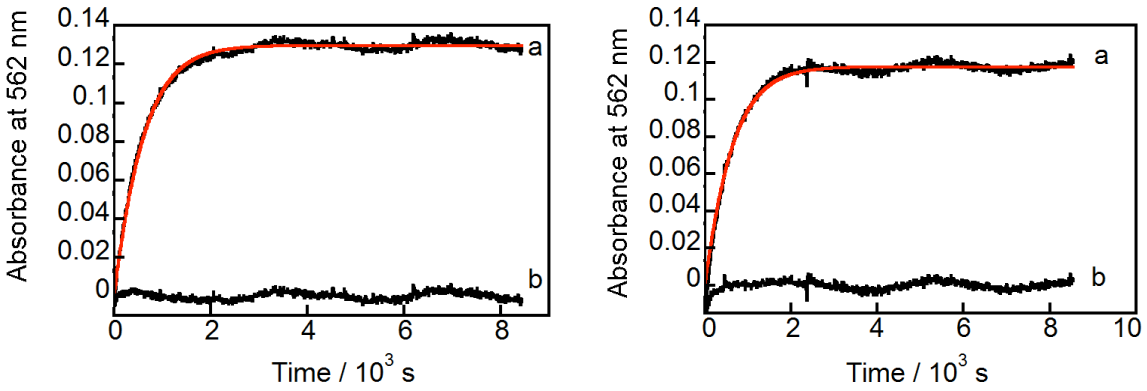

Figure 5.4: Absorbance at 562 nm during irradiation of DAE at 287 nm in cyclohexane. a) Experimental data (black) and numerical fit (red); b) Residuals between the experimental data and the fit. T = 15 ^{o}C. The two graphs correspond to independent experiments.

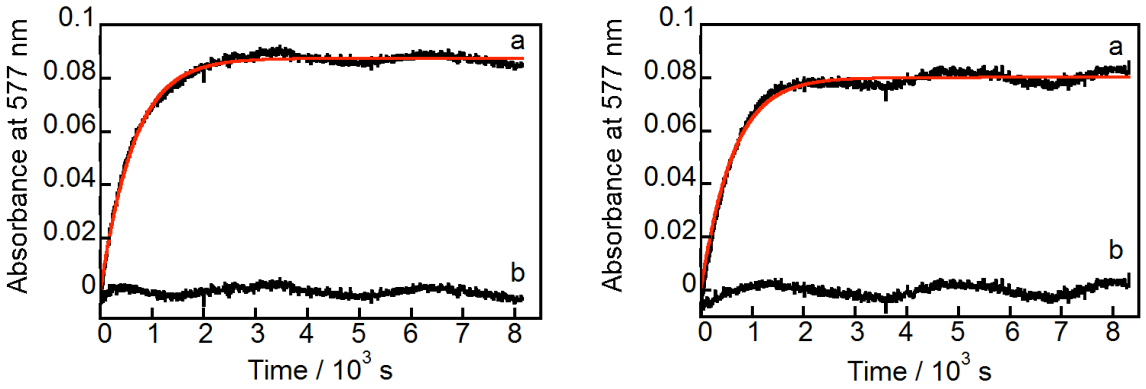

Figure 5.5: Absorbance at 577 nm during irradiation of DAE at 292 nm in NaC 80 mM/NaCl 0.2 M. a) Experimental data (black) and numerical fit (red); b) Residuals between the experimental data and the fit. T = 15 ^{o}C. The two graphs correspond to independent experiments.

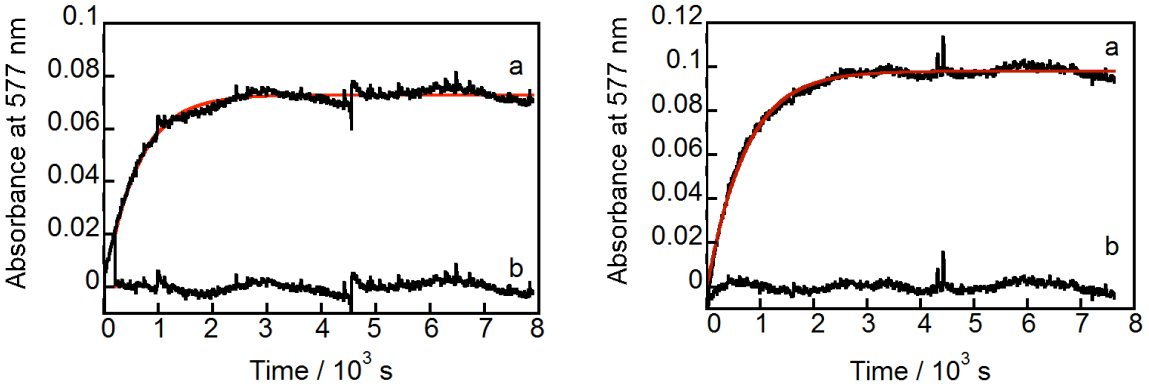

Figure 5.6: Absorbance at 577 nm during irradiation of DAE at 292 nm in NaC 80 mM/NaCl 1M. a) Experimental data (black) and numerical fit (red); b) Residuals between the experimental data and the fit. T = 15 ^{o}C. The two graphs correspond to independent experiments.

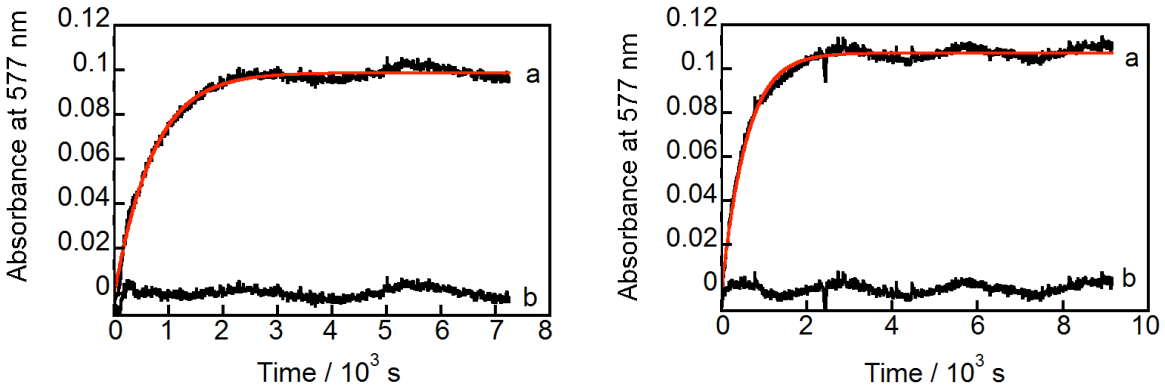

Figure 5.7: Absorbance at 577 nm during irradiation of DAE at 292 nm in NaDC 80 mM/NaCl 0.2 M. a) Experimental data (black) and numerical fit (red); b) Residuals between the experimental data and the fit.. T = 25 ^{o}C. The two graphs correspond to independent experiments.

The errors for Φ_{AB} and Φ_{BA} obtained from the fit were very small. For two independent experiments, the errors were also small in most of the conditions. However, the parameters determined by other experiments and fixed during the fitting also have an error associated with them. The parameter that most affects the quantum yields is $\varepsilon_{\mathbf{B}}^{\mathrm{vis}}$; therefore, the fitting was done considering the minimum and maximum values for $\varepsilon_{\mathbf{B}}^{\mathrm{vis}}$ and keeping other parameters as their average values. The results showed that the quantum yield could change as much as ± 0.02 when considering the experimental error of $\varepsilon_{\mathbf{B}}^{\mathrm{vis}}$. Therefore, an uncertainty of ± 0.02 was assumed for all the quantum yield values except where a larger error was observed for independent experiments. The values of Φ_{AB} and Φ_{BA} for DAE isomerization irradiating at the isosbestic point was found to be, within error, the same in all the conditions studied (Table 5.1).

Table 5.1: Quantum yield for the photochemical isomerization of DAE irradiated at the isosbestic point[a]

Medium/ irradiation wavelength	Φ_{AB}	Φ_{BA}
Cyclohexane (2) / 287 nm	0.39 ± 0.02	0.07 ± 0.02
NaC 80 mM/NaCl 0.2 M (2) / 292 nm	0.39 ± 0.02	0.06 ± 0.02
NaC 80 mM/NaCl 1 M (2) / 292 nm	0.36 ± 0.03	0.07 ± 0.02
NaDC 80 mM/NaCl 0.2 M (2) / 292 nm	0.36 ± 0.03	0.05 ± 0.02

[a]The numbers in parenthesis correspond to independent experiments.

The photocoloration of NSP was studied irradiating the solutions at the isosbestic point. The reaction was carried out in ethanol (Figure 5.8) and in aqueous solution containing NaC 80 mM/NaCl 0.2 M (Figure 5.9), NaC 80 mM/NaCl 1.0 M (Figure 5.10), NaDC 80 mM/NaCl 0.2 M (Figure 5.11) and NaTC 80 mM/NaCl 0.2 M (Figure 5.12). Two independent experiments were performed for each condition mentioned.

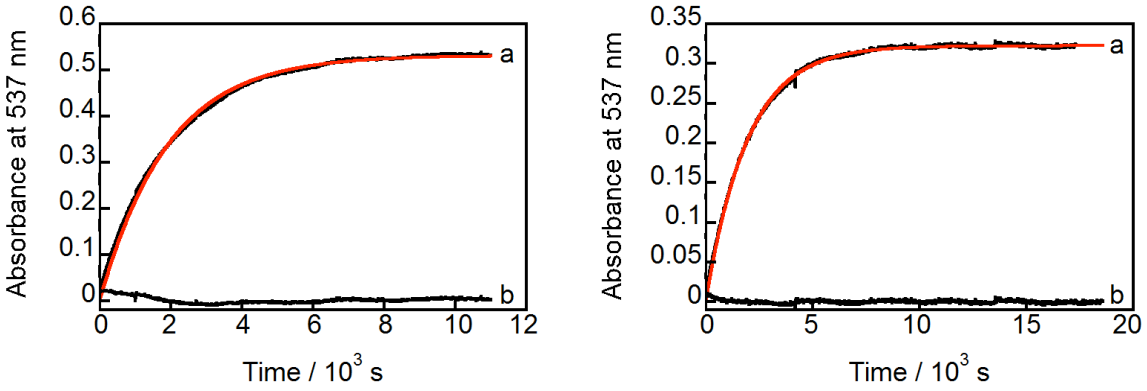

Figure 5.8: Absorbance at 537 nm during irradiation of NSP at 298 nm in ethanol. a) Experimental data (black) and numerical fit (red); b) Residuals between the experimental data and the fit. T = 15 °C. The two graphs correspond to independent experiments.

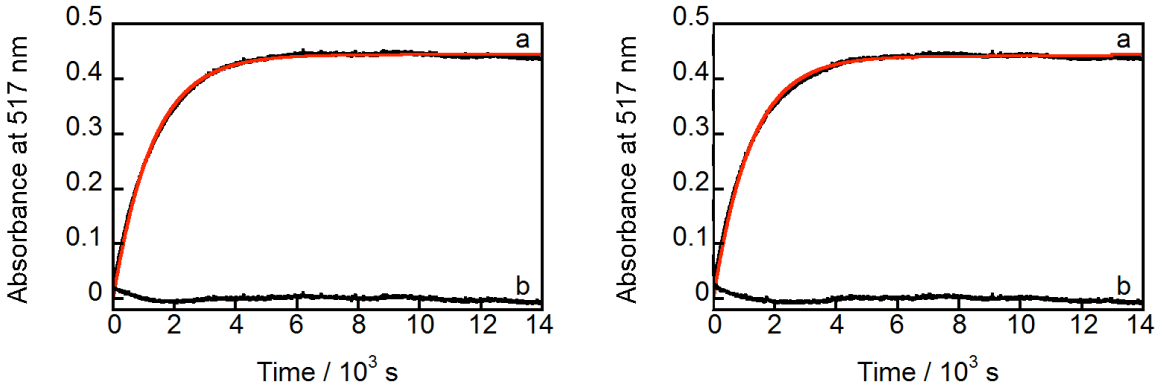

Figure 5.9: Absorbance at 517 nm during irradiation of NSP at 299 nm in NaC 80 mM/NaCl 0.2 M. a) Experimental data (black) and numerical fit (red); b) Residuals between the experimental data and the fit. T = 15 ^{o}C. The two graphs correspond to independent experiments.

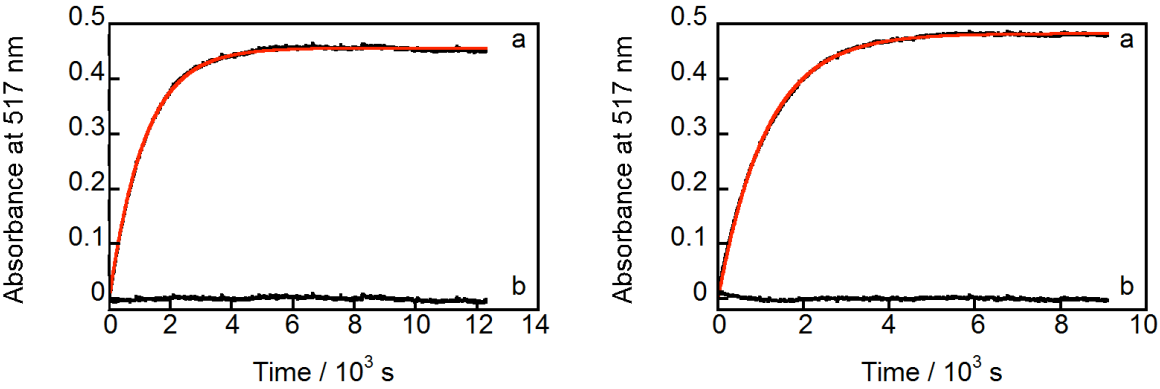

Figure 5.10: Absorbance at 517 nm during irradiation of NSP at 299 nm in NaC 80 mM/NaCl 1.0 M. a) Experimental data (black) and numerical fit (red); b) Residuals between the experimental data and the fit. T = 15 ^{o}C. The two graphs correspond to independent experiments.

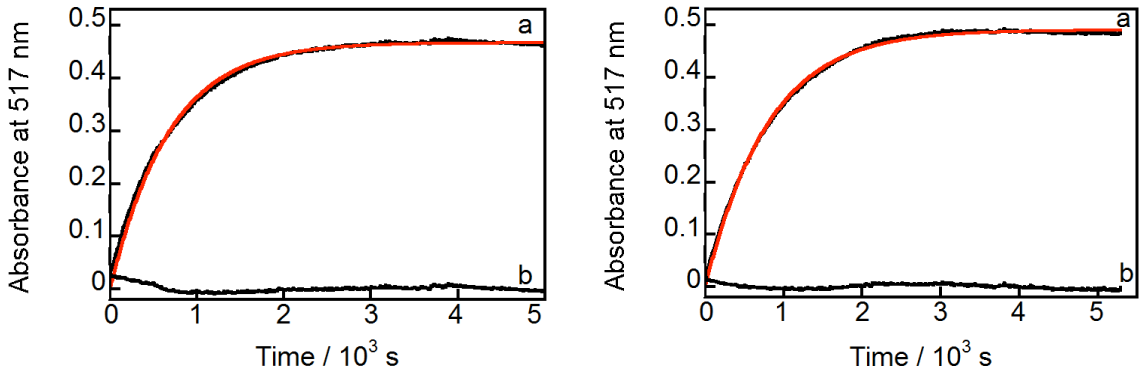

Figure 5.11: Absorbance at 517 nm during irradiation of NSP at 302 nm in NaDC 80 mM/NaCl 0.2 M. a) Experimental data (black) and numerical fit (red); b) Residuals for the fit. T = 25 °C. The two graphs correspond to independent experiments.

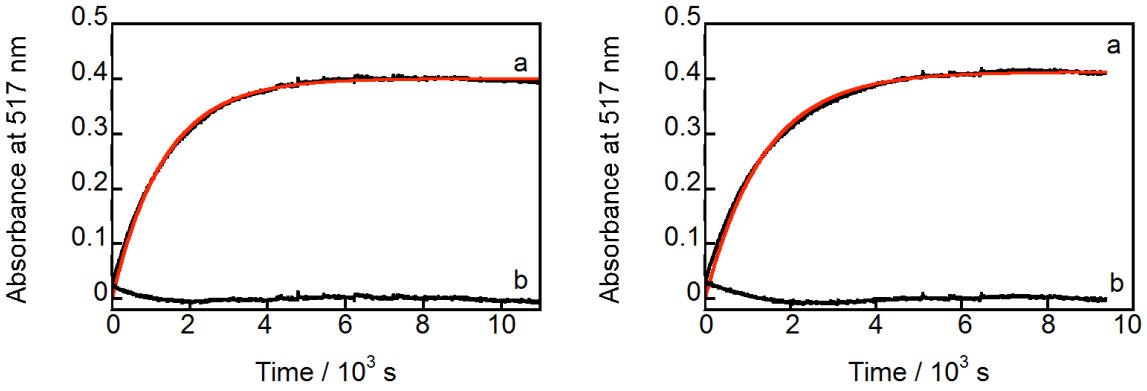

Figure 5.12: Absorbance at 517 nm during irradiation of at 299 nm in NaTC 80 mM/NaCl 0.2 M a) Experimental data (black) and numerical fit (red); b) Residuals between the experimental data and the fit. T = 15 °C. The two graphs correspond to independent experiments.

As observed for DAE, the error on Φ_{AB} and Φ_{BA} was very small for the fit and for independent experiments in most of the conditions. The fitting was then performed considering the experimental error on $\varepsilon_{\mathbf{B}}^{vis}$, k_{AB} and k_{BA}. The values of Φ_{AB} and Φ_{BA} vary around ± 0.01 depending on the experimental error on these fixed parameters. Therefore, the quantum yields were expressed with an error of ± 0.01 unless a larger error was

obtained for independent experiments. Differently from DAE, the quantum yield for the photocoloration of NSP is greatly affected by the medium. Both Φ_{AB} and Φ_{BA} are smaller in ethanol than in aqueous solutions containing bile salt. The value of Φ_{AB} also depends on the structure of the bile salt. The largest value for Φ_{AB} was found in the presence of NaDC and the smallest one in the presence of NaTC (Table 5.2).

Table 5.2: Quantum yield for the photochemical isomerisation of NSP irradiated at the isosbestic point[a]

Medium/ irradiation wavelength	Φ_{AB}	Φ_{BA}
Ethanol (2) / 298 nm	0.15 ± 0.01	0.04 ± 0.01
NaC 80 mM/NaCl 0.2 M (2) / 299 nm	0.30 ± 0.01	0.14 ± 0.01
NaC 80 mM/NaCl 1 M (2) / 299 nm	0.32 ± 0.01	0.15 ± 0.02
NaDC 80 mM/NaCl 0.2 M (2) / 302 nm	0.51 ± 0.03	0.15 ± 0.02
NaTC 80 mM/NaCl 0.2 M (2) / 299 nm	0.26 ± 0.01	0.15 ± 0.01

[a]The numbers in parenthesis correspond to independent experiments.

5.6 Discussion

The methods to determine the quantum yield of photochromic reactions can be divided into photostationary and photokinetic methods. The photostationary method consists of evaluating the photostationary state in different reaction conditions. In 1967, Fisher[105] described a procedure to determine the absorption spectrum for an isomer **B** at equilibrium with the isomer **A** in a photoisomerization reaction. The solution had to be irradiated at two wavelengths and the photostationary state obtained was analyzed

assuming that the ratio Φ_{AB}/Φ_{BA} was the same at both wavelengths. The absorption spectrum of **A** had to be known and the system had to be thermally and photochemically stable. Others groups employed the photostationary method to determine quantum yields and a series of assumptions had to be made depending on the complexity of the system.[106-108]

The photokinetic method analyzes the kinetic curves obtained by irradiation with monochromatic light. The set of equations used in this method was first described by Zimermann[109] in 1958. Pimienta et al. successfully determined Φ_{AB}, Φ_{BA} and the ε value for the colored form of a spiropyran,[89] a spironaphthoxazine[103] and a spirooxazine.[110] They used numerical analysis to fit kinetic curves of samples irradiated at two wavelengths. In these studies, the quantum yields were also assumed to be wavelength independent. The photokinetic method described in this thesis analyses the data for irradiation at a single wavelength. This is advantageous, since some studies show that the quantum yield of DAE can change with the irradiation wavelength.[41,80,111] Also, this method determines absolute quantum yields instead of relying on the comparison with the colorability of another compound.

For the isomerization of DAE, the quantum yield values obtained were the same in bile salt solutions and cyclohexane. The quantum yield for this reaction takes into account the amount of anti-parallel conformers in solution, which are the active species that undergo the cyclization reaction. Therefore, the results seem to indicate that the solvent does not affect neither the amount of anti-parallel conformers nor the quantum yield for the conversion of anti-parallel DAE_a into DAE_b. Another possibility is that

the quantum yield is affected by the solvent but the amount of anti-parallel conformers is also affected and compensates this effect.

A change in the solvent can affect the energy levels of A and B to different extents. The relaxation process can be more effective in some conditions than in others, resulting in quantum yields that differ from solvent to solvent. Unlike DAE, the isomers involved in the photochromism of NSP have very different polarities. As discussed in Chapter 4, the colored isomer NSP_b is a zwitterionic species that is located in a polar environment inside the bile salt aggregates. Therefore, a change in the medium could affect the quantum yield for NSP and not for DAE. Chibisov and Görner[112] reported that the quantum yield for the coloration of NSP decreases in more polar solvent. For different bile salts that would indicate that the polarity order is NaDC<NaC<NaTC. From the analysis of the equilibrium constants for the dark reaction, the same polarity order was observed. According to pyrene I/III ratio, the polarity on primary aggregates also follows this trend.[113,114] Considering the equilibrium constants, a smaller quantum yield would be expected for the solution of NaC containing NaCl 1 M compared to the solution of NaC containing NaCl 0.2 M. However, the quantum yield is the same in both conditions. Also, the quantum yield in ethanol is smaller than in solutions containing bile salts, although the wavelength of maximum absorption for NSP_b indicates that the environment is more polar in bile salts than in ethanol. These results indicate that bile salts are complex systems that have specific interactions and cannot be analyzed exclusively in terms of polarity.

Both NSP and DAE could be switched between their colored and colorless isomers in aqueous solutions containing bile salts. The solubility achieved allows the use of these

systems where aqueous medium is required, for instance in biological applications. Moreover, the rate constants for the decomposition reaction, dark reaction and photocoloration of NSP could be modulated by changing the bile salt and the concentration of NaCl in the system. The proven ability of bile salts to alter reactivity is interesting for applications of the systems presented in this thesis, and should also be explored for the reaction of other compounds.

6 Conclusion

The studies presented in this thesis explore the effect of bile salt aggregates on the photochromism of NSP and DAE. These aggregates provide solubilization of NSP and DAE in water and affect the reactivity of NSP.

The relaxation kinetics for the dark reaction of NSP can be modulated by the concentrations of NaC and NaCl and also by the structure of the bile salt. The dark reaction rate constant increases with the increase on NaCl concentration and at a smaller degree with the increase on the NaC concentration. For different bile salts, the dark reaction rate constant is smaller in NaTC and has approximately the same value in NaC and NaDC. The changes could be due to different polar environments inside the aggregates. The presence of bile salts also slows down the decomposition of NSP compared to the decomposition of water-soluble derivatives in water.

The determination of quantum yields for photochromic systems is not a trivial task. A photokinetic method was developed and has the advantage of analyzing a single kinetic curve. The sample is irradiated with monochromatic light at a controlled temperature while the absorbance of the colored isomer is monitored. In order to use this method, the molar absorptivity coefficient of both isomers has to be determined by an independent experiment. The quantum yield for the coloration and decoloration of DAE and NSP was determined at the isosbestic point. For DAE, Φ_{AB} and Φ_{BA} are the same in bile salts and cyclohexane. The quantum yield for the coloration of NSP depends on the bile salt employed and increases in the order NaTC < NaC < NaDC. A method using HPLC was

developed to determine the molar absorptivity coefficient of the colored forms of NSP and DAE. This method has the advantage of not requiring the isolation of the isomers.

7 Bibliography

(1) Bouas-Laurent, H.; Durr, H. *Pure Appl. Chem.* **2001**, *73*, 639.

(2) Irie, M. *Proc. Jpn. Acad., Ser. B* **2010**, *86*, 472.

(3) Brown, G. H. In *Photochromism*; Brown, G. H., Ed.; Wiley-Interscience: New York, 1971; Vol. 3, p 1.

(4) Irie, M. *Chem. Rev.* **2000**, *100*, 1683.

(5) Vernon, L. P.; Ke, B. In *Photochromism*; Brown, G. H., Ed.; Wiley-Interscience: New York, 1971; Vol. 3, p 687.

(6) Hampp, N. *Chem. Rev.* **2000**, *100*, 1755.

(7) Förster, T. *Pure Appl. Chem.* **1970**, *24*, 443.

(8) Gauglitz, G. In *Photochromism: Molecules and Systems: Revised Edition*; Dürr, H., Bouas-Laurent, H., Eds.; Elsevier Science B.V.: Amsterdam, 2003, p 15.

(9) Appriou, P.; Guglielmetti, R.; Garnier, F. *J. Photochem.* **1978**, *8*, 145.

(10) McArdle, C. B.; Blair, H.; Barraud, A.; Ruaudel-Teixier, A. *Thin Solid Films* **1983**, *99*, 181.

(11) Zhang, C.; Zhang, Z.; Fan, M.; Yan, W. *Dyes Pigm.* **2008**, *76*, 832.

(12) Tomasulo, M.; Yildiz, I.; Raymo, F. M. *Inorg. Chim. Acta* **2007**, *360*, 938.

(13) Gaeva, E. B.; Pimienta, V.; Micheau, J. C.; Metelitsa, A. V.; Voloshin, N. A. *Mol. Cryst. Liq. Cryst.* **2005**, *430*, 81.

(14) Yokoyama, Y.; Shiroyama, T. *Chem. Lett.* **1995**, 71.

(15) Van, G. B. *Mol. Cryst. Liq. Cryst. Sci. Technol., Sect. A* **2000**, *344*, 57.

(16) Fischer, E.; Hirshberg, Y. *J. Chem. Soc.* **1952**, 4522.

(17) Hirshberg, I. Y.; Fischer, E. *J. Chem. Soc.* **1954**, 297.

(18) Hirshberg, Y.; Fischer, E. *J. Chem. Soc.* **1954**, 3129.

(19) Guglielmetti, R. In *Photochromism: Molecules and Systems: Revised Edition*; Dürr, H., Bouas-Laurent, H., Eds.; Elsevier Science B.V.: Amsterdam, 2003, p 314.

(20) Bercovici, T.; Heiligman-Rim, R.; Fischer, E. *Mol. Photochem.* **1969**, *1*, 23.

(21) Koelsch, C. F. *J. Org. Chem.* **1951**, *16*, 1362.

(22) Heiligman-Rim, R.; Hirshberg, Y.; Fischer, E. *J. Phys. Chem.* **1962**, *66*, 2465.

(23) Ernsting, N. P.; Arthen-Engeland, T. *J. Phys. Chem.* **1991**, *95*, 5502.

(24) Gorner, H. *Phys. Chem. Chem. Phys.* **2001**, *3*, 416.

(25) Barachevskii, V. A.; Karpov, R. E. *High Energy Chem.* **2007**, *41*, 188.

(26) Krongauz, V. A.; Parshutkin, A. A. *Photochem. Photobiol.* **1972**, *15*, 503.

(27) Krongauz, V. A.; Fishman, S. N.; Goldburt, E. S. *J. Phys. Chem.* **1978**, *82*, 2469.

(28) Kalisky, Y.; Williams, D. J. *Macromolecules* **1984**, *17*, 292.

(29) Onai, Y.; Mamiya, M.; Kiyokawa, T.; Okuwa, K.; Kobayashi, M.; Shinohara, H.; Sato, H. *J. Phys. Chem.* **1993**, *97*, 9499.

(30) Onai, Y.; Kasatani, K.; Kobayashi, M.; Shinohara, H.; Sato, H. *Chem. Lett.* **1990**, 1809.

(31) Hirshberg, Y. *J. Am. Chem. Soc.* **1956**, *78*, 2304.
(32) Ikeda, S.; Saso, Y. *Colloids Surf.* **1992**, *67*, 21.
(33) Tamaki, T.; Sakuragi, M.; Ichimura, K.; Aoki, K.; Arima, I. *Polym. Bull.* **1990**, *24*, 559.
(34) Zhou, J.; Sui, Q.; Huang, B. *J. Photochem. Photobiol., A* **1998**, *117*, 129.
(35) Hochstrasser, R. M. *Pure Appl. Chem.* **1980**, *52*, 2683.
(36) Waldeck, D. H. *Chem. Rev.* **1991**, *91*, 415.
(37) Saltiel, J.; Sun, Y. P. In *Photochromism: Molecules and Systems: Revised Edition*; Dürr, H., Bouas-Laurent, H., Eds.; Elsevier Science B.V.: Amsterdam, 2003, p 64.
(38) Orlandi, G.; Siebrand, W. *Chem. Phys. Lett.* **1975**, *30*, 352.
(39) Srinivasan, R.; Powers, J. C., Jr. *J. Chem. Phys.* **1963**, *39*, 580.
(40) Laarhoven, W. H. *Pure Appl. Chem.* **1984**, *56*, 1225.
(41) Irie, M.; Mohri, M. *J. Org. Chem.* **1988**, *53*, 803.
(42) Kellogg, R. M.; Groen, M. B.; Wynberg, H. *J. Org. Chem.* **1967**, *32*, 3093.
(43) Nakamura, S.; Irie, M. *J. Org. Chem.* **1988**, *53*, 6136.
(44) Irie, M.; Sakemura, K.; Okinaka, M.; Uchida, K. *J. Org. Chem.* **1995**, *60*, 8305.
(45) Irie, M.; Miyatake, O.; Uchida, K. *J. Am. Chem. Soc.* **1992**, *114*, 8715.
(46) Takeshita, M.; Irie, M. *Chem. Commun.* **1997**, 2265.
(47) Takeshita, M.; Kato, N.; Kawauchi, S.; Imase, T.; Watanabe, J.; Irie, M. *J. Org. Chem.* **1998**, *63*, 9306.
(48) Yamada, M.; Takeshita, M.; Irie, M. *Mol. Cryst. Liq. Cryst. Sci. Technol., Sect. A* **2000**, *345*, 107.
(49) Hofmann, A. F.; Mysels, K. J. *Colloids Surf.* **1988**, *30*, 145.
(50) Hofmann, A. F.; Eckmann, L. *Proc. Natl. Acad. Sci. U. S. A.* **2006**, *103*, 4333.
(51) Begley, M.; Gahan, C. G. M.; Hill, C. *FEMS Microbiol. Rev.* **2005**, *29*, 625.
(52) Carey, M. C.; Small, D. M. *J. Clin. Invest.* **1978**, *61*, 998.
(53) Haslewood, G. A. D. *J. Lipid Res.* **1967**, *8*, 535.
(54) Small, D. M.; Penkett, S. A.; Chapman, D. *Biochim Biophys Acta* **1969**, *176*, 178.
(55) Kawamura, H.; Murata, Y.; Yamaguchi, T.; Igimi, H.; Tanaka, M.; Sugihara, G.; Kratohvil, J. P. *J. Phys. Chem.* **1989**, *93*, 3321.
(56) Esposito, G.; Giglio, E.; Pavel, N. V.; Zanobi, A. *J. Phys. Chem.* **1987**, *91*, 356.
(57) Campanelli, A. R.; Candeloro, d. S. S.; Giglio, E.; Pavel, N. V.; Quagliata, C. *J. Inclusion Phenom. Mol. Recognit. Chem.* **1989**, *7*, 391.
(58) Madenci, D.; Egelhaaf, S. U. *Curr. Opin. Colloid Interface Sci.* **2010**, *15*, 109.
(59) O'Connor, C. J.; Ch'ng, B. T.; Wallace, R. G. *J. Colloid Interface Sci.* **1983**, *95*, 410.
(60) Norman, A. *Acta Chem. Scand.* **1960**, *14*, 1300.
(61) Ju, C.; Bohne, C. *Photochem. Photobiol.* **1996**, *63*, 60.

(62) Rinco, O.; Nolet, M.-C.; Ovans, R.; Bohne, C. *Photochem. Photobiol. Sci.* **2003**, *2*, 1140.

(63) Amundson, L. L.; Li, R.; Bohne, C. *Langmuir* **2008**, *24*, 8491.

(64) Li, R.; Carpentier, E.; Newell, E. D.; Olague, L. M.; Heafey, E.; Yihwa, C.; Bohne, C. *Langmuir* **2009**, *25*, 13800.

(65) Mazer, N. A.; Carey, M. C.; Kwasnick, R. F.; Benedek, G. B. *Biochemistry* **1979**, *18*, 3064.

(66) Barros, T. C.; Stefaniak, K.; Holzwarth, J. F.; Bohne, C. *J. Phys. Chem. A* **1998**, *102*, 5639.

(67) Murphy, R. S.; Barros, T. C.; Mayer, B.; Marconi, G.; Bohne, C. *Langmuir* **2000**, *16*, 8780.

(68) Auletta, T.; de Jong, M. R.; Mulder, A.; van Veggel, F. C. J. M.; Huskens, J.; Reinhoudt, D. N.; Zou, S.; Zapotoczny, S.; Schönherr, H.; Vancso, G. J.; Kuipers, L. *J. Amer. Chem. Soc.* **2004**, *126*, 1577.

(69) Bohne, C. *Langmuir* **2006**, *22*, 9100.

(70) Norman, A. *Acta Chem. Scand.* **1960**, *14*, 1295.

(71) Roda, A.; Hofmann, A. F.; Mysels, K. J. *J. Biol. Chem.* **1983**, *258*, 6362.

(72) Crano, J. C.; Flood, T.; Knowles, D.; Kumar, A.; Van Gemert, B. *Pure Appl. Chem.* **1996**, *68*, 1395.

(73) Kawata, S.; Kawata, Y. *Chemical Reviews* **2000**, *100*, 1777.

(74) Levy, D.; Einhorn, S.; Avnir, D. *Journal of Non-Crystalline Solids* **1989**, *113*, 137.

(75) Willner, I. *Acc. Chem. Res.* **1997**, *30*, 347.

(76) Li, Y.; Holzwarth, J. F.; Bohne, C. *Langmuir* **2000**, *16*, 2038.

(77) Hatchard, C. G.; Parker, C. A. *Proc. R. Soc. London, Ser. A* **1956**, *235*, 518.

(78) Murov, S. L.; Carmichael, I.; Hug, G. L. *Handbook of Photochemistry*; 2nd ed.; Marcel Dekker, Inc.: New York, 1993.

(79) Shibata, K.; Kobatake, S.; Irie, M. *Chem. Lett.* **2001**, 618.

(80) Santos, A. R.; Ballardini, R.; Belser, P.; Gandolfi, M. T.; Iyer, V. M.; Moggi, L. *Photochem. Photobiol. Sci.* **2009**, *8*, 1734.

(81) Skoog, D. A.; Holler, F. J.; Nieman, T. A. *Princípios de Análise Instrumental*; 5 ed.; Bookman: Porto Alegre, 2002.

(82) Fuentealba, D.; Thurber, K.; Bovero, E.; Pace, T. C. S.; Bohne, C. *Photochem. Photobiol. Sci.* **2011**.

(83) Flannery, J. B., Jr. *J. Am. Chem. Soc.* **1968**, *90*, 5660.

(84) Song, X.; Zhou, J.; Li, Y.; Tang, Y. *J. Photochem. Photobiol., A* **1995**, *92*, 99.

(85) Zhang, S.; Zhang, Q.; Ye, B.; Li, X.; Zhang, X.; Deng, Y. *J. Phys. Chem. B* **2009**, *113*, 6012.

(86) Heller, C. A.; Fine, D. A.; Henery, R. A. *J. Phys. Chem.* **1961**, *65*, 1908.

(87) di, N. M. R.; Gentili, P. L.; Romani, A.; Favaro, G. *ChemPhysChem* **2008**, *9*, 768.

(88) Ortica, F.; Romani, A.; Blackburn, F.; Favaro, G. *Photochem. Photobiol. Sci.* **2002**, *1*, 803.

(89) Pimienta, V.; Lavabre, D.; Levy, G.; Samat, A.; Guglielmetti, R.; Micheau, J. C. *J. Phys. Chem.* **1996**, *100*, 4485.

(90) Keum, S. R.; Hur, M. S.; Kazmaier, P. M.; Buncel, E. *Can. J. Chem.* **1991**, *69*, 1940.

(91) Li, R.; Santos, C. S.; Norsten, T. B.; Morimitsu, K.; Bohne, C. *Chem. Commun.* **2010**, *46*, 1941.

(92) Stafforst, T.; Hilvert, D. *Chem. Commun.* **2009**, 287.

(93) Rinco, O.; Kleinman, M. H.; Bohne, C. *Langmuir* **2001**, *17*, 5781.

(94) Pattabiraman, M.; Kaanumalle, L. S.; Ramamurthy, V. *Langmuir* **2006**, *22*, 2185.

(95) Kratohvil, J. P.; Hsu, W. P.; Jacobs, M. A.; Aminabhavi, T. M.; Mukunoki, Y. *Colloid Polym. Sci.* **1983**, *261*, 781.

(96) Garidel, P.; Hildebrand, A.; Neubert, R.; Blume, A. *Langmuir* **2000**, *16*, 5267.

(97) Coello, A.; Meijide, F.; Rodriguez Nunez, E.; Vazquez Tato, J. *J. Phys. Chem.* **1993**, *97*, 10186.

(98) Güveli, D. E. *Colloid Polym. Sci.* **1986**, *264*, 707.

(99) Carey, M. C.; Small, D. M. *J Colloid Interface Sci* **1969**, *31*, 382.

(100) Rau, H. *J. Photochem.* **1984**, *26*, 221.

(101) Ottavi, G.; Ortica, F.; Favaro, G. *Int. J. Chem. Kinet.* **1999**, *31*, 303.

(102) Maafi, M. *Molecules* **2008**, *13*, 2260.

(103) Pimienta, V.; Froute, C.; Deniel, M. H.; Lavabre, D.; Guglielmetti, R.; Micheau, J. C. *J. Photochem. Photobiol., A* **1999**, *122*, 199.

(104) Jackson, R. L.; Lishan, D. G. *J. Phys. Chem.* **1984**, *88*, 5986.

(105) Fischer, E. *J. Phys. Chem.* **1967**, *71*, 3704.

(106) Rau, H.; Greiner, G. *EPA Newsl.* **1991**, *41*, 40.

(107) Gregoire, F.; Lavabre, D.; Micheau, J. C.; Gimenez, M.; Laplante, J. P. *J. Photochem.* **1985**, *28*, 261.

(108) Wilkinson, F.; Hobley, J.; Naftaly, M. *J. Chem. Soc., Faraday Trans.* **1992**, *88*, 1511.

(109) Zimmerman, G.; Chow, L.-Y.; Paik, U.-J. *J. Am. Chem. Soc.* **1958**, *80*, 3528.

(110) Gaeva, E. B.; Pimienta, V.; Delbaere, S.; Metelitsa, A. V.; Voloshin, N. A.; Minkin, V. I.; Vermeersch, G.; Micheau, J. C. *J. Photochem. Photobiol., A* **2007**, *191*, 114.

(111) Ern, J.; Bens, A. T.; Martin, H.-D.; Kuldova, K.; Trommsdorff, H. P.; Kryschi, C. *J. Phys. Chem. A* **2002**, *106*, 1654.

(112) Chibisov, A. K.; Görner, H. *J. Photochem. Photobiol., A* **1997**, *105*, 261.

(113) Zana, R.; Guveli, D. *J. Phys. Chem.* **1985**, *89*, 1687.

(114) Zhang, S.-Z.; Xie, J.-W.; Liu, C.-S. *Anal. Chem.* **2003**, *75*, 91.

Appendix A Determination of ε values for DAE and NSP

DAE in hexane – trial 1

Absorption spectrum and HPLC response curve of DAE_a (Figure A.1):

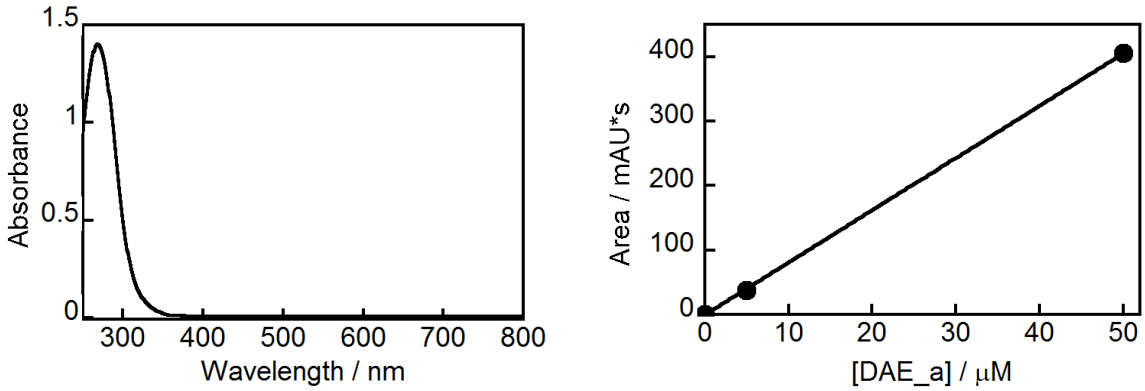

Figure A.1: Absorption spectrum (left) and HPLC response curve (right) of DAE_a 50 μM in hexane. The linear fit was set to pass through zero and has a slope of 8.1032; the correlation coefficient is 0.99997.

Absorption spectrum and HPLC chromatogram of DAE irradiated at 285 nm (Figure A.2):

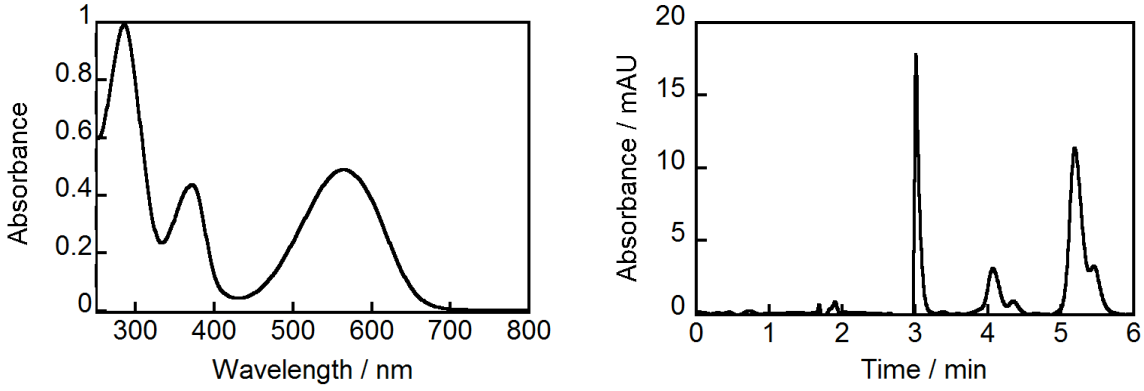

Figure A.2: Absorption spectrum (left) and HPLC chromatogram (right) of DAE 50 μM irradiated at 285 nm in hexane.

The area under the peaks at 4.1 and 4.3 min is 34.48 mAU × s, so the [DAE_a] is equal to 4.26 μM and the [DAE_b] is equal to 45.74 μM. The ε of DAE_b at 562 nm was found to be 1.07×10^4 cm^{-1} M^{-1} (Figure A.3).

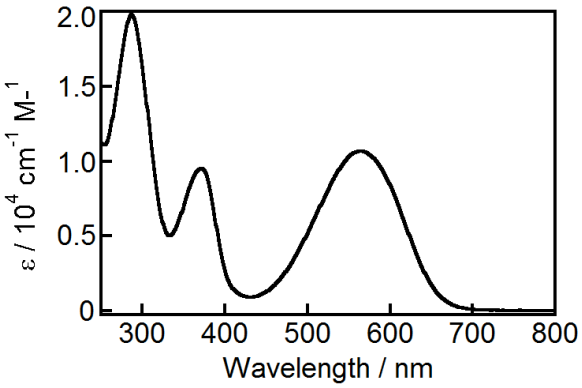

Figure A.3: Absorption spectrum of DAE_b in hexane.

DAE in hexane – trial 2

Absorption spectrum and HPLC response curve of DAE_a (Figure A.4):

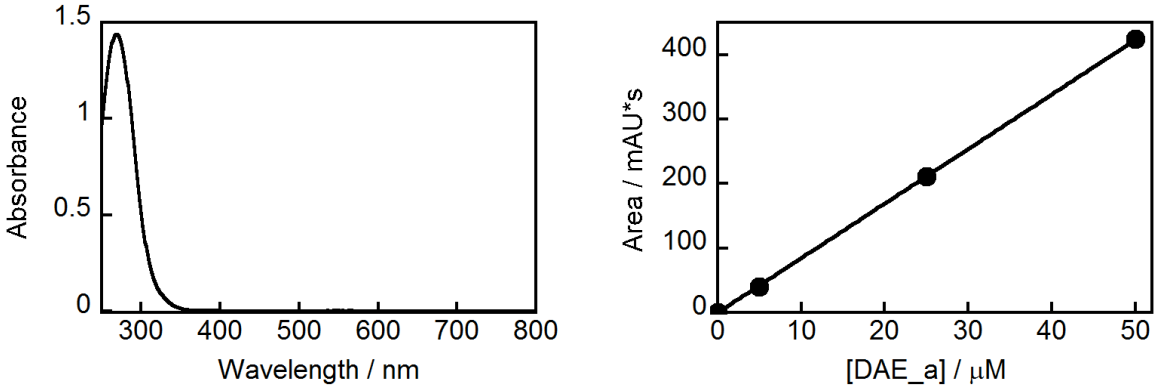

Figure A.4: Absorption spectrum (left) and HPLC response curve (right) of DAE_a 50 μM in hexane. The linear fit was set to pass through zero and has a slope of 8.463; the correlation coefficient is 0.99996.

Absorption spectrum and HPLC chromatogram of DAE irradiated at 287 nm (Figure A.5):

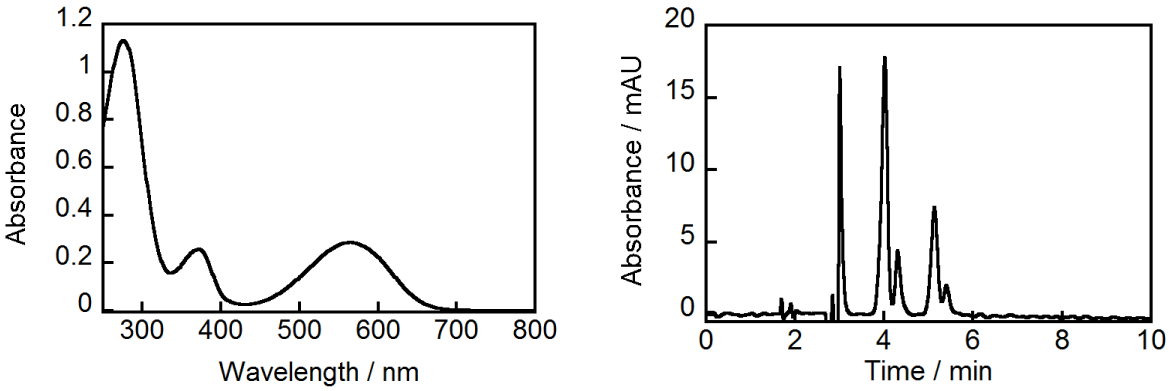

Figure A.5: Absorption spectrum (left) and HPLC chromatogram (right).of DAE 50 µM irradiated at 287 nm in hexane.

The area under the peaks at 4.1 and 4.3 min is 212.18 mAU × s, so the [DAE_a] is equal to 25.07 µM and the [DAE_b] is equal to 24.93 µM. The ε of DAE_b at 562 nm was found to be 1.14×10^4 cm^{-1} M^{-1} (Figure A.6).

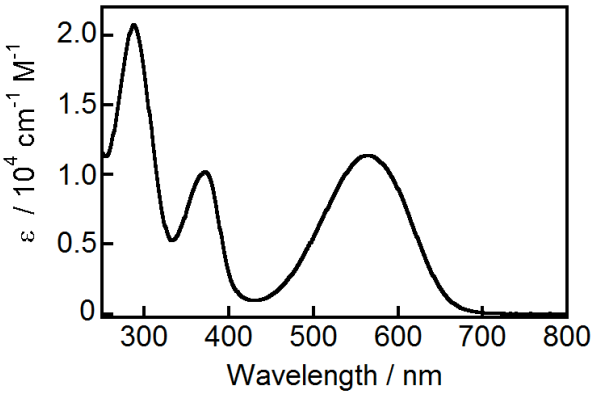

Figure A.6: Absorption spectrum of DAE_b in hexane.

DAE in NaC 80 mM/NaCl 0.2 M – trial 1

Absorption spectrum and HPLC response curve of DAE_a (Figure A.7):

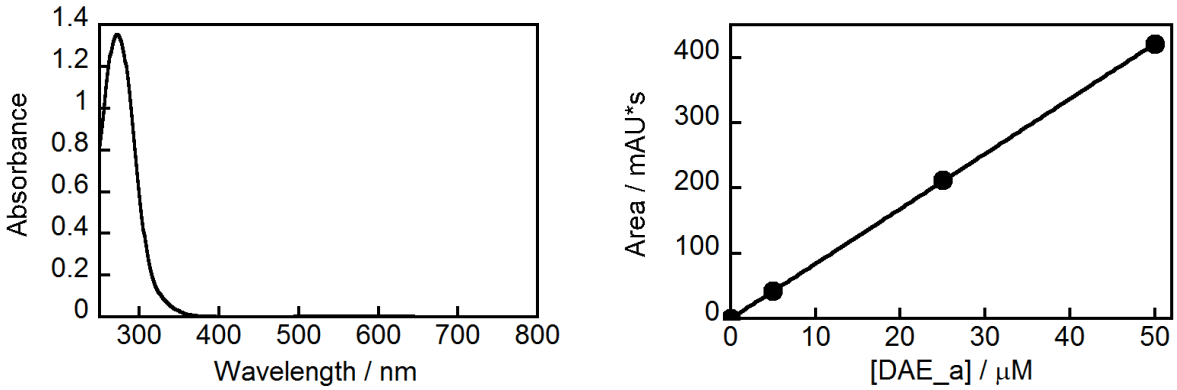

Figure A.7: Absorption spectrum (left) and HPLC response curve (right) of DAE_a 50 μM in NaC 80 mM/NaCl 0.2 M. The linear fit was set to pass through zero and has a slope of 8.426; the correlation coefficient is 0.99998.

Using the same work solution, two samples were irradiated at 287 nm and the absorption and chromatogram registered (Figure A.8):

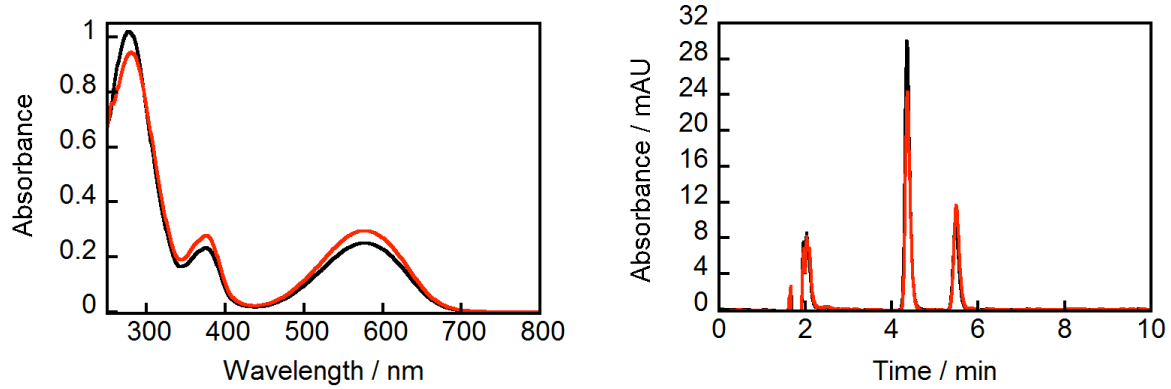

Figure A.8: Absorption spectra (left) and HPLC chromatogram (right).of DAE 50 μM irradiated at 287 nm in NaC 80 mM/NaCl 0.2 M. Sample 1 (---), sample 2 (---).

The area under the peak at 4.3 min is 240.5 mAU × s for sample 1 and 194.7 mAU × s for sample 2. Therefore, the [DAE_a] is equal to 28.54 μM and 23.11 μM, respectively. The [DAE_b] is equal to 21.46 μM and 26.89 μM, respectively. The ε of DAE_b at 577 nm was found to be in average 1.12×10^4 cm^{-1} M^{-1}(Figure A.9).

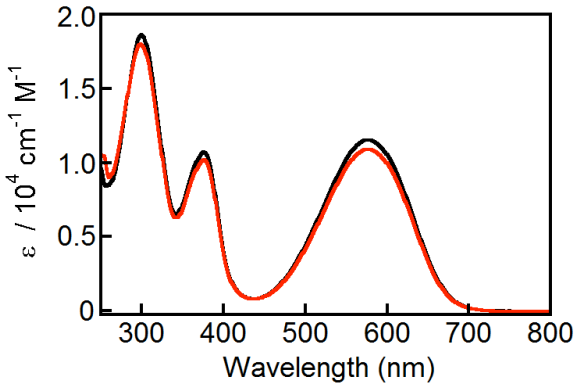

Figure A.9: Absorption spectra of DAE_b in NaDC 80 mM/NaCl 0.2. Sample 1 (---), sample 2 (---).

DAE in NaC 80 mM/NaCl 0.2 M – trial 2

Absorption spectrum and HPLC response curve of DAE_a (Figure A.10):

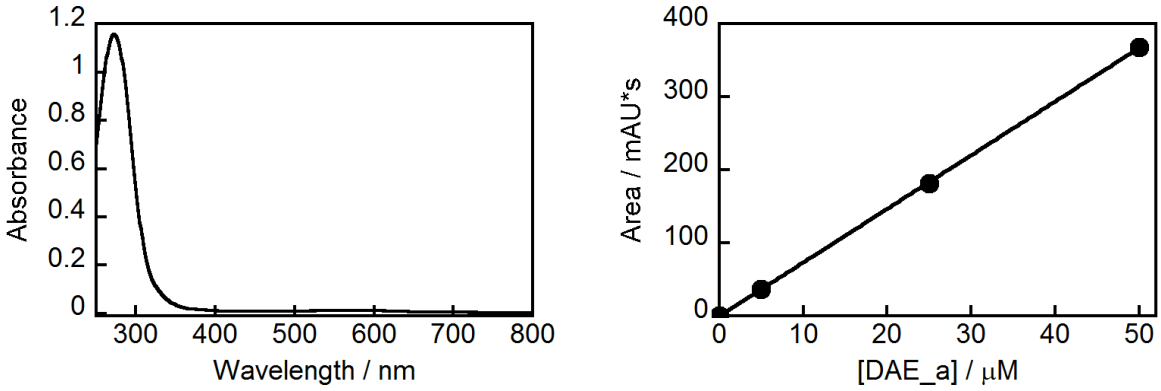

Figure A.10: Absorption spectrum (left) and HPLC response curve (right) of DAE_a 50 μM in NaC 80 mM/NaCl 0.2 M. The linear fit was set to pass through zero and has a slope of 7.3432; the correlation coefficient is 0.99996.

Absorption spectrum and HPLC chromatogram of DAE irradiated at 287 nm (Figure A.11):

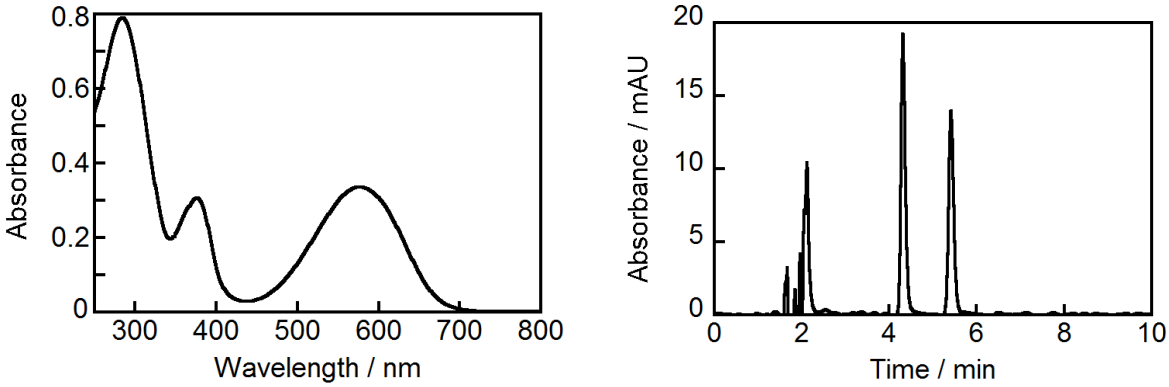

Figure A.11: Absorption spectrum (left) and HPLC chromatogram (right) of DAE 50 µM irradiated at 287 nm in NaC 80 mM/NaCl 0.2 M.

The area under the peak at 4.3 min is 134.3 mAU × s, so the [DAE_a] is equal to 18.29 µM and the [DAE_b] is equal to 31.71 µM. The ε of DAE_b at 577 nm was found to be 1.046×10^4 cm^{-1} M^{-1} (Figure A.12).

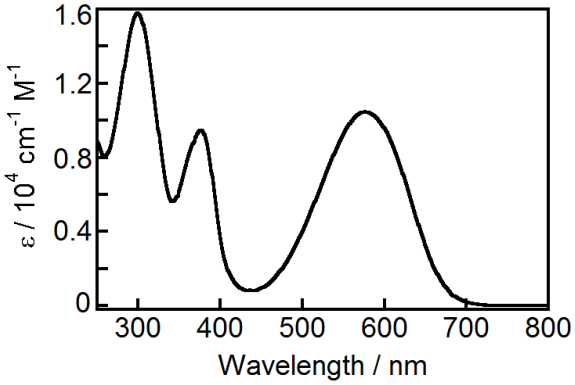

Figure A.12: Absorption spectrum of DAE_b in NaC 80 mM/NaCl 0.2 M.

DAE in NaDC 80 mM/NaCl 0.2 M – trial 1

Absorption spectrum and HPLC response curve of DAE_a (Figure A.13):

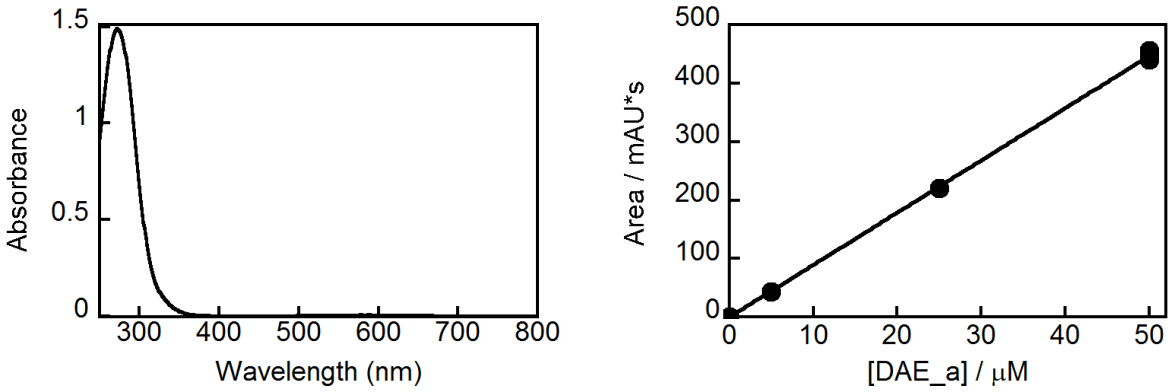

Figure A.13: Absorption spectrum (left) and HPLC response curve (right) of DAE_a 50 μM in NaDC 80 mM/NaCl 0.2 M. The linear fit was set to pass through zero and has a slope of 8.9346; the correlation coefficient is 0.99969.

Using the same work solution, three samples were irradiated at 287 nm and the absorption and chromatogram registered (Figure A.14).

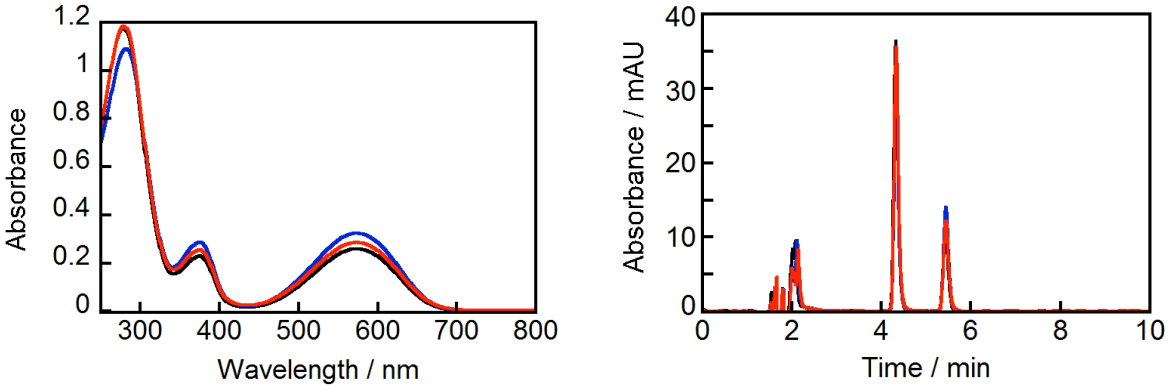

Figure A.14: Absorption spectra (left) and HPLC chromatogram (right).of DAE 50 μM irradiated at 287 nm in NaDC 80 mM/NaCl 0.2 M. Sample 1 (---), sample 2 (---), sample 3 (---).

The area under the peak at 4.3 min is 261.9 mAU × s for sample 1, 203.9 mAU × s for sample 2 and 253.9 mAU × s for sample 3. Therefore, the [DAE_a] is equal to 29.21 μM, 22.82 μM and 28.42 μM, respectively. The [DAE_b] is equal to 20.79 μM, 27.18μM and 21.58 μM, respectively. The ε of DAE_b at 577 nm was found to be in average 1.22 $\times 10^4$ cm^{-1} M^{-1} (Figure A.15).

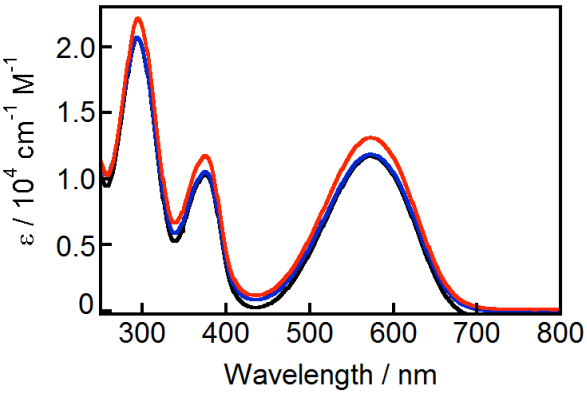

Figure A.15: Absorption spectra of DAE_b in NaDC 80 mM/NaCl 0.2. Sample 1 (black), sample 2 (blue), sample 3 (red).

DAE in NaDC 80 mM/NaCl 0.2 M – trial 2

Absorption spectrum and HPLC response curve of DAE_a (Figure A.16):

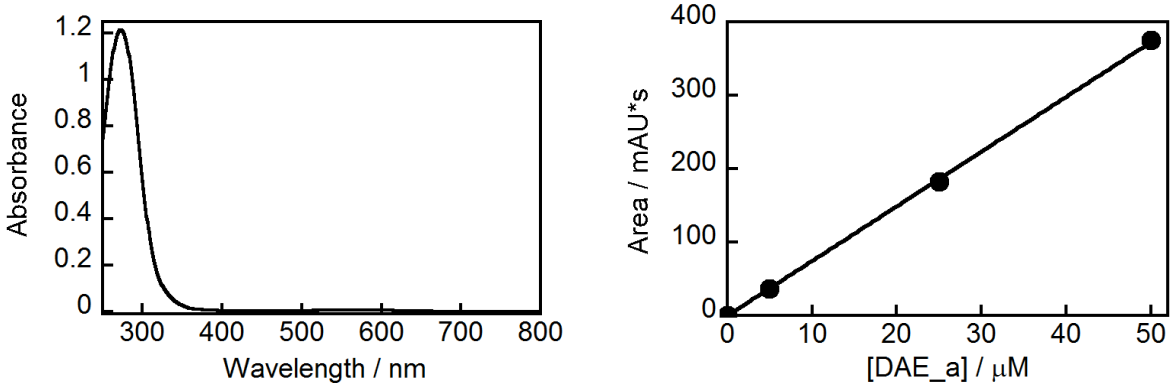

Figure A.16: Absorption spectrum (left) and HPLC response curve (right) of DAE_a 50 μM in NaDC 80 mM/NaCl 0.2 M. The linear fit was set to pass through zero and has a slope of 7.4527; the correlation coefficient is 0.99985.

Absorption spectrum and HPLC chromatogram of DAE irradiated at 287 nm (Figure A.17):

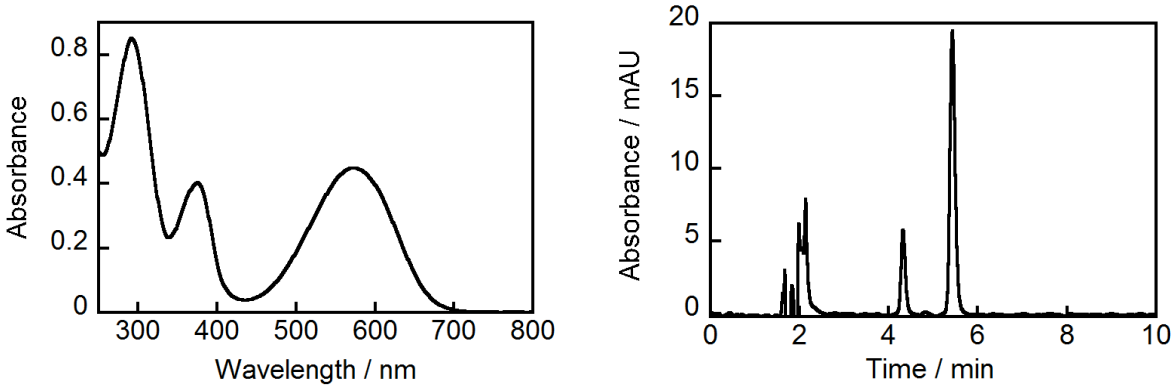

Figure A.17: Absorption spectrum (left) and HPLC chromatogram (right) of DAE 50 µM irradiated at 287 nm in NaDC 80 mM/NaCl 0.2 M.

The area under the peak at 4.3 min is 41.05 mAU × s, so the [DAE_a] is equal to 5.508 µM and the [DAE_b] is equal to 44.492 µM. The ε of DAE_b at 577 nm was found to be 1.00×10^4 cm^{-1} M^{-1} (Figure A.18).

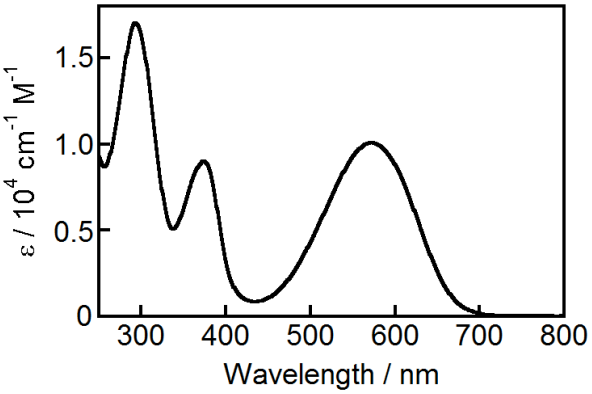

Figure A.18: Absorption spectrum of DAE_b in NaDC 80 mM/NaCl 0.2 M.

NSP in ethanol – trial 1

Absorption spectrum and HPLC response curve of NSP_a (Figure A.19):

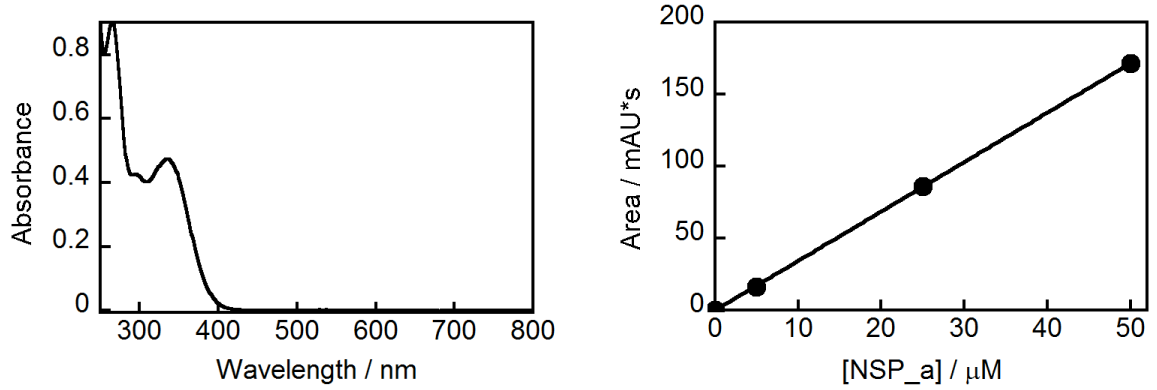

Figure A.19: Absorption spectrum (left) and HPLC response curve (right) of NSP_a 50 μM in ethanol. The linear fit was set to pass through zero and has a slope of 3.432; the correlation coefficient is 0.99997.

Absorption spectrum and HPLC chromatogram of NSP irradiated at 338 nm (Figure A.20):

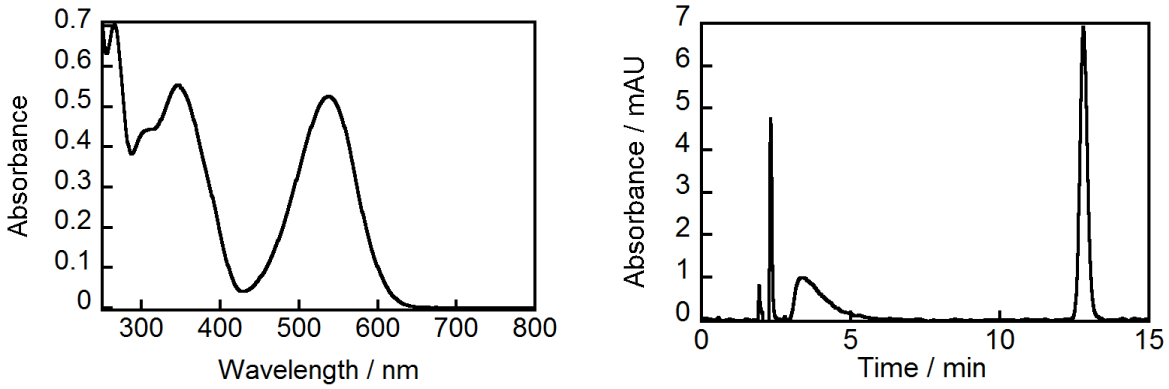

Figure A.20: Absorption spectrum (left) and HPLC chromatogram (right).of NSP 50 μM irradiated at 338 nm in ethanol.

The area under the peak at 12.8 min is 122.42 mAU × s, so the [NSP_a] is equal to 35.67 μM and the [NSP_b] is equal to 14.33 μM. The ε of NSP_b at 537 nm was found to be 3.65×10^4 cm^{-1} M^{-1} (Figure A.21).

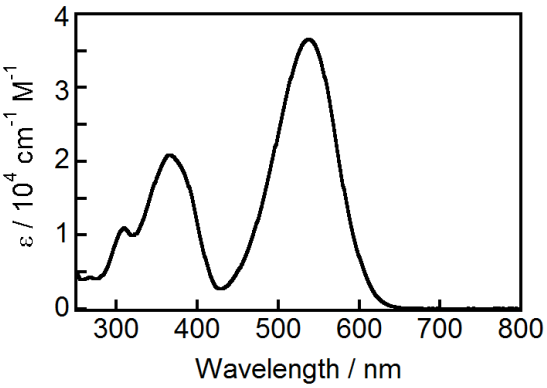

Figure A.21: Absorption spectrum of NSP_b in ethanol.

NSP in ethanol – trial 2

Absorption spectrum and HPLC response curve of NSP_a (Figure A.22):

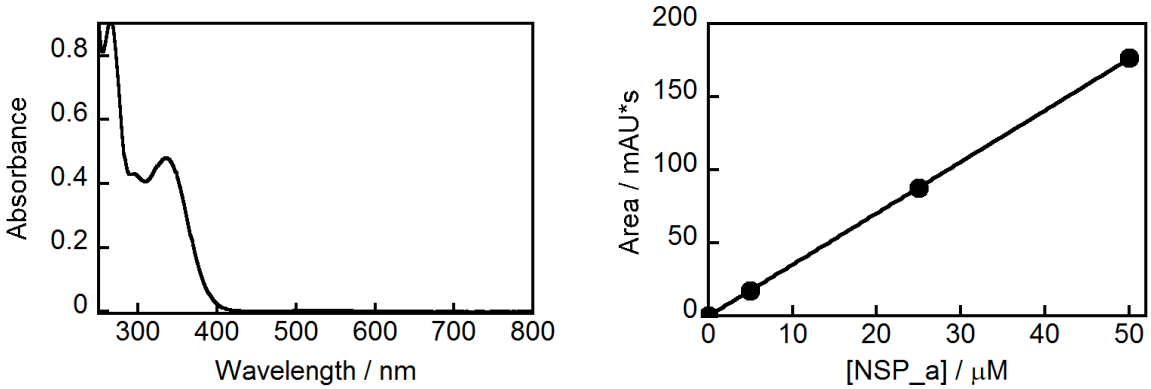

Figure A.22: Absorption spectrum (left) and HPLC response curve (right) of NSP_a 50 μM in ethanol. The linear fit was set to pass through zero and has a slope of 3.5191; the correlation coefficient is 0.99997.

Absorption spectrum and HPLC chromatogram of NSP irradiated at 338 nm (Figure A.23):

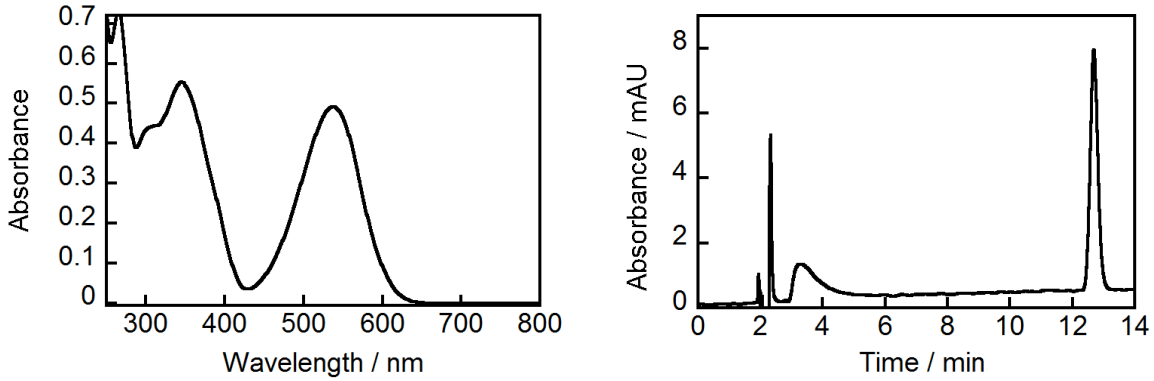

Figure A.23: Absorption spectrum (left) and HPLC chromatogram (right).of NSP 50 µM irradiated at 338 nm in ethanol.

The area under the peak at 12.8 min is 129.46 mAU × s, so the [NSP_a] is equal to 36.79 µM and the [NSP_b] is equal to 13.21 µM. The ε of NSP_b at 537 nm was found to be 3.70×10^4 cm^{-1} M^{-1} (Figure A.24).

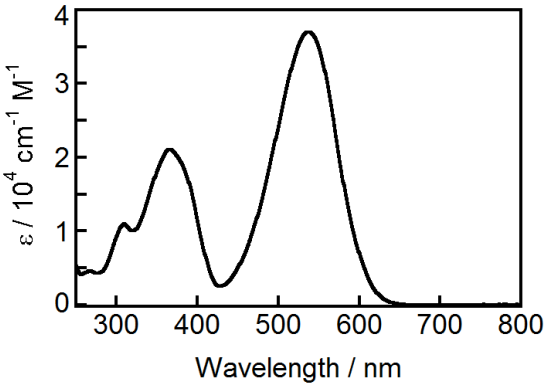

Figure A.24: Absorption spectrum of NSP_b in ethanol.

NSP in NaC 80 mM/NaCl 0.2 M – trial 1

Absorption spectrum and HPLC response curve of NSP_a (Figure A.25):

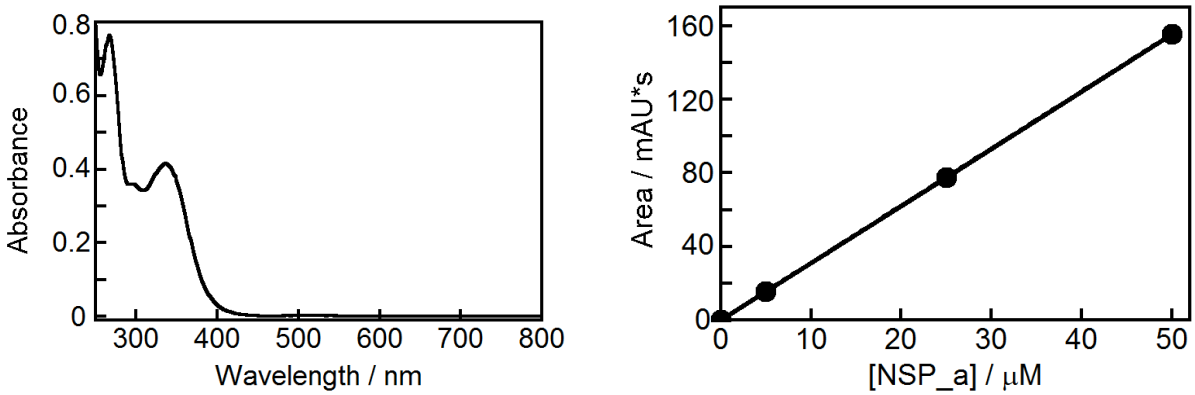

Figure A.25: Absorption spectrum (left) and HPLC response curve (right) of NSP_a 50 μM in NaC 80 mM/NaCl 0.2 M. The linear fit was set to pass through zero and has a slope of 3.1076; the correlation coefficient is 1.

Absorption spectrum and HPLC chromatogram of NSP irradiated at 338 nm (Figure A.26):

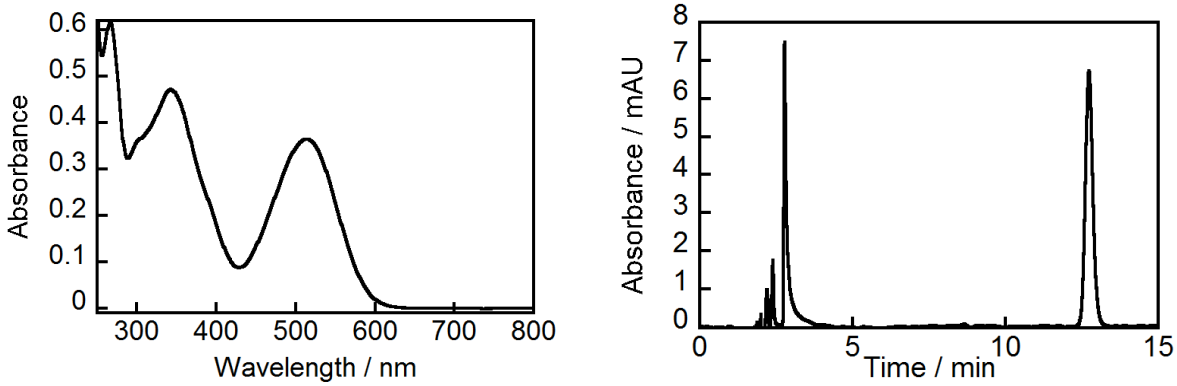

Figure A.26: Absorption spectrum (left) and HPLC chromatogram (right).of NSP 50 μM irradiated at 338nm nm in NaC 80 mM/NaCl 0.2 M.

The area under the peak at 12.7 min was 114.87 mAU × s, so the [NSP_a] was equal to 36.96 μM and the [NSP_b] was equal to 13.04 μM. The ε of NSP_b at 517 nm was found to be 2.78×10^4 cm^{-1} M^{-1} (Figure A.27).

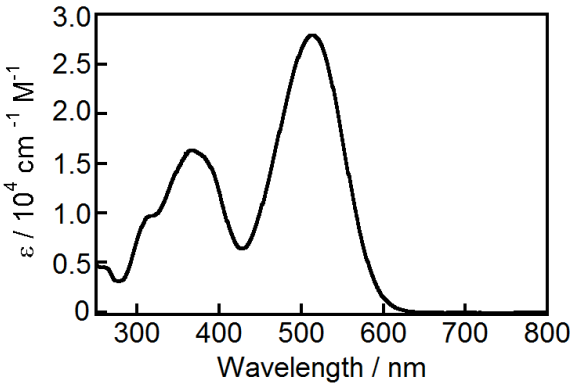

Figure A.27: Absorption spectrum of NSP_b in NaC 80 mM/NaCl 0.2 M.

NSP in NaC 80 mM/NaCl 0.2 M – trial 2

Absorption spectrum and HPLC response curve of NSP_a (Figure A.28):

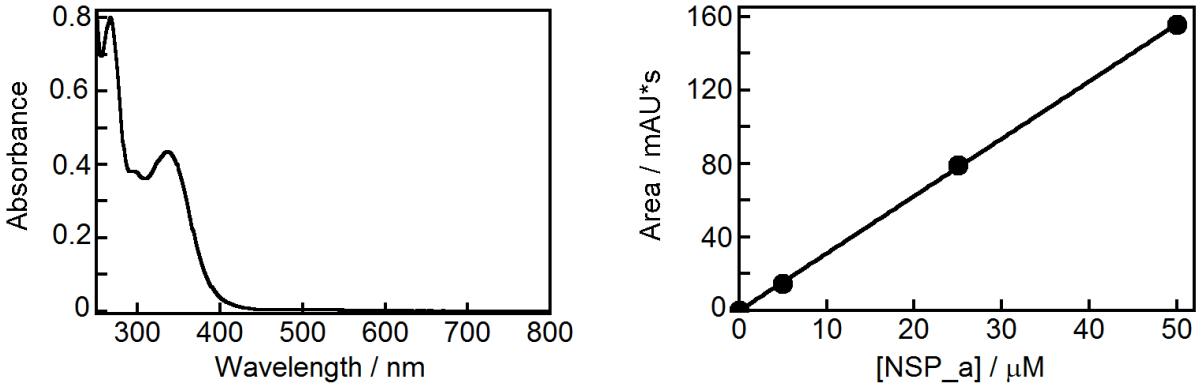

Figure A.28: Absorption spectrum (left) and HPLC response curve (right) of NSP_a 50 μM in NaC 80 mM/NaCl 0.2 M. The linear fit was set to pass through zero and has a slope of 3.1204; the correlation coefficient is 0.99992.

Absorption spectrum and HPLC chromatogram of NSP irradiated at 338 nm (Figure A.29):

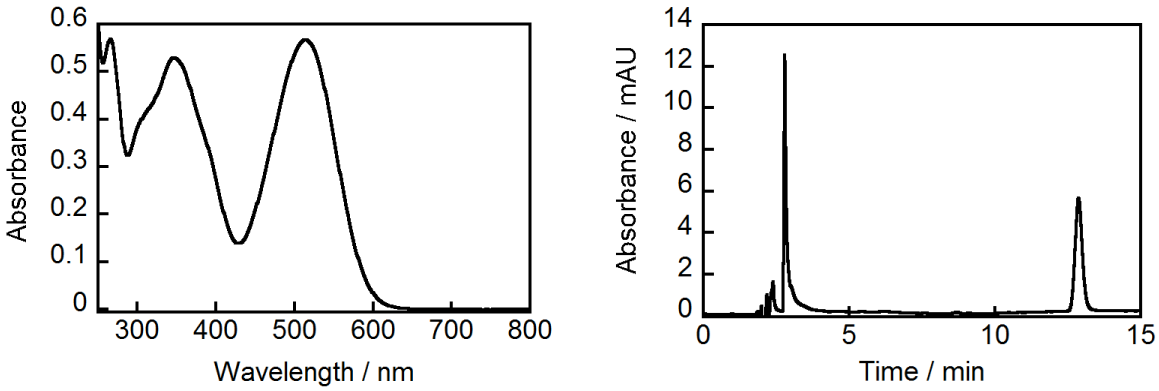

Figure A.29: Absorption spectrum (left) and HPLC chromatogram (right) of NSP 50 µM irradiated at 338 nm in NaC 80 mM/NaCl 0.2 M.

The area under the peak at 12.8 min is 95.22 mAU × s, so the [NSP_a] is equal to 30.52 µM and the [NSP_b] is equal to 19.48 µM. The ε of NSP_b at 517 nm was found to be 2.89×10^4 cm^{-1} M^{-1} (Figure A.30).

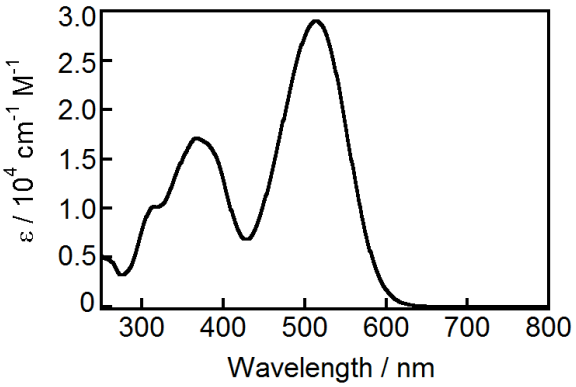

Figure A.30: Absorption spectrum of NSP_b in NaC 80 mM/NaCl 0.2 M.

NSP in NaDC 80 mM/NaCl 0.2 M – trial 1

Absorption spectrum and HPLC response curve of NSP_a (Figure A.31):

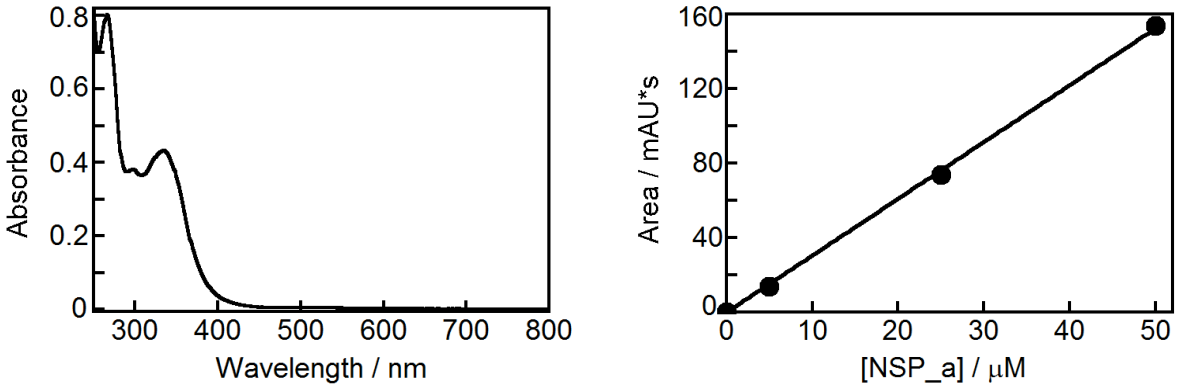

Figure A.31: Absorption spectrum (left) and HPLC response curve (right) of NSP_a 50 μM in NaDC 80 mM/NaCl 0.2 M. The linear fit was set to pass through zero and has a slope of 3.0476; the correlation coefficient is 0.99966.

Absorption spectrum and HPLC chromatogram of NSP irradiated at 338 nm (Figure A.32):

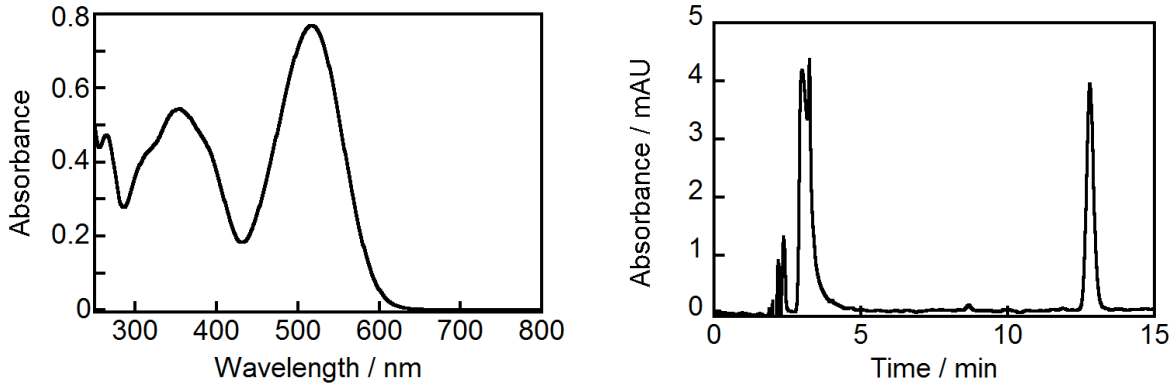

Figure A.32: Absorption spectrum (left) and HPLC chromatogram (right).of NSP 50 μM irradiated at 338 nm in NaDC 80 mM/NaCl 0.2 M.

The area under the peak at 12.8 min is 66.39 mAU × s, so the [NSP_a] is equal to 21.78 μM and the [NSP_b] is equal to 28.22 μM. The ε of NSP_b at 517 nm was found to be 2.72×10^4 cm^{-1} M^{-1} (Figure A.33).

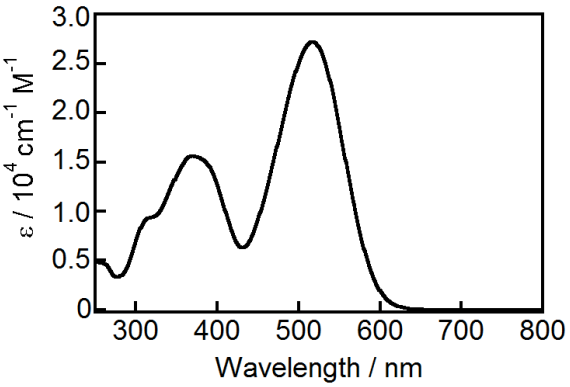

Figure A.33: Absorption spectrum of NSP_b in NaDC 80 mM/NaCl 0.2 M.

NSP in NaDC 80 mM/NaCl 0.2 M – trial 2

Absorption spectrum and HPLC response curve of NSP_a (Figure A.34):

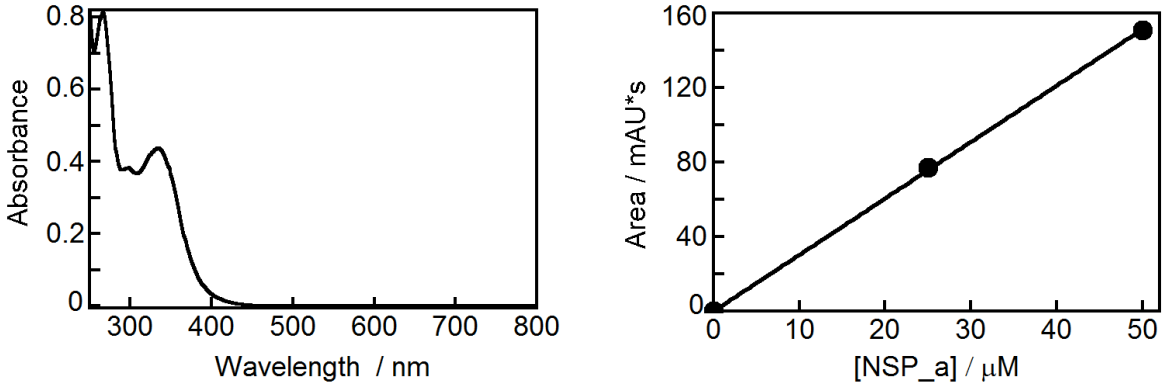

Figure A.34: Absorption spectrum (left) and HPLC response curve (right) of NSP_a 50 μM in NaDC 80 mM/NaCl 0.2 M. The linear fit was set to pass through zero and has a slope of 3.0297; the correlation coefficient is 0.9999.

Absorption spectrum and HPLC chromatogram of NSP irradiated at 338 nm (Figure A.35):

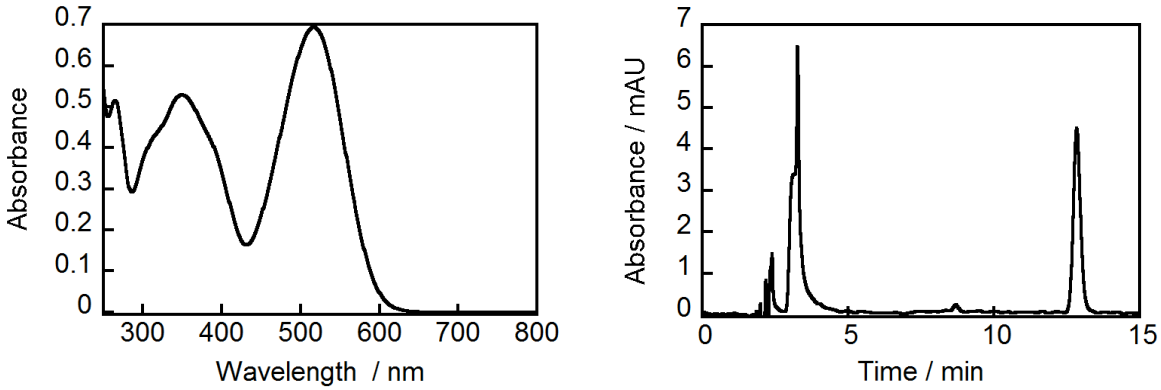

Figure A.35: Absorption spectrum (left) and HPLC chromatogram (right).of NSP 50 µM irradiated at 338nm in NaDC 80 mM/NaCl 0.2 M.

The area under the peak at 12.8 min is 77.10 mAU × s, so the [NSP_a] is equal to 25.45 µM and the [NSP_b] is equal to 24.55 µM. The ε of NSP_b at 517 nm was found to be 2.82×10^4 cm^{-1} M^{-1} (Figure A.36).

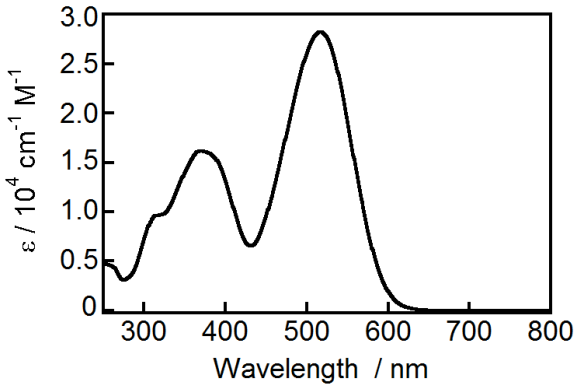

Figure A.36: Absorption spectrum of NSP in NaDC 80 mM/NaCl 0.2 M

NSP in NaTC 80 mM/NaCl 0.2 M – trial 1

Absorption spectrum and HPLC response curve of NSP_a (Figure A.37):

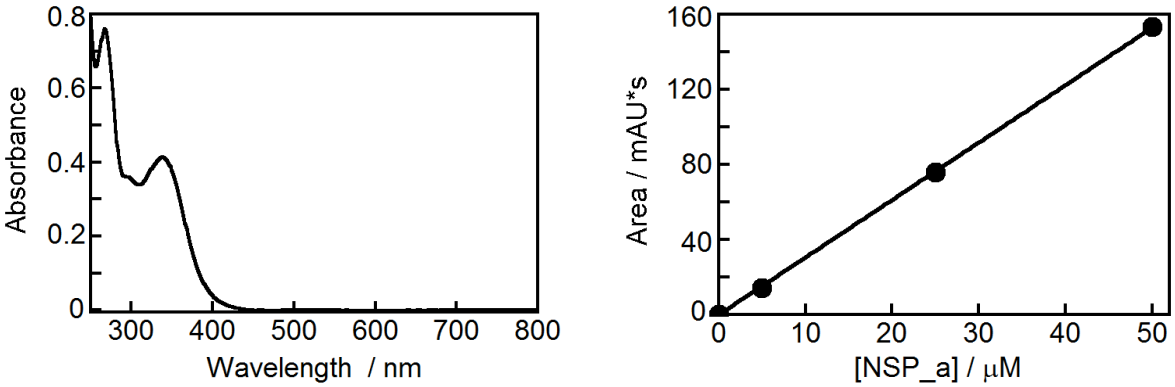

Figure A.37: Absorption spectrum (left) and HPLC response curve (right) of NSP_a 50 μM in NaTC 80 mM/NaCl 0.2 M. The linear fit was set to pass through zero and has a slope of 3.0585; the correlation coefficient is 0.99994.

Absorption spectrum and HPLC chromatogram of NSP irradiated at 338 nm (Figure A.38):

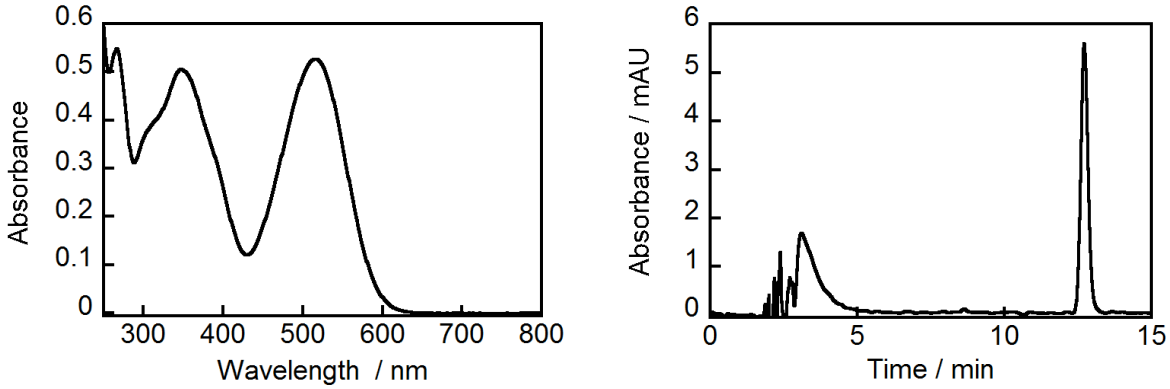

Figure A.38: Absorption spectrum (left) and HPLC chromatogram (right).of NSP 50 μM irradiated at 338 nm in NaTC 80 mM/NaCl 0.2 M.

The area under the peak at 12.8 min is 95.60 mAU × s, so the [NSP_a] is equal to 31.26 μM and the [NSP_b] is equal to 18.74 μM. The ε of NSP_b at 517 nm was found to be 2.81×10^4 cm^{-1} M^{-1} (Figure A.39).

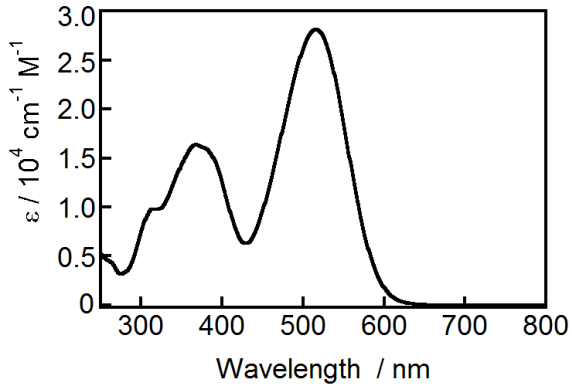

Figure A.39: Absorption spectrum of NSP_b in NaTC 80 mM/NaCl 0.2 M.

NSP in NaTC 80 mM/NaCl 0.2 M – trial 2

Absorption spectrum and HPLC response curve of NSP_a (Figure A.40):

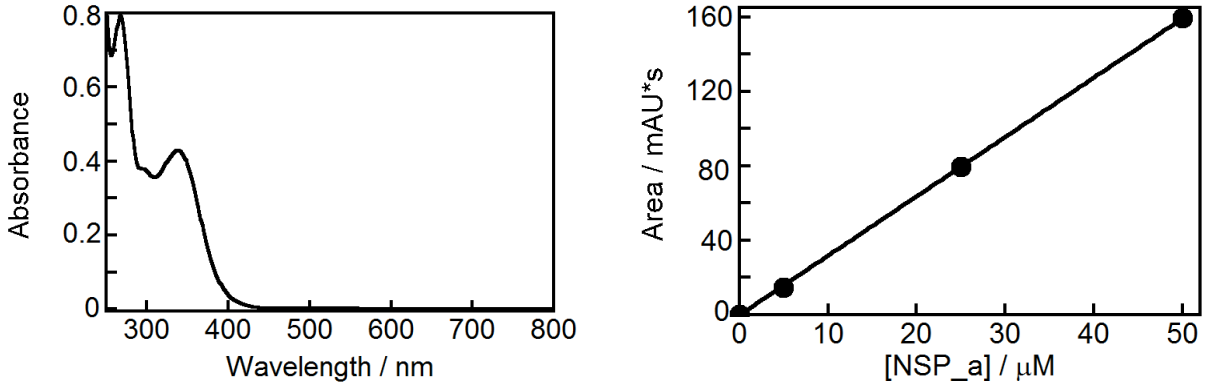

Figure A.40: Absorption spectrum (left) and HPLC response curve (right) of NSP_a 50 μM in NaTC 80 mM/NaCl 0.2 M. The linear fit was set to pass through zero and has a slope of 3.1862; the correlation coefficient is 0.99995.

Absorption spectrum and HPLC chromatogram of NSP irradiated at 338 nm (Figure A.41):

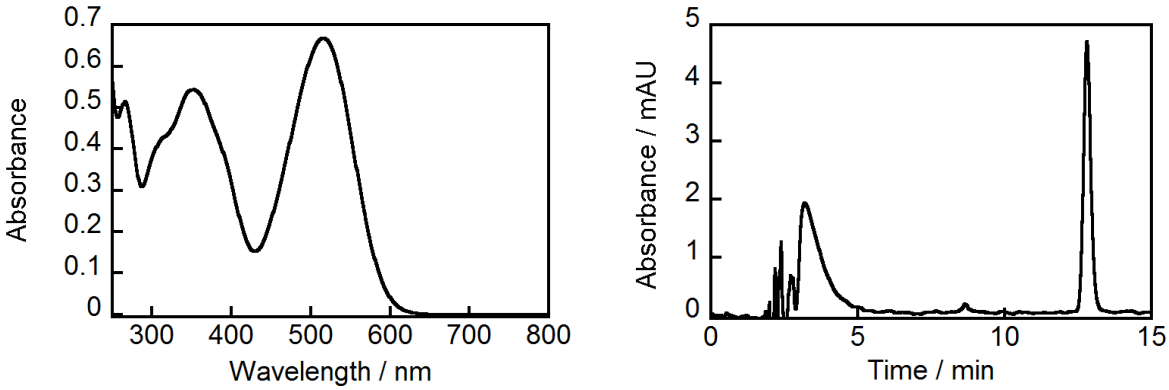

Figure A.41: Absorption spectrum (left) and HPLC chromatogram (right).of NSP 50 µM irradiated at 338 nm in NaTC 80 mM/NaCl 0.2 M.

The area under the peak at 12.8 min is 80.60 mAU × s, so the [NSP_a] is equal to 25.30 µM and the [NSP_b] is equal to 24.70 µM. The ε of NSP_b at 517 nm was found to be 2.70×10^4 cm^{-1} M^{-1} (Figure A.42).

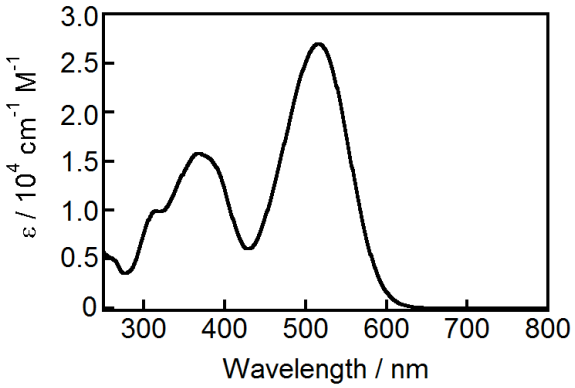

Figure A.42: Absorption spectrum of NSP_b in NaTC 80mM/NaCl 0.2 M.

Appendix B Arrhenius and Eyring plots for NSP dark reaction

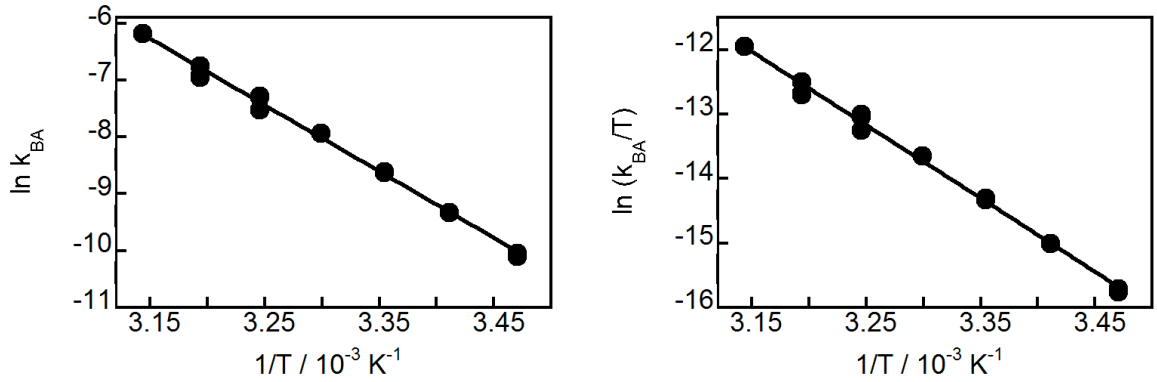

Figure B.1: Temperature studies of NSP dark reaction in NaC 80 mM/NaCl 1.0 M. **Left**: Arrhenius plot for k_{BA}. **Right**: Eyring plot k_{BA}.

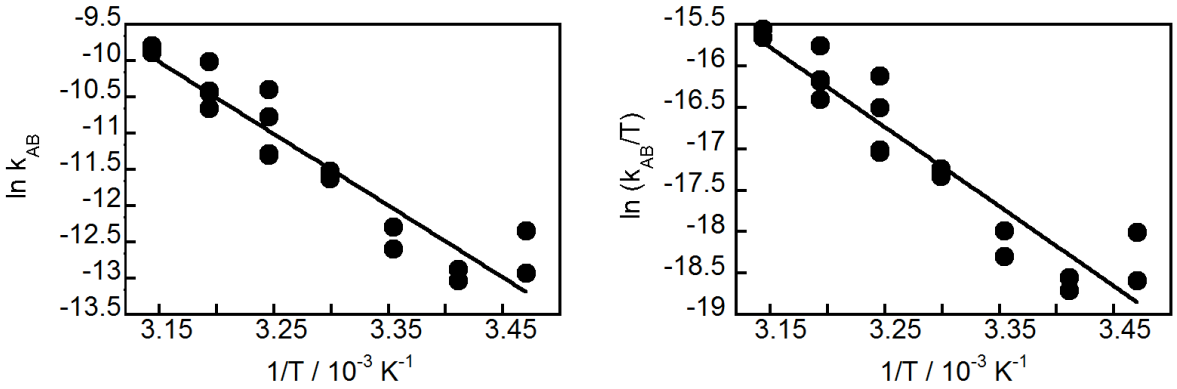

Figure B.2: Temperature studies of NSP dark reaction in NaC 80 mM/NaCl 1.0 M. **Left**: Arrhenius plot for k_{AB}. **Right**: Eyring plot k_{AB}.

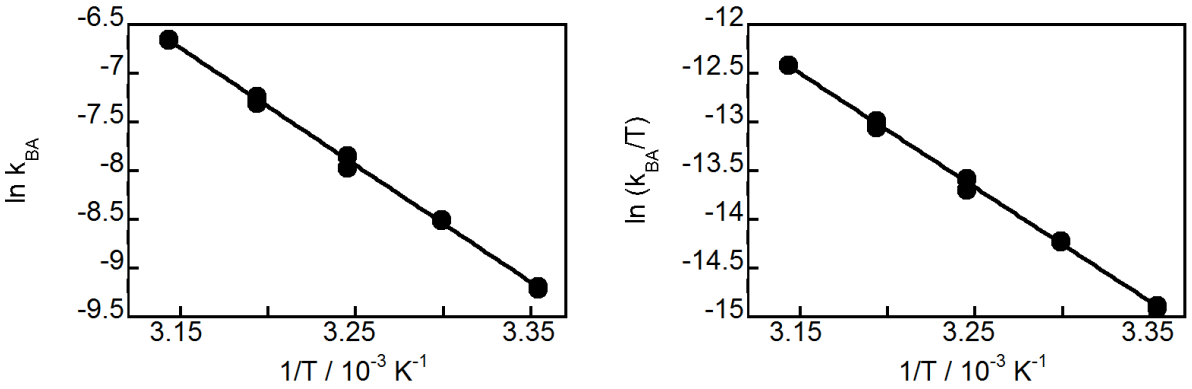

Figure B.3: Temperature studies of NSP dark reaction in NaDC 80 mM/NaCl 0.2 M. **Left**: Arrhenius plot for k_{BA}. **Right**: Eyring plot k_{BA}.

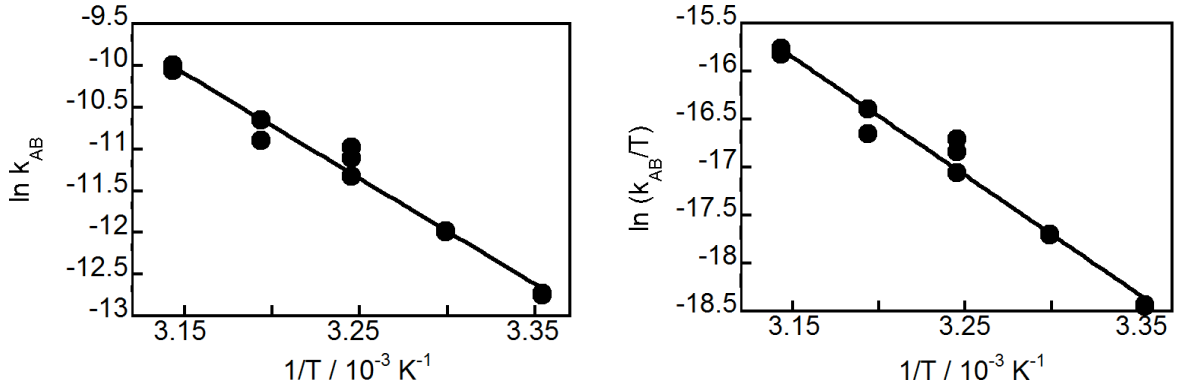

Figure B.4: Temperature studies of NSP dark reaction in NaDC 80 mM/NaCl 0.2 M. **Left**: Arrhenius plot for k_{AB}. **Right**: Eyring plot k_{AB}.

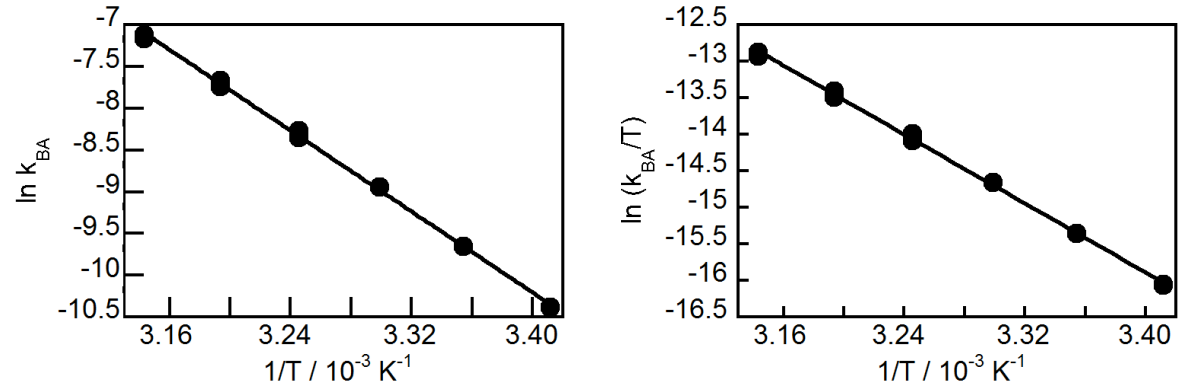

Figure B.5: Temperature studies of NSP dark reaction in NaTC 80 mM/NaCl 0.2 M. **Left**: Arrhenius plot for k_{BA}. **Right**: Eyring plot for k_{BA}.

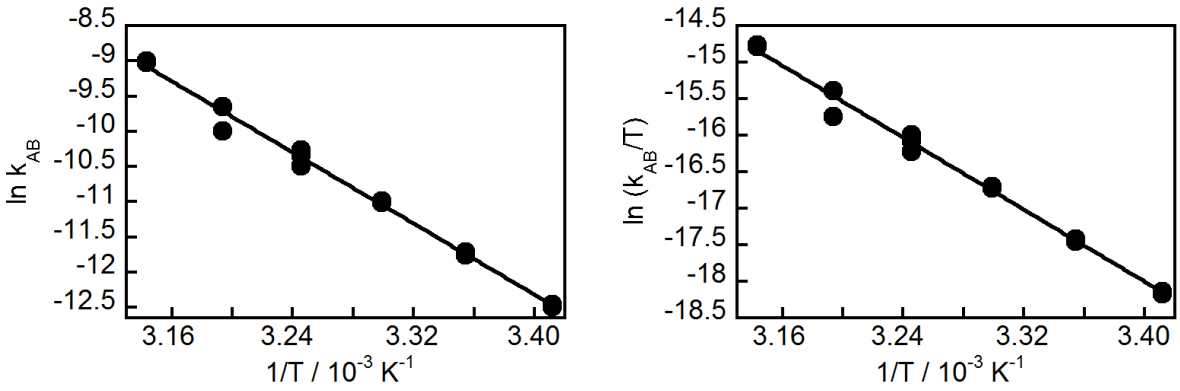

Figure B.6: Temperature studies of NSP dark reaction in NaTC 80 mM/NaCl 0.2 M. **Left**: Arrhenius plot for k_{AB}. **Right**: Eyring plot k_{AB}.